



Fakultät für Medizin

Institut für Virologie

Characterization of Endogenous Major Histocompatibility Complex Class II Antigen Processing Pathways for Modified Vaccinia Virus Ankara Infection

Yi Zhang

Vollständiger Abdruck der von der Fakultät für Medizin der Technischen Universität München zur Erlangung des akademischen Grades eines

Doctor of Philosophy (Ph.D.)

genehmigten Dissertation.

Vorsitzender: Univ.-Prof. Dr. Agnes Görlach

Betreuer: Univ.-Prof. Dr. Ingo Drexler

Prüfer der Dissertation:

1. apl. Prof. Dr. Anne Krug

2. Priv.-Doz. Dr. Klaus-Peter Janssen

Die Dissertation wurde am 27.11.2013 bei der Fakultät für Medizin der Technischen Universität München eingereicht und durch die Fakultät für Medizin am 29.01.2014 angenommen.

Table of Contents

Table of Contents	I
Index of Figures	V
Index of Tables	VII
Abbreviations	VIII
1. Introduction	1
1.1 Dendritic cells (DCs) are highly efficient antigen-presenting cells	1
1.1.1 Distinct DCs maturation process facilitates the antigen accumulation and T cell stimulation	1
1.1.2 Antigen processing and presentation by APCs	3
1.1.2.1 Direct and cross presentation by MHC I	3
1.1.2.2 Exogenous and endogenous antigen presentation by MHC II	6
1.2 MVA and its immunogenicity	9
1.2.1 MVA is a potent recombinant vaccine candidate	9
1.2.2 The life cycle of VACV/MVA	10
1.2.3 Innate anti-viral responses after poxvirus infection	12
1.2.4 Adaptive immunity against MVA infection	13
1.3 Autophagy and its role in antigen presentation	15
1.3.1 Functional autophagy is constituted of autophagosome formation and autophagic flux 15	
1.3.2 Autophagy contributes to innate and adaptive immunity	18
2. Aims of the study	20
3. Material and Methods	22
3.1 Materials	22
3.1.1 Plasmids	22
3.1.2 Antibodies	22
3.1.3 Cells, viruses and mice	24
3.1.3.1 Cells	24
3.1.3.2 Viruses	25
3.1.3.3 Mice	26
3.1.4 Buffers, solutions and media.....	27

3.1.4.1	Media for cell culture.....	27
3.1.4.2	Solutions for cell culture applications.....	28
3.1.4.3	Buffers for IF	28
3.1.4.4	Buffers and solutions for protein biochemistry	30
3.1.4.5	Buffers for Flow Activated Cell Sorting (FACS).....	31
3.2	Methods.....	32
3.2.1	Tissue culture	32
3.2.1.1	Cell lines	32
3.2.1.2	Primary cells	33
3.2.1.2.1	Generation and culture of bone marrow derived DCs	33
3.2.1.2.2	Isolation and culture of primary dermal fibroblasts.....	33
3.2.1.3	Cultivation of C4H3 hybridoma and production of C4H3 antibodies.....	34
3.2.1.4	Cryopreservation of cells.....	35
3.2.1.5	Transient transfection of cell lines and BMDCs.....	35
3.2.1.5.1	Transfection of cell lines.....	36
3.2.1.5.2	Transfection of BMDCs.....	36
3.2.2	Virological methods.....	36
3.2.2.1	In vitro infection of cells with MVA and VACV	36
3.2.2.2	Virus amplification and crude stock preparation	37
3.2.2.3	Virus purification.....	37
3.2.2.4	Virus titration and growth kinetics	38
3.2.3	Confocal laser scanning microscopy (CLSM).....	38
3.2.3.1	Intracellular IF	38
3.2.3.2	Live cell imaging and co-localization analysis.....	39
3.2.4	Protein biochemistry	40
3.2.4.1	Preparation of cell lysates	40
3.2.4.2	Determination of protein concentration	40
3.2.4.3	Immunoprecipitation (IP).....	40
3.2.4.4	Polyacrylamide gel electrophoresis	41
3.2.4.5	Immunoblotting (IB).....	42
3.2.5	Flow chemistry.....	43
4.	Results.....	44
4.1	MVA induced autophagy and the molecular mechanisms behind.....	44
4.1.1	MVA accumulates LC3 to induce autophagosome formation.....	44
4.1.1.1	LC3 is increased in BMDCs, BMDMs, and HeLa cells after MVA infection	44
4.1.1.2	VACV enhances LC3 lipidation	45
4.1.1.3	LC3-II conversion is abolished in Atg7-deficient BMDCs	46
4.1.2	Autophagic flux is enhanced by MVA	48

4.1.2.1	Autophagosomes and autolysosomes are detectable by immunofluorescence after transfecting mRFP-EGFP-LC3 plasmids.....	48
4.1.2.2	EGFP-LC3 is degraded in the lysosome upon MVA infection	52
4.1.2.3	Fusion of autophagosome with lysosomes is increased.....	55
4.1.3	MVA-induced autophagy requires the TLRs adaptor protein MyD88.....	57
4.1.3.1	MyD88 and Beclin-1 levels are upregulated	57
4.1.3.2	MVA infection fails to induce autophagy in MyD88 ^{-/-} BMDCs	58
4.1.3.3	Starvation-induced autophagy is functional in MyD88 ^{-/-} BMDCs	59
4.1.3.4	Autophagy induction requires viral replication intermediates.....	60
4.2	Endogenous MHC II presentation of MVA-produced HEL.....	63
4.2.1	Infected BMDCs fail to endocytose exogenous apoptotic cell debris	63
4.2.2	Endogenous viral antigens are presented to CD4 ⁺ T cells	65
4.2.3	HEL-MHC II complexes are detected in the cytoplasm and on the cell membrane....	66
4.2.3.1	Aw3.18 mAb only recognizes surface antigen-MHC II complexes	66
4.2.3.2	C4H3 monoclonal antibodies recognize intracellular pHEL/I-A ^k	68
4.2.3.3	Self-produced C4H3 mAb additionally recognizes the pHEL46-61/I-A ^k complexes.....	70
4.2.4	Endogenously loaded pHEL46-61/I-A ^k are present in BMDCs infected with MVA-HEL	70
4.2.5	The presentation of pHEL46-61/I-A ^k associates with MHC II.....	71
4.3	Detection of viral antigens and intracellular organelles by confocal laser scanning microscopy	73
4.3.1	Spatiotemporal distribution pattern of foreign gene expression under control of early or late promoters by recombinant MVA.....	73
4.3.1.1	EGFP expression pattern.....	73
4.3.1.2	OVA expression pattern.....	75
4.3.2	Spatiotemporal distribution pattern of viral antigens during infection.....	76
4.3.2.1	H3 is present around viral factories and then transported to the cell membrane.....	76
4.3.2.2	A27 is present around viral factories only.....	77
4.3.3	Cellular organelles undergo morphological changes upon infection.....	78
4.3.3.1	Early endosomes do not co-localize with viral factories	78
4.3.3.2	The Golgi complexes co-localize with viral factories	80
4.3.3.3	Detection of the MHC II containing compartment (MIIC)	84
4.3.3.3.1	MIIC transforms into a large tubular structure only upon MVA infection.....	84
4.3.3.3.2	MIIC co-localize with viral factories.....	84
4.3.3.4	MHC II co-localize with MIIC and then move on to the cell surface during cell maturation	86
4.3.3.5	MHC II co-localizes with lysosomes.....	87

5. Discussion	89
5.1 Autophagy is important for MVA-related MHC class II antigen processing and presentation	89
5.1.1 Methods and limitations to monitor autophagy in BMDCs.....	89
5.1.1.1 Interpretation of LC3-turnover analysis by immunoblotting.....	89
5.1.1.2 Dissection of autophagy maturation by EGFP/mRFP-LC3 lysosomal delivery and proteolysis	91
5.1.2 Both MVA and VACV infection activate autophagy in BMDCs.....	93
5.1.2.1 Atg7 is required for MVA induced autophagy in BMDCs.....	93
5.1.2.2 MVA infection induces stronger autophagy than VACV infection.....	94
5.1.3 MVA induces autophagy through a TLRs adaptor protein.....	94
5.2 Endogenous antigen presentation of HEL peptides.....	97
5.2.1 Endocytotic ability of MVA-infected BMDCs is impaired.....	97
5.2.2 Infected BMDCs can present endogenous antigens to CD4 ⁺ T cells on MHC II.....	98
5.2.3 Endogenous HEL peptides are processed and presented by MHC II	99
5.3 Excellular and intracellular events in MVA infected BMDCs	101
5.3.1 Expression and spatiotemporal distribution pattern of viral products	101
5.3.2 Co-localization of viral factory, MIIC and Golgi complex	102
6. Conclusions and Outlook	105
7. References.....	106
8. Appendix.....	119
8.1 Equipment	119
8.2 Consumables.....	120
Acknowledgment.....	122
Curriculum Vitae.....	123

Index of Figures

Figure 1. Comparison of immature and mature DCs reflects a dramatic change in morphology and function	3
Figure 2. Schematic diagram of antigen presentations by MHC I and MHC II	5
Figure 3. Four models of endogenous antigens processing and presentation pathways exist in DCs.....	8
Figure 4. Infectious cycle of VACV in permissive cells	11
Figure 5. Biogenesis of autophagy and its inhibitors.....	17
Figure 6. Kinetic expression of LC3 in MVA infected BMDCs, BMDMs and HeLa cells	45
Figure 7. The expression of LC3 in VACV infected BMDCs	46
Figure 8. The expression of LC3 in Atg7-deficient BMDCs	47
Figure 9. Transient transfection of HeLa cells with the mRFP-EGFP-LC3 expression plasmid.....	50
Figure 10. Optimization of chloroquine concentration in mRFP-EGFP-LC3 transfected HeLa cells	52
Figure 11. mRFP-EGFP-LC3 quenching assay in HeLa cells.....	54
Figure 12. Autophagic flux in MVA-EGFP P7.5 infected HeLa cells.....	56
Figure 13. Kinetic analysis of Beclin-1 and MyD88 expression in MVA infected BMDCs	58
Figure 14. Analysis of Beclin-1 and LC3 in MVA or VACV infected BMDCs.....	59
Figure 15. Expression of LC3 in MVA or VACV-infected MyD88 deficient BMDCs	60
Figure 16. The expression of LC3 under conditions that block viral DNA replication	62

Figure 17. Schematic presentation of endocytosis assay methods.....	64
Figure 18. Stimulation of CD4^{ova} T cells by OVA peptide or MVA-OVA PK1L infected BMDCs	65
Figure 19. Presentation of HEL antigens was detected by FACS using Aw3.18 mAb 68	
Figure 20. Comparison of pHEL/MHC II immunofluorescence by using Aw3.18 mAb and C4H3 mAb	69
Figure 21. Intracellular staining of pHEL46-61/I-A^k by using purified C4H3 mAb or hybridoma supernatant	70
Figure 22. Kinetics of pHEL46-61/I-A^k expression in MVA-HEL P7.5 infected BMDCs 71	
Figure 23. Co-localization of C4H3 and MHC II in MVA-HEL P7.5 infected BMDCs 72	
Figure 24. Detection of EGFP expression under the control of MVA early (PK1L) or late (P11) promoters.....	74
Figure 25. Characterization of recombinant OVA expression in the cytoplasm.....	75
Figure 26. Spatiotemporal distribution of H3 in MVA-infected HeLa cells	76
Figure 27. Characterization of viral antigen A27 localization in the cytoplasm.....	77
Figure 28. Kinetics of recombinant gene expression and localization of early endosomes in MVA infected DC 2.4 or HeLa cells	80
Figure 29. Temporal distribution of Golgi complexes and viral factories in infected HeLa cells or BMDCs	83
Figure 30. Monitoring the MIIC transformation upon MVA infection or LPS stimulation 86	
Figure 31. Transport of MHC II during the maturation of BMDCs.....	87
Figure 32. MHC II co-localizes with LAMP-2	88

Index of Tables

Table 1. Plasmids for immunofluorescence (IF) and immunoprecipitation (IP).....	22
Table 2. Primary antibodies for immunofluorescence (IF) , immunoblotting (IB) and immunoprecipitation (IP) and flow chemistry	22
Table 3. Secondary antibodies for IF, IB, IP, flow chemistry and dye for live imaging	24
Table 4. Cell lines and primary cells	24
Table 5. Index of viruses	25
Table 6. Index of mouse strains	26
Table 7. Cell culture media	27
Table 8. Solutions for cell culture application.....	28
Table 9. Buffers used for IF	28
Table 10. Buffers and solutions used for protein biochemistry.....	30
Table 11. Buffers for FACS analysis.....	31
Table 12. Composition of SDS-PAGE gels	41

Abbreviations

Abs/mAbs	Antibodies/monoclonal Abs
APCs/pAPCs	Antigen presenting cells/ professional APCs
Atg	Autophagy related protein
BMDCs/DCs	Bone marrow derived dendritic cells/dendritic cells
CD	Cluster of differentiation
CLIP	Class-II-associated Ii peptide
CLSM	Confocal laser scan microscope
CQ	chloroquine
CTL	Cytotoxic T Lymphocyte
CVA	Chorioallantois vaccinia virus
ddH ₂ O	Double distilled water
EGFP	Enhanced green fluorescent protein
ER	Endoplasmic reticulum
FACS	Fluorescence activated cell sorting
GM-CSF	Granulocyte-macrophage colony-stimulating factor
HEL	Hen egg lysozyme
HLA-DM	Human leukocyte antigen-DM

Hsp	Heat shock protein
IB	Immunoblotting
IFN	Interferon
Ii	Invariant chain
IL	Interleukin
IP	Immunoprecipitation
LAMP	Lysosome associated membrane protein
LC	Microtubule-associated protein light chain
LPS	Lipopolysaccharide
MAL	MyD88-adaptor like
MHC	Major histocompatibility complex
MIIC	MHC II containing compartment
MOI	Multiplicity of infection
mRFP	Monomeric red fluorescent protein
MVA	Modified vaccinia virus Ankara
MyD88	Myeloid differentiation primary response gene 88
OVA	Chicken ovalbumin
PAGE	Polyacrylamide gel electrophoresis
PAMPs	Pathogen-associated molecular patterns

PCR	Poly chain reaction
PE	Phosphatidylethanolamine
p.i.	Post transfection
PRR	Pathogen recognition receptor
p.t.	Post transfection
PUVA	Psoralen in combination with ultraviolet (UVA) radiation treatment
RT	Room temperature
SARM	Sterile α -and armadillo motif-containing protein
TAP(s)	Transporter(s) associated with antigen processing
TLR	Toll like receptor
TNF	Tumor necrosis factor
TRAM	TRIF-related adaptor molecule
TRIF	Toll/interleukin-1 receptor domain-containing adapter protein
VACV	Vaccinia virus
v/v	Volume per volume
w/o	Without
w/v	Weight per volume

1. Introduction

1.1 Dendritic cells (DCs) are highly efficient antigen-presenting cells

The cells that first encounter the antigenic particles and then process and consequently present the recognizable antigens to T cells are called antigen-presenting cells (APCs). Though several cell types can exert antigen-presenting function *in vivo*, certain cells including B cells, macrophages and dendritic cells (DCs) that are very efficient for this work are further considered as professional APCs (pAPCs).

1.1.1 Distinct DCs maturation process facilitates the antigen accumulation and T cell stimulation

Dendritic cells (DCs), a talented member of professional APCs, are a key link between the innate and adaptive immune system. They are endowed with the strong capability of sensing and ingesting microorganisms by using several cellular pathways and numerous receptors on the cell surface as well as endoplasmic reticulum membrane. Upon pathogen recognition, they can secrete large amount of cytokines (e.g. type I interferons, IFN I) to limit the spread of infection, thus providing first line of defense against invading pathogens.¹ DCs are also superior at controlling the quality of T cell responses by secretion of cytokines or costimulatory molecules that drive naïve lymphocytes into distinct kinds of effectors. They alert helper T cells, which allow the activation of macrophages, natural killer cells as well as B cells. Cytotoxic T cells can be authorized by helper T cells-licensed DCs to lyse the infected cells. Thereby, DCs successfully initiate primary immune responses.²

Most DCs have long finger-like processes, similar to the dendrites of neurons. This morphological characteristic of DCs helps to accumulate a diverse array of antigens from the surrounding environment by endocytosis, as well as facilitates extensive interaction with T cells. The migration of DCs from peripheral sites to the secondary lymphoid organs is accompanied by degradation of the internalized pathogens and changes of surface molecules, which benefit the subsequent presentation of antigens to T cells via major

histocompatibility complexes (MHC) I/II.³

In vivo and *in vitro*, DCs exist in two functional and phenotypical stages: immature DCs and mature DCs (Fig. 1). Immature DCs are specialized in pathogen uptake by macropinocytosis, receptor-mediated endocytosis and phagocytosis,⁴ while expressing low levels of surface MHC I and II molecules as well as costimulatory signals such as CD (cluster of differentiation) 40, CD80, and CD86. Thus, immature DCs can capture and process antigens, but are insufficient to activate T cells because the antigen presentation lacks the adequate costimulation.⁵ In order to stimulate T cells, immature DCs need to undergo a maturation process that is started once DCs receive a stimuli, for example through components of the bacterial wall (e.g. lipopolysaccharide, LPS), viral gene products (e.g. double stranded RNA, dsRNA) or inflammatory cytokines (e.g. tumor necrosis factor α , TNF- α).⁶ After that, DCs redistribute MHC II molecules from intracellular endocytic compartments to the cell surface, while selectively decreasing their internalization activity but dramatically upregulating costimulatory molecules on the plasma membrane to be ready for recognition by T cells.⁷ Upon maturation, DCs migrate from peripheral sites to lymph nodes to share the antigenic peptides with lymph node-resident macrophages that disseminate the dangerous information, and most importantly they complete their task to stimulate T-cells.⁸

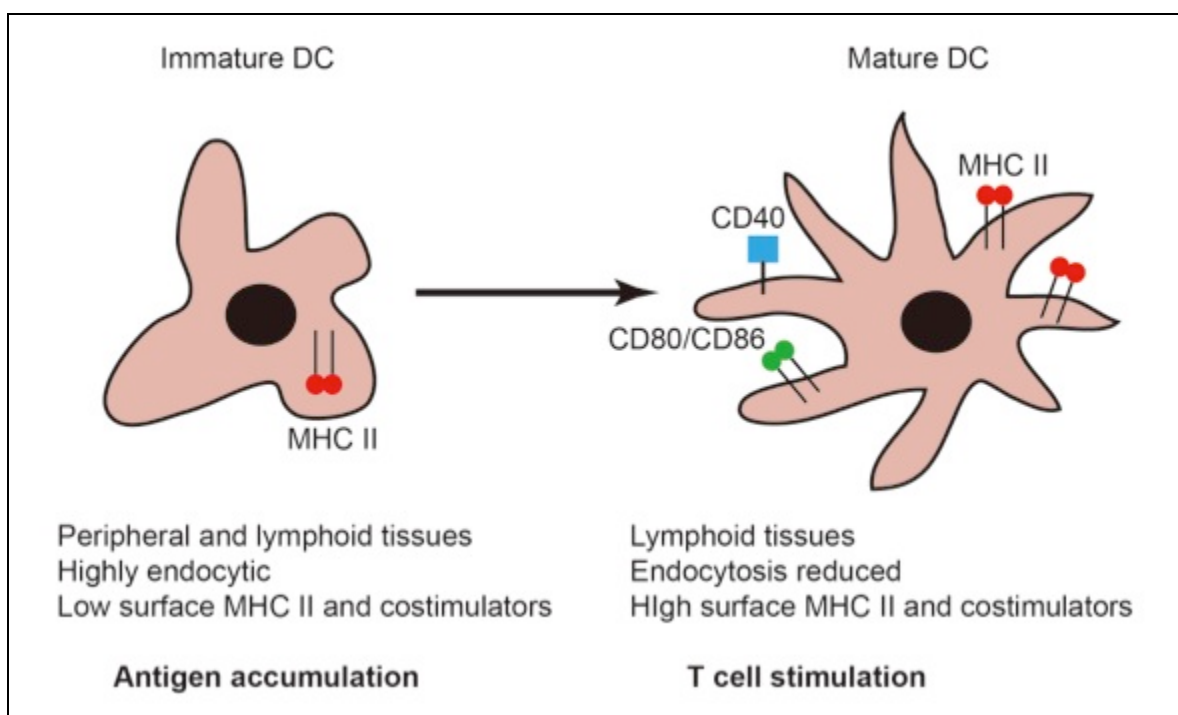


Figure 1. Comparison of immature and mature DCs reflects a dramatic change in morphology and function

The maturation process allows DCs travelling from a peripheral site of infection to a secondary lymphoid tissue. The migration is accompanied with the changes in expression of surface MHC II as well as costimulatory molecules. Whereas immature DCs (left) are active in endocytosis, antigen processing and accumulation, mature DCs (right) lose these properties during the movement to lymphoid organs but gain the capacity to present antigenic peptides at the membrane via MHC I/II, associated with increased costimulators (e.g. CD80/CD86) for the recognition by naïve T cells. MHC II rests in endocytic compartment when DCs are immature, and are subsequently transported to the membrane upon maturation.

1.1.2 Antigen processing and presentation by APCs

The generation of peptides from native proteins is commonly referred to as antigen processing, whereas the display of the peptides at the cell surface by the MHC I/II is referred to as antigen presentation.⁹ T cells play a central role in cell-mediated immunity, however cannot recognize antigens directly. They depend on the APCs to process the pathogens to peptide fragments and present the peptides by the MHC molecules. Then, the T cell receptors present on the surface of T cells are responsible for recognizing the antigens bound to MHC molecules. Therefore, MHC I/ II restricted antigen processing pathways decide the fate of processed peptides to the subtype of T cells they are presented to.

1.1.2.1 Direct and cross presentation by MHC I

The antigens presented by MHC I are recognized by cytotoxic T lymphocytes (CTLs). Classically, endogenous cellular antigens (e.g. ovalbumin amino acids 257-264, SIINFEKL) designed for presentation on MHC I molecules are ubiquitinated in the cytosol and subsequently fed to the proteasome.¹⁰ Proteins generated in the cytosol, are subjected to customized cleavage of the amino acid chain after hydrophobic or basic amino acids during proteolysis, in order to favor the subsequent transportation to the lumen of the endoplasmic reticulum (ER) via transporters associated with antigen processing (TAPs). These transporters consist of two subtypes: TAP-1 and TAP-2. In the ER lumen, the resulting peptide fragments may need further amino-terminal trimming by aminopeptidases (e.g. ER aminopeptidase 1, ERAP1) to the correct size for MHC I binding.¹¹ This process is termed direct or conventional presentation by MHC I (Fig. 2).

However, the restriction of this direct MHC I pathway is insufficient to activate naïve CTLs in two scenarios: the intracellular pathogen does not infect APCs (e.g. tumors pathogens) or compromises their direct MHC I presentation (e.g. Measles virus and vaccinia virus¹²) by preventing the appearance of the peptide/MHC I complex on the cell surface. As a consequence, this flaw of direct presentation can be utilized by some viruses and tumors to evade lymphocyte recognition so that avoid the host immune surveillance.¹³ This phenomenon strongly suggested that other possible pathways exist besides the classical rule of antigen presentation.

In line with this, in 1976 Bevan *et al.* have shown that exogenous antigens endocytosed by APCs can also elicit potent CTL responses, a process which was later on named “cross-presentation”.¹⁴ Although the mechanistic details need to be further elucidated, it has been proven that exogenous antigens leak out from endosomal vesicles and enter the ER to be loaded on MHC I. This alternative presentation pathway is critical for the induction of adaptive immune responses against viral antigens or tumor antigens which are not endogenously synthesized within APCs, but are able to license CTLs by neighboring APCs (Fig. 2).¹⁵ Using the attenuated vaccinia virus (VACV) strain– modified vaccinia virus Ankara (MVA), our group demonstrated that the primary CTL response against VACV-produced antigens is dominated by cross-priming *in vivo*, while infected DCs failed to induce primary CTL responses.¹⁶⁻¹⁸ Therefore, theoretically, any viral infection may induce CTLs by combining the direct presentation and cross presentation by MHC class I.

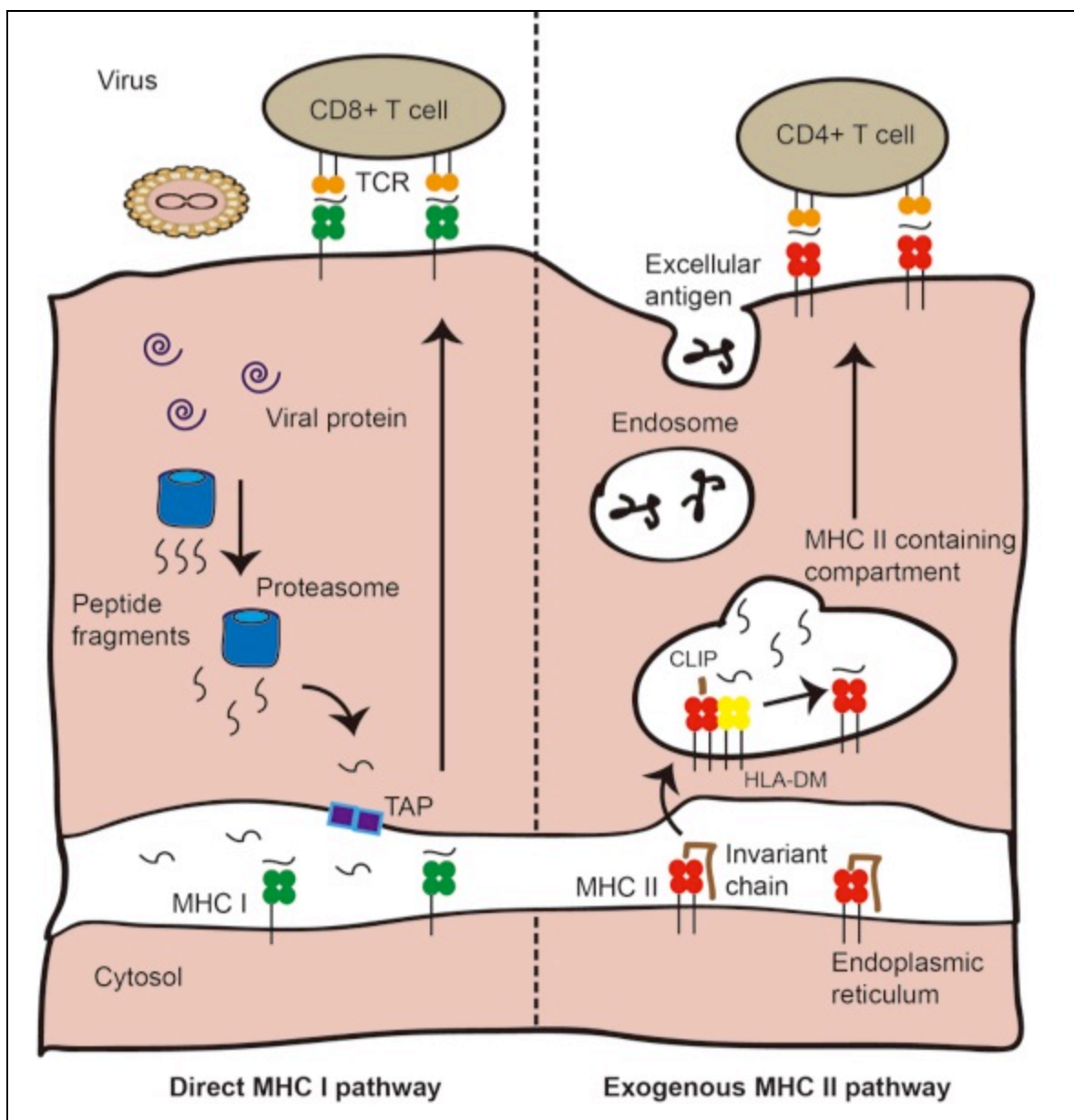


Figure 2. Schematic diagram of antigen presentations by MHC I and MHC II

Direct MHC I pathway (left): Viral proteins produced in infected DCs are degraded in the proteasome. The resulting peptide fragments can be transported to the lumen of the endoplasmic reticulum via transporters associated with antigen processing (TAPs). In there, peptides are trimmed into the precise size to be loaded on the newly synthesized MHC I molecules and later on delivered to the membrane surface. The peptide/MHC I complex is recognized by T cell receptors (TCRs) on CD8⁺ T cells, which stimulate a CTL response. **Exogenous MHC II pathway** (right): Apoptotic bodies derived from neighboring infected DCs are ingested by uninfected DCs. The endocytosed antigens are digested into antigenic peptides in the endosomes and lysosomes that subsequently replace the class-II-associated Ii peptide (CLIP) in the binding groove with the help of HLA-DM. The peptide/MHC II complex is then displayed on the cell surface waiting to be recognized by the TCRs of CD4⁺ T cells. Therefore, antigens presented by the MHC II pathway are responsible for activation of helper T cells.

1.1.2.2 *Exogenous and endogenous antigen presentation by MHC II*

Whereas MHC I is designed to present endogenous peptides to CTLs, MHC II molecules present exogenous protein fragments to CD4⁺ helper T cells. After microbes or viral products have been endocytosed, they are digested into peptides of 13-17 amino acids length and loaded on MHC II in the endocytic compartment. Newly synthesized MHC II molecules are targeted from the Golgi complex to vesicular compartments through a signal in the cytoplasmic tail of the invariant chain (Ii) of MHC II (Fig. 2). Once MHC class II arrives there, Ii is gradually degraded, leaving only a class-II-associated Ii peptide (CLIP) in the binding groove. With the help of the MHC II-like molecule HLA-DM (in human, H2-M in mouse), CLIP is released from the groove, which allows antigen peptides to bind. Particularly, the Ii cleavage and peptides exchange with CLIP that bound to MHC II occurs in a specific late endosomal compartment called the MHC class II containing compartment (MIIC). Afterwards, MHC II molecules are released from MIIC and transported to the plasma membrane to present the cargo peptides to CD4⁺ T cells. This process is termed MHC II-restricted exogenous antigen presentation.

Similar to MHC I, the presentation of endocytic peptides is not exclusive to MHC II, which has been already demonstrated by several studies.¹⁹⁻²¹ But unlike MHC I, the routes by which endogenous antigens meet MHC class II are very diverse. It has been shown that endogenous peptides derived from endosomal and plasma membrane, as well as mitochondrial or nuclear generated peptides are all able to enter the MHC II antigen presentation pathway.²² There are four models proposed to elucidate how these endogenous peptides can access MHC II (Fig. 3). Briefly, the first two possibilities are similar to the direct MHC I processing pathway, in which cytosolic peptides are imported into the ER via TAP or some other ER membrane transporters (e.g. Sec61). The peptides either travel together with MHC class II-Ii to endosomal compartments and then with the help of HLA-DM are loaded onto MHC II (e.g. influenza hemagglutinin, HA)²³ or they occupy the peptide-binding groove of MHC class II ahead of Ii when MHC II still remains in the ER (e.g. a 12-mer HA peptide)²⁴. The third pathway is suggested to be dependent on lysosome associated membrane protein 2a (LAMP-2a, the chaperone-mediated autophagy transporter) rather than TAP. In this pathway, proteins (e.g. Glutamate decarboxylase 65,

GAD65) are degraded initially by the proteasome and subsequently imported into MIIC by LAMP-2a transporter. The fourth pathway postulated suggests that antigens are delivered to the lysosome for MHC II processing by macroautophagy (refer to Chapter 1. 3). Up to date, the last route has been demonstrated for some antigens, such as Epstein-Barr virus nuclear antigen 1 (EBNA-1) and influenza matrix protein 1 (MP1). Paludan *et al.* demonstrated that blocking autophagy by 3-MA or using small interfering RNA (siRNA) downregulating Atg12, leads to EBNA-1 slowly accumulating in cytosolic autophagosomes. Therefore, MHC class II-restricted presentation of endogenous EBNA-1 to T cells was reduced.²⁵ Additionally, it was reported that targeting of MP1 to autophagosomes via fusion of the autophagosome-associated protein in DCs led to strongly enhanced MHC II presentation to CD4⁺ T cells clones.²⁶

In conclusion, DCs are unique among all APCs in many critical ways. Unlike macrophages or B cells, which are emphasized by the extraordinary capacity for endocytosis or antibody secretion, the primary function of DCs appears to be antigen presentation. They have distinct maturation and migration properties, enabling them to proactively seek naïve T cells to present the carried antigens. These specialties have interesting implications for how DCs may use several mechanisms to process antigens from diverse sources and choose different T cells populations for presentation.

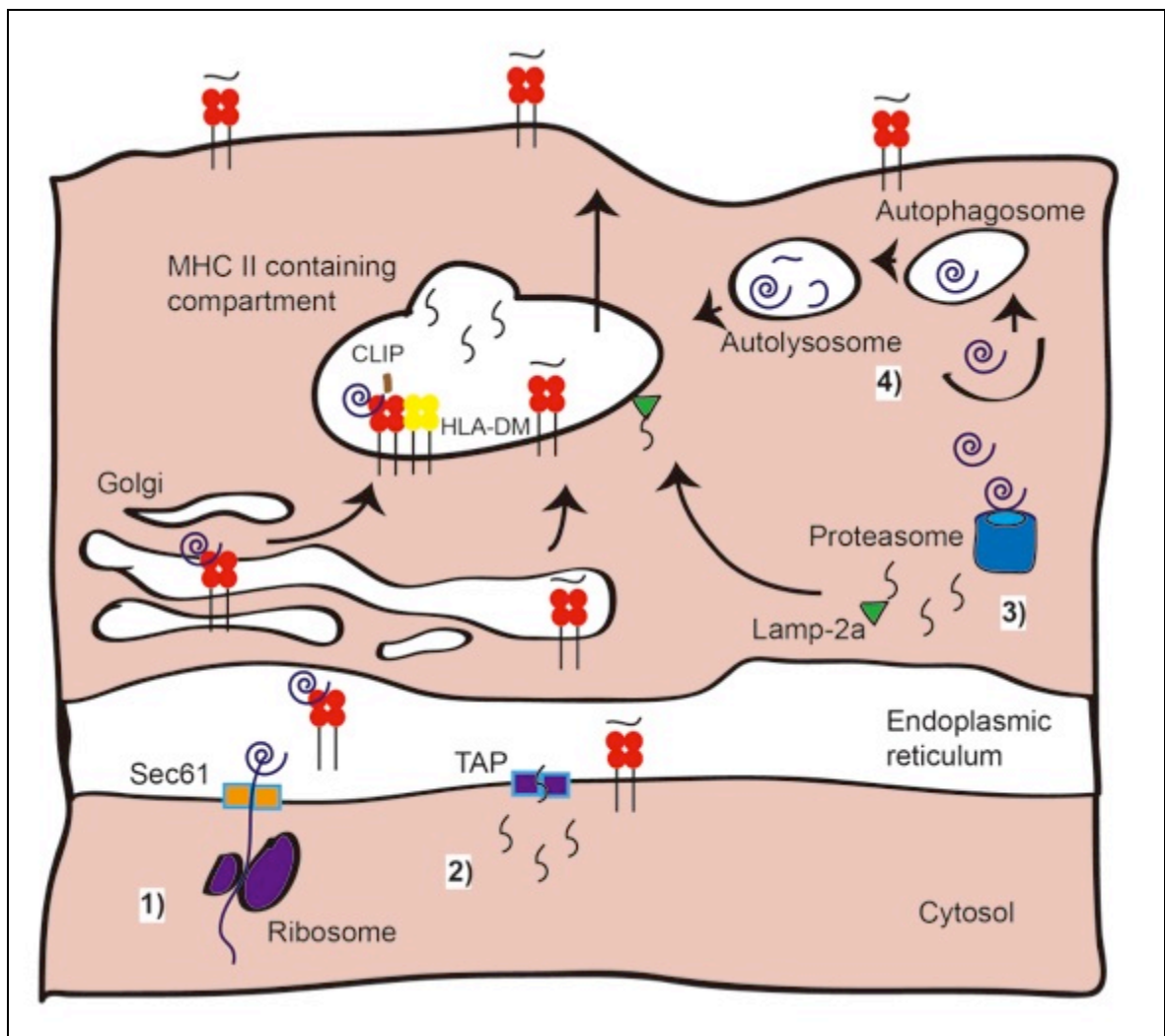


Figure 3. Four models of endogenous antigen processing and presentation pathways exist in DCs

1) Secreted/transmembrane proteins can associate with newly synthesized MHC II after their translocation into the ER via transporters (e.g. Sec61), and later on enter MIIC for further degradation and peptide loading. 2) Cytosolic peptides can be imported to the ER via TAP and occupy the peptide-binding groove of MHC II, which failed to associate the Ii. 3) Other cytosolic proteins degraded by the proteasome are transported by LAMP-2a to enter the MIIC. 4) Antigens are engulfed into autophagosomes and then degraded via fusion with lysosomes.

1.2 MVA and its immunogenicity

1.2.1 MVA is a potent recombinant vaccine candidate

The poxviruses comprise a family of double-stranded DNA (dsDNA) viruses that replicate in the cytoplasm of vertebrate and invertebrate cells.²⁷ One of the famous members in this family is variola virus, the cause of smallpox, which once altered human history by leading to the devastating disease in the mid-18th century.²⁸ In 1980, the World Health Organization (WHO) announced the eradication of smallpox. Since then potential life-threatening viral infections caused by poxviruses are rare but can occur, e.g. monkeypox which are sporadically spreading out in the human populations.²⁹ Since Edward Jenner used cowpox as a prophylactic agent against smallpox in 1798, vaccination has been greatly developed including VACV as a vaccine.³⁰ VACV contains a dsDNA genome of approximately 190 kb encoding more than 200 proteins. Some characteristics of VACV, such as a large packaging capacity for recombinant DNA, precise virus-specific control of target gene expression, lack of persistence or genomic integration into the host genome and an extremely effective immunogenicity, made VACV the first generation of vaccines used worldwide.³¹ However, as live VACV contained these vaccines, between 14 and 52 people per 1 million people vaccinated for the first time experienced potentially life-threatening reactions such as serious skin rashes and inflammation of the brain (<http://www.bt.cdc.gov/agent/smallpox/vaccination/facts.asp>). Hence, for safety considerations including the fact that the number of immunosuppressed individuals is growing, the next generation of vaccines is asking for a candidate, which is replication-defective in human cells and qualified for expressing recombinant antigens of interest. To address this demand, the attenuated VACV strain–MVA was developed and profoundly investigated by the German scientist Professor Anton Mayr.³²

After more than 570 tissue culture passages in chicken embryo fibroblasts (CEF), 15% of the VACV genome including host range genes was removed in MVA.³³ MVA replication is non-permissive in human cells due to a blockage in viral replication, which occurs late at the stage of virus assembly.³⁴ Because of the high safety record, strong immunogenicity, as well as the large packaging capacity, MVA is designed as a prevaccine at the end of the small pox eradication campaign, and is considered as one of the prospective vaccine candidates against Hepatitis B virus (HBV) or Human Immunodeficiency Virus (HIV),

or for the immunotherapy of malignant diseases.^{31,35}

1.2.2 The life cycle of VACV/MVA

As illustrated in Fig. 4, the replication cycle of VACV has been well studied and two distinct entry forms have been characterized: 1) the intracellular matured virions (IMV) which bind to the cell surface and subsequently fuse with the cell membrane; 2) the extracellular enveloped virions (EEV) which enter the cell by endocytosis that lose the extra outer membrane in the low pH condition to expose the IMV.³⁶ Once the viral and host membranes fuse with each other, the viral core is released into the cytoplasm to start the early mRNA transcription, leading to the expression of a variety of proteins including DNA polymerases, intermediate transcription factors, and RNA polymerases, which are required for the subsequent cascade of gene replication. After that, uncoating of the virus core enables the viral DNA replication and the subsequent waves of intermediate and late gene transcription. Unlike the early mRNA transcription which is strictly controlled by the viral transcriptional factors, intermediate and late gene expression require additional host-derived transcription factors to accelerate gene expression, indicating that viruses hijack the host cellular machinery to serve for its own replication cycle. As a specialty of VACV, viral DNA replication occurs outside of the nuclei, in an organelle named “viral factory”. It is a discrete cytoplasmic structure that forms during the intermediate and late gene transcription, and it is also the place where the early VACV proteins accumulate. This distinct cellular compartment is investigated in many studies as it is speculated to have close relation with the host cellular organelles and components, such as the ER^{37, 38} and vimentin intermediate filaments (IFs)³⁹. The IMV assemble in viral factory and subsequently migrate via microtubule mediated trafficking and wrapping with Golgi-derived membranes to form intracellular enveloped viruses (IEV). The IEV are further transported to the cell periphery on microtubules where they fuse with the plasma membrane to form cell-associated enveloped (CEV), which are later on released directly as free EEV particles.⁴⁰

Further studies by Meyer *et al.* revealed that six major deletions reduced the size of the entire genome in VACV wild-type-strain chorioallantois vaccinia virus Ankara (CVA) to 177 kb for the MVA strain. The elimination of host range genes such as K1L or C7L results in the lack of late gene expression in several MVA infected human and murine cell

lines, indicating that the two genes are essential for completing the MVA life cycle.^{33, 41} Furthermore, recent research indicates that deletion of interferon resistance gene E3L inhibits MVA antigen production in HeLa cells at the late gene expression level, suggesting that E3L can prevent activation of additional host factors which affect the completion of the MVA molecular life cycle.⁴² To date, only a small portion of host range genes in VACV/MVA have been characterized and a large number of unknown mechanisms underlying the host-virus interaction needs to be identified.

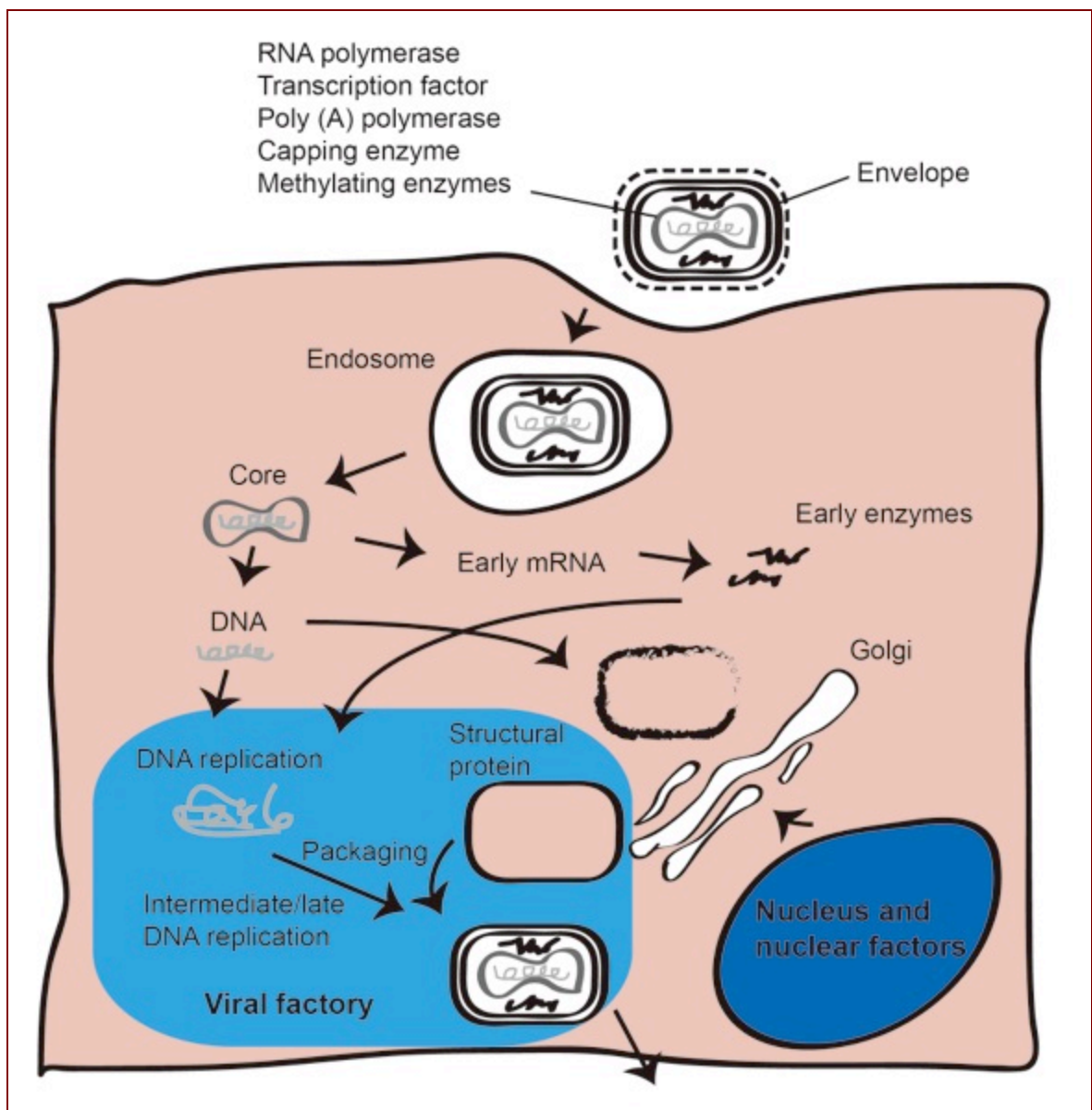


Figure 4. Infectious cycle of VACV in permissive cells

The infectious cycle of VACV is constituted of virion entry, early transcription, DNA replication, virus assembly and egress. When VACV enters a permissive cell, the viral core is released into the cytoplasm. The early mRNA is produced inside the core and subsequently released and then used

to generate early enzymes, which serve for viral DNA replication. The DNA replication cascade lasts around 2 to 12h to allow the expression of late genes that are required for virion assembly. Newly synthesized DNA and viral components are then recruited to the viral factory to be packaged into virions and wrapped into enveloped virus.

1.2.3 Innate anti-viral responses after poxvirus infection

Techniques of genetic engineering now enable researchers to reduce the virulence of poxviruses in order to generate safer and optimized vaccines that can stimulate the immune response. On the other side, the host immune response also attempts to control the viral spread by introducing characteristic cellular changes such as apoptosis and necrosis. Therefore, it is important to understand these intracellular events that restrict viral infection in order to design an effective vaccine with the capability to strengthen the anti-viral defense. Based on the efforts of several research groups, it is now believed that binding and entry of poxviruses into mammalian cells is an efficient process, and that any restriction events which limit the viral replication, e.g. in non-permissive cells like human DCs or for replication-deficient viral strains such as MVA will occur after the virus has entered the host cell.^{43,44} Once the virus core is released into the cytoplasm, the battle between virus and host starts. Though the mechanisms have not been completely elucidated, four categories of restriction points in cells regulating the poxvirus infection have been proposed. The first event is control of the cell cycle in infected cells. It was reported that deletion of the growth factor genes in VACV results in attenuation in infected animals, suggesting that the viruses encode growth factors to stimulate quiescent cells so that the viral replication levels in these infected or the neighboring cells are increased.⁴⁵ MVA infection in HeLa cells was demonstrated to upregulate the gene encoding interleukin 1A (IL-1A) and to stimulate the expression of nuclear factor kappa B (NF- κ B) components, which are involved in host resistance.⁴⁶ Secondly, different cell types restrict virus replication to be abolished at different stages. Human DCs are not permissive for the replications of both VACV and MVA,³⁴ that the infection was abortive after early gene expression,¹⁶ whereas late viral products are detected in MVA infected murine myeloid DCs (Thiele and Zhang, unpublished data). The third category includes the complementing factors from host cells such as trans-acting transcription factors. The virus usurps these factors to complete the viral activities, like core uncoating, intermediate and late gene transcription, protein synthesis and virion trafficking. For example, the chaperon

protein–heat shock protein 90 (Hsp90) that assists proteins to fold properly and stabilizes protein structures was shown to modulate VACV replication by interacting with the viral core protein 4a.⁴⁷ The fourth intracellular event comprises the signal transduction pathways (e.g. interferon (IFN) pathway, Toll-like receptor (TLR) pathways and NF- κ B signaling pathway) that respond to viral infection and are critical for the anti-viral defense. Of these, the best-studied pathway may be the IFN-mediated antiviral state. Since host and virus have exerted powerful selective pressure on each other, almost all viruses have evolved defense mechanisms to avoid recognition by the host immune system. In line with this, García-Arriaza *et al.* deleted VACV genes (C6L and K7R), which encode inhibitors of the IFN pathway, to improve adaptive and memory immune responses of a MVA based HIV vaccine.⁴⁸ Up to date, the knowledge of which regulatory factors control the intracellular steps that determine a given poxvirus infection to be permissive or restrictive is still growing.

1.2.4 Adaptive immunity against MVA infection

It has been well characterized that the primary target of MVA infection *in vivo* are APCs, such as DCs, and macrophages.⁴⁹ In MVA infected peripheral blood mononuclear cells (PBMCs), it was also shown that CD8⁺ T cell epitopes are dominant in early, and non-structural viral genes and transcription factors, while CD4⁺ T cell epitopes are concentrated in late, viral structural proteins and enzymes involved in viral replication.⁵⁰ This evidence suggests that the adaptive immunity has developed clear labor division to respond to the different levels of viral invasion.

One major aim in vaccination and immunotherapy is the induction of strong CTL activation in APCs directly against the viral or tumor antigens respectively. With the purpose to improve CD8⁺ T cells responses as one potential strategy to optimize the vaccine, it has been investigated how processing and MHC I restricted presentation of antigenic peptides can be enhanced (PhD Thesis of Dr. Georg Gasteiger, The Role of Antigen Presentation and Immunodominance for the Induction and Expansion of Cytotoxic T cell Responses with MVA Vector Vaccines, <http://mediatum.ub.tum.de/node?id=647691>). It has been demonstrated that cross-priming can dominate the induction of CTL responses to a virus that efficiently infects DCs and allows strong antigen-presentation by the APCs.¹⁷

On the other hand, infection of CD4⁺ T cell deficient mice resulted in delayed viral clearance, increased mortality and failure to develop virus-specific antibody responses, suggesting that CD4⁺ T cells are essential for the maintenance and recall of CTL responses.³⁰ The CD4⁺ T cells can also elicit a protective antibody response to some VACV proteins (e.g. A27L, B5R) that are known to be strongly targeted by humoral and cellular responses upon VACV vaccination.⁵¹ Recently, Sette *et al.* have reported that the antibody response to each particular protein target needs to be accompanied by a matched CD4⁺ T cells response.⁵² Although covalent linkage of the B cell-T cell epitopes is not necessary for the generation of antibodies in all cases, it seems required for a large virus like VACV. Therefore, the induction of efficient CD4⁺ T cell responses is becoming a hot spot in the development of potent candidate vaccines.

To sum up, replication-deficient MVA preferentially targets APCs and can stimulate strong CTL responses by direct as well as cross presentation especially in DCs. This attenuated virus strain has low virulence and high expression levels of foreign fusion proteins, which makes it an ideal vector for both prophylactic and therapeutic vaccination. However, the requirements for efficient induction and activation of CD4⁺ T cells needs to be further characterized.

1.3 Autophagy and its role in antigen presentation

1.3.1 Functional autophagy is constituted of autophagosome formation and autophagic flux

Autophagy is an evolutionary ancient cellular system for cell survival that reacts to a variety of stresses, including bacteria and virus infection, as well as starvation. By developing an intracellular bulk pathway, autophagy delivers cytoplasmic materials to lysosomes to be degraded, thus providing energy for cell metabolism or eliminating pathogens by lysosomal lysis. This process starts with the generation of a double-membrane organelle termed “autophagosome”, which engulfs the surrounding proteins and organelles, and undergoes maturation by emerging with the lysosome to form the “autolysosome” that can share the acidic environment and lysosomal enzymes for degradation of inner cargo. This multi-step dynamic process is called “autophagic flux”. Together with autophagosome initiation, it represents the function of autophagy.

Autophagy is classified as macroautophagy, microautophagy and chaperone-mediated autophagy, out of which the most extensively studied class is macroautophagy.⁵³ Microautophagy is a mechanism for invagination, protrusion and septation part of lysosomal membrane to uptake the cytosolic material. Chaperone-mediated autophagy involves the direct translocation of cytosolic proteins across lysosomal membranes for rapid degradation, which requires selective proteins to be recognized by chaperone proteins.⁵⁴ This thesis will mainly focus on the macroautophagy (simply referred as autophagy hereafter).

As depicted in Fig. 5, autophagy is a highly regulated process that comprises several stages. Briefly, the first autophagic regulatory process involves the de-repression of the mammalian target of rapamycin (mTOR) Serine/Threonine (Ser/Thr) kinase, which inhibits autophagy by phosphorylating autophagy related gene-encoded protein (Atg)-13 (Atg13).⁵⁵ When mTOR is downregulated, the re-association of de-phosphorylated Atg13 with Atg1 stimulates its catalytic activity and initiates autophagosome formation. Among the first step, Beclin-1 (the mammalian orthologue of Atg6) plays an important role in forming a complex with phosphoinositide-3 kinase class III (PIK3C3). For incorporation into this complex, Beclin-1 has to dissociate with anti-apoptotic Bcl-2 and Bcl-xL, which

anchor Beclin-1 at the ER membrane. There is evidence showing that Bcl-2 by binding with Beclin-1 interferes with the interaction of Beclin-1 and PIK3C3, which functions as a brake of autophagy and autophagic cell death.⁵⁶ Additionally, autophagy maturation is also enhanced by association of the Beclin-1-PIK3C3 complex with UV irradiation resistance-associated gene (UVRAG).⁵⁷ Two ubiquitin-like conjugation systems constitute the autophagosome elongation process. In both pathways, E1-like enzyme Atg7 essentially contributes to the complex conjugation, especially the phosphatidylethanolamine (PE) to microtubule-associated protein light chain 3 (LC3, mammalian homologue of Atg8), which leads to the turnover from the cytosolic form LC3-I to the autophagic-associated form LC3-II. When the autolysosome has emerged, LC3-II on the inner membrane as well as the luminal contents of autophagic vacuoles are consequently degraded within this acidic compartment.⁵⁵

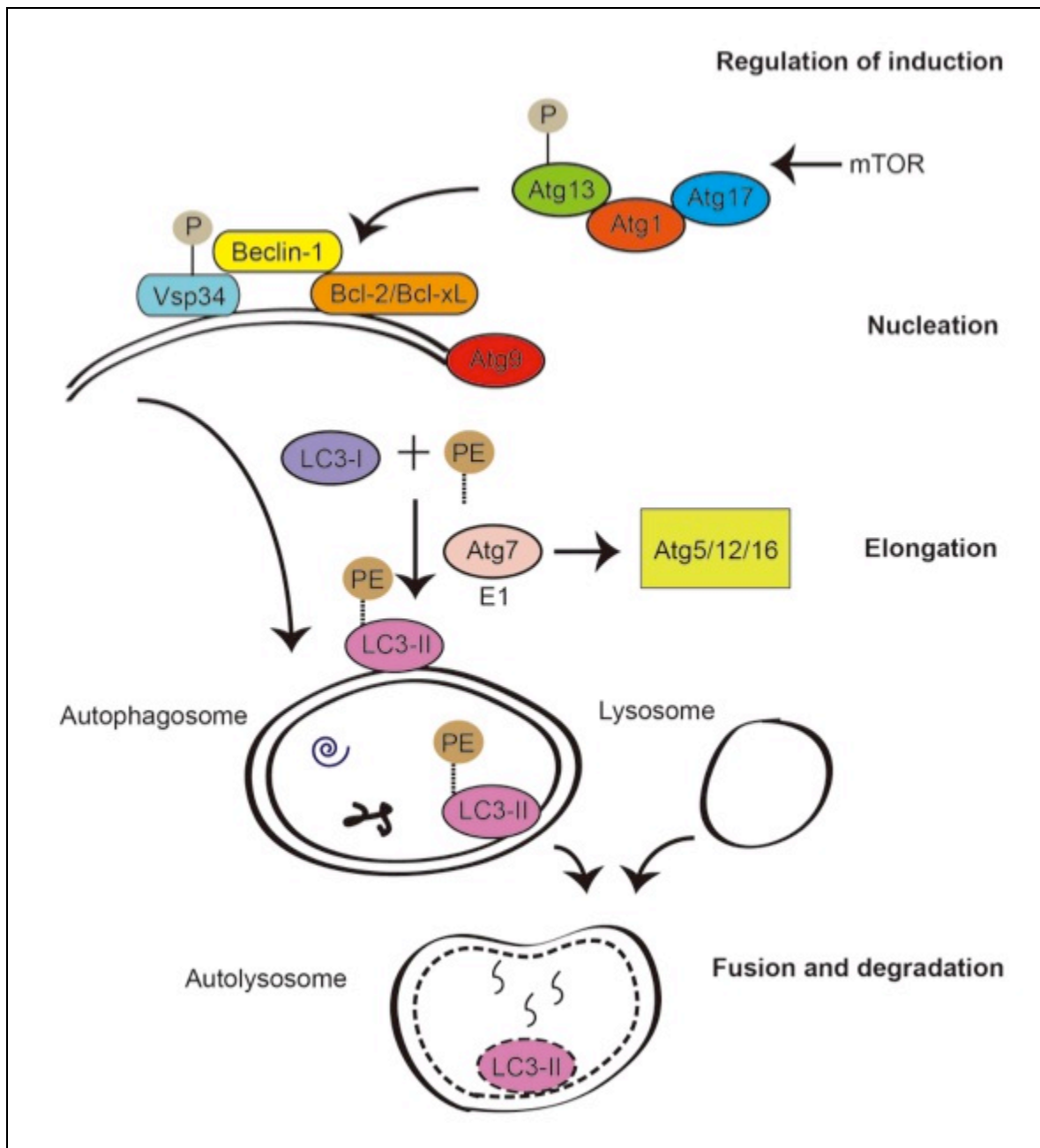


Figure 5. Biogenesis of autophagy and its inhibitors

Biogenesis of autophagy is evolutionarily conserved and involves the following stages: 1) regulation of induction, 2) nucleation, 3) elongation, 4) fusion and degradation. The initiation of autophagy starts with regulation of the mammalian target of rapamycin (mTOR) Serine/Threonine (Ser/Thr) kinase, which is an inhibitor of autophagy by phosphorylating autophagy protein-13 (Atg13). Once mTOR is de-repressed, Atg13 re-associates with Atg1 kinase and Atg17 that triggers the Atg1 kinase activity and induces autophagy vesicle nucleation. The second step is to activate the lipid kinase of the class III phosphatidylinositol-3(PI3K)-Vps 34, which forms a complex with Beclin-1 (the mammalian orthologue of yeast Atg6) and subsequently integrates upstream signals to induce the downstream Atg conjugation cascade. Two ubiquitin-like conjugation systems are part of the vesicle elongation process. One involves the association of the Atg5-Atg12 conjugate with Atg16. This Atg 5/12/16 complex with the help of E1-like enzyme Atg7, further facilitates the second conjugation of phosphatidylethanolamine (PE) to LC3-I (mammalian paralogue of Atg8). The lipidation of LC3-I functions together with other factors

(such as Atg9) to assemble the phagophore, elongate the membrane of the autophagosome and lead to the fusion with the lysosome. The autophagosome fuses with the lysosome to generate the autolysosome, where the inner membrane as well as the inside contents are degraded by lysosomal enzymes which are active in this acidic compartment. Red blocking arrows indicate the inhibitors of autophagy. Bcl2 and Bcl-xL are regulators of Beclin-1.

1.3.2 Autophagy contributes to innate and adaptive immunity

Autophagy ingests intracellular microorganisms into autophagosomes and subsequently delivers these pathogens to lysosomes for hydrolysis, suggesting a direct antimicrobial function of autophagy. It is suggested that autophagy provides a series of barriers against the invasion of viruses and bacteria.⁵⁸ Except for degradation of engulfed pathogens in the autolysosome, the LC3-associated phagocytosis involves the engagement of the autophagic machinery while the bacterium is captured by phagosomes. Evidence showed that LC3 and Beclin-1 were recruited to the phagosomes, facilitating phagosomes fusion with the lysosome, thus allowing a rapid acidification and enhanced killing of the ingested organism.⁵⁹ Furthermore, a group of autophagic adaptors, known as sequestosome 1-like receptors (SLRs), can recognize molecular tags (such as ubiquitin) present on invading pathogens or damaged host components that activate autophagy in order to restrict the proliferation of bacteria.⁶⁰

To initiate autophagy, mammalian cells detect the presence, location and extent of the pathogen invasion. Different pattern recognition receptor (PRR) families identify distinct pathogen-associated molecular patterns (PAMPs) on the cell surface and intracellularly.⁵⁷ Toll-like receptors (TLRs) represent a conserved family of innate immune recognition receptors that play key roles in the recognition of PAMPs leading to the induction of innate and adaptive immune responses.⁶¹ They are critical PRRs that are in charge of recognizing both extracellular pathogen products (such as LPS and lipopeptide recognized by TLR4, 2 and 6 respectively) and endosomal dangerous molecules (such as single-stranded DNA, single-stranded RNA and double-stranded RNA recognized by TLR9, 7, 8 and 3 respectively). Delgado *et al.* have found out that ssRNA induces the autophagy in a Beclin-1-dependent manner, which functionally eliminates the intracellular pathogens via myeloid differentiation factor 88 (MyD88).⁶² In return, it was also shown that autophagy transports Sendai and Vesicular stomatitis virus replication intermediates to TLR7/8 that is required for IFN- α production by DCs in response to these viral infections.⁶³ Furthermore, Shi and

colleagues have demonstrated TLR signaling pathways enhance autophagy via the adapter proteins MyD88 and Toll-IL-1 receptor (TIR)-domain-containing adapter-inducing interferon- β (TRIF).^{56, 64} These evidences indicate a close link between the TLR signaling pathway and the autophagic system, revealing that TLRs and autophagy influence each other, thereby amplifying the outputs of both systems in response to pathogen invasion.

The function of autophagy is not only confined in direct elimination of microorganisms, it is also called a bulk “topological inverter” by transporting proteins from the cytoplasm into antigen-processing compartments.⁵⁸ Since the autophagosome contains a double membrane and internal membrane sheets, MHC II was observed to obtain a typical multilaminar morphology by fusion with the autophagosome under the electron microscope.⁶⁵ As a byproduct of this, MHC II received more peptides from hydrolysis in autolysosome degradation. Accordingly, antigen processing for MHC II presentation to CD4⁺ helper T cells is benefited. Lee *et al.* showed that Atg5 deficiency in DCs compromised the development of CD4⁺ T cells responses upon herpes simplex virus (HSV) infection of mice.⁶⁶

In summary, autophagy influences innate and adaptive immune responses through its effects on eating-and-killing the microorganisms, TLR mediated cytokine secretion, antigen presentation, CD4⁺ T cell stimulation as well as some other functions that are too extensive to be covered in this introduction.

2. Aims of the study

Using the attenuated VACV strain MVA, it was demonstrated that primary CTL responses against VACV-derived antigens were dominated by cross-priming *in vivo*, while infected DCs failed to induce primary CTLs. Recently, our group discovered that inhibition of autophagy by chemical inhibitors leads to decreased specific CD4⁺ T cell responses against endogenous MVA antigen. Though it has not yet been proven that these MHC II ligands are generated from autophagy substrates, at least this result suggests that autophagy facilitates the presentation process of these. Given that MVA-infected DCs are prone to apoptosis quite fast and that the endocytic ability of infected DCs is significantly impaired, the endogenous antigen presentation through autophagy seems able to reconstitute the loss of exogenously acquired MHC class II antigens to some extent. Especially in DCs, where the endocytic system seem to be leaky and releases exogenous antigen for cross-presentation on MHC I, autophagic re-transfer of these cytoplasmic antigens that have escaped from endosomes back to its original destinations seems very likely. Finally, TLRs have been shown to play an important role in the sensing of MVA. The TLR2-TLR6-MyD88, MDA-5-IPS-1 and NALP3 inflammasome pathway has been described as one of the main innate sensors of MVA in bone marrow derived macrophages (BMDMs) and bone marrow derived dendritic cells (BMDCs).⁶⁷ Therefore, the induction of the TLR signaling might stimulate downstream autophagy, resulting in a cooperation of both sensing and effector system in the responses to the viral infection.

To prove this hypothesis, the central objective of this thesis was to investigate and characterize the cellular events and the underlying molecular mechanisms that control and shape the MHC II restricted endogenous antigen presentation pathway in professional APCs and cell lines during acute MVA infection. To address this aim, the experimental work consists of the following three parts:

A. Monitor the change of autophagy behavior during MVA infection.

- 1) Determine if the autophagy system contributes to the delivery of endogenous viral antigens into endocytic compartments for peptide-MHC II complex formation and presentation.

2) Include of fluorescently labelled recombinant MVA expressing MHC II model antigens (e.g. MVA-mRFP-HEL).

3) Investigate of the intracellular trafficking of HEL-MHC II complex in DCs and characterization of the activation of CD4⁺ T cell populations by BMDCs upon MVA-mRFP-HEL infection to verify the endogenous presentation pathway.

B. Investigate the influence of the TLR signaling pathway on the autophagic system upon MVA infection.

1) Analyse of the protein expression levels of autophagy associated gene products (e.g. Beclin-1 and LC3-I/II) and TLR adaptors (e.g. MyD88) in the steady state condition, upon viral infection and after amino acids starvation.

2) Investigate the interactions between these proteins and their influence on autophagy function.

C. Determine the spatiotemporal pattern of viral antigen expression and localization/redistribution of structural or non-structural viral gene products in cellular compartments during the course of infection. The main focus here is to analyse the co-localization of the viral factory with cellular organelles as well as the cell skeleton.

3. Material and Methods

3.1 Materials

For detailed information on equipment, consumable items and reagents as well as kits and enzymes please refer to the lists provided in Chapter 8. Appendix.

3.1.1 Plasmids

The plasmids listed in Table 1 were either commercially available or kind gifts.

Table 1. Plasmids for immunofluorescence (IF) and immunoprecipitation (IP)

Name	Description	Source
ptfLC3	mRFP-EGFP-LC3	Addgene, #21074
pEGFP-LC3	EGFP-LC3	Addgene, #21073
pmRFP-LC3	mRFP-LC3	Addgene, #21075
pcDNA4-Beclin 1-HA	HA-tagged Beclin 1	Addgene, #24399
Flag-MyD88	Flag-tagged MyD88	Gift from Dr. Katharina Eisenächer

3.1.2 Antibodies

Table 2. Primary antibodies for immunofluorescence (IF), immunoblotting (IB) and immunoprecipitation (IP) and flow chemistry

Antigens	Species	Working concentration/dilution	Source, catalog Nr.
H3L	rabbit	1:100	Genesis, GB 10432
GFP	goat	1:400	Abcam, ab6673

GOLPH4	rabbit	1:400	Abcam, ab28049
EEA1	rabbit	2.5 µg/ml	Abcam, ab50313
HLA-DM	rabbit	1:400	Abnova, H00003108-D01
LC3B	rabbit	1:200/1:1000*	Sigma, L7543
MHC II (I A-b,d,q and I E- d, k)	mouse	1:600	eBioscience, 14-5321
ER (Anti-Calnexin)	rabbit	1:300	Sigma, C4731
LAMP-2	rabbit	1:400	Abcam, ab37024
MHC II (I A-k,s)	mouse	1:200	BD, 554926
C4H3	rat	1:4**/1:200	NIH or self-made
Beclin-1	rabbit	1:100***/1:1000*	Cell signaling, 3738
MyD88	rabbit	1:100***/1:1000*	Abcam, ab2064
Flag (clone M2)	mouse	1:1000	Sigma, F3165
HA (clone 3F10)	rat	1:100***/1:2000*	Roche, 11867431001
β-actin	rabbit	1:5000	Abcam, ab8227
CD16/CD32	rat	1:100	BD, 553142
Biotynilated Aw3.18	–	–	Provided by Dr. Jacob Loschoko

*: for IB; ** hybridoma supernatant; ***: for IP

The purified C4H3 antibodies and hybridoma was kindly provided by Dr. Ronald N Germain from the National Institutes of Health (NIH), Bethesda, USA.

Table 3. Secondary antibodies for IF, IB, IP, flow chemistry and dye for live imaging

Specificity	Species	Dilution	Source, catalog Nr.
Alexa Fluor® 594 anti-rabbit	chicken	1:800	Invitrogen A-21442
647 anti-rat	chicken	1:800	Invitrogen A-21472
Alexa Fluor® 488 anti-goat	donkey	1:800	Invitrogen A-11055
PE anti-mouse	goat	1:200	Jackson research, 115-116-071
Anti-rabbit	goat	1:7500	Jackson research, 110-035-144
Alexa Fluor® 647 anti-mouse	goat	1:800	Abcam, ab150115
Alexa Fluor® 488 anti-rat	goat	1:800	Abcam, ab 150157
Biotin anti-Aw3.18	–	1:100	Provided by Dr. Jacob Loschko

3.1.3 Cells, viruses and mice

3.1.3.1 Cells

Cells listed in Table 4 were commercially obtained or from our lab storage.

Table 4. Cell lines and primary cells

Name	Description	Source, Catalog Nr.
HeLa	Human epithelioid carcinoma, cervix	ATCC CCL-2

DC 2.4	Murine dendritic cell line	Gift from Dr. KL Rock
NIH 3T3	Murine fibroblasts	CRL-1658
HaCaT	Human keratinocytes	CLS #300493
C4H3	Hybridoma (producing rat IgG2b mAb specific for the HEL 46-61 peptide in the context of I-A ^k)	Dr. Ronald N Germain (NIH)
B16-F10	Granulocyte macrophage colony-stimulating factor (GM-CSF) transduced murine melanoma cells	Lab storage
CEF	Primary chicken embryo fibroblasts	SPF eggs freshly prepared
BMDCs	Primary murine bone marrow derived dendritic cells	Femurs and tibias from SPF mice

3.1.3.2 Viruses

Table 5. Index of viruses

Name	Description
MVA-EGFP P7.5	Recombinant MVA expressing EGFP under the control of vaccinia virus promoter P7.5
MVA-EGFP P11	Recombinant MVA expressing EGFP under the control of vaccinia virus promoter P11
MVA-EGFP PK1L	Recombinant MVA expressing EGFP under the control of vaccinia virus promoter PK1L
MVA-mCherry PK1L	Recombinant MVA expressing mCherry under the control of vaccinia virus promoter PK1L

MVA-II_{new}	Wild type MVA
MVA-OVA P7.5	Recombinant MVA expressing ovalbumin
MVA-HEL P7.5	Recombinant MVA expressing hen egg lysozyme
MVA-HEL-RFP P7.5	Recombinant MVA expressing hen egg lysozyme with red fluorescence protein (RFP)
Vaccinia virus (western reserve strain)	Wild-type vaccinia virus

3.1.3.3 Mice

Table 6. Index of mouse strains

Name	Description	Source
C57BL/6	H2 ^b	Charles River
Balb/c	H2 ^d	Charles River
C3H	H2 ^k	Charles River
MyD88^{-/-}	H2 ^b (originated from C57BL/6)	Kind gift from Dr. Dirk Busch
Atg7 loxP/loxP CD11c x Cre^{+/-} heterozygous	H2 ^b (originated from C57BL/6)	Kind gift from Dr. Frank Thiele
TLR7^{-/-}	H2 ^b (originated from C57BL/6)	Kind gift from Dr. Percy Knolle
TLR9^{-/-}	H2 ^b (originated from C57BL/6)	Kind gift from Dr. Percy Knolle

MyD88^{-/-} and Atg7 loxP/loxP CD11c x Cre^{+/-} heterozygous mice were used on a C57BL/6 genetic background. Mice were kept under specific pathogen-free conditions in the animal facility of the Klinikum rechts der Isar at the Technical University Munich and Helmholtz

Zentrum Munich. Experiments are performed in accordance with the German animal care and ethics legislation and approved by the local government authorities.

3.1.4 Buffers, solutions and media

3.1.4.1 Media for cell culture

If not mentioned, otherwise a general growth medium was used to culture most cell lines.

Table 7. Cell culture media

Name of cell line	Medium composition
C4H3	500 ml DMEM (PAA, # E15-810) 10% (v/v) Fetal bovine serum (FBS, GIBCO, # 10500-064) 1% (v/v) Penicillin/Streptomycin (GIBCO, # 15140-122) 1% (v/v) N-2-Hydroxyethylpiperazine-N-2-Ethane Sulfonic Acid (HEPES, GIBCO, # 15630-056) 1% (v/v) Sodium pyruvate (PAA, # S11-003) 1% (v/v) Non-essential amino acids (PAA, # M11-003) 0.1% (v/v) β -mercaptoethanol (50mM pre-prepared stock, Sigma, # M3148) 2% (v/v) Zap-Hybridoma (InVitria, # 7772AP003)
Primary dermal fibroblasts	500 ml DMEM (PAA, E15-810) 10% Fetal bovine serum (FBS, GIBCO, # 10500-064) 1% (v/v) Penicillin/Streptomycin (GIBCO, # 15140-122)
BMDCs	500 ml RPMI (Lonza, # BE12-702F) 10% Fetal bovine serum (FBS, GIBCO, # 10500-064) 1% (v/v) Penicillin/Streptomycin (GIBCO, # 15140-122) 10% GM-CSF (self-made from B16-F10 hybridoma cell line)

General	500 ml RPMI (Lonza, # BE12-702F) 10% Fetal bovine serum (FBS, GIBCO, # 10500-064) 1% (v/v) Penicillin/Streptomycin (GIBCO, # 15140-122)
Freezing medium	70% complete culture medium of the respective cell line 20% FCS Fetal bovine serum (FBS, GIBCO, # 10500-064) 10% DMSO (Sigma, # D2650)

3.1.4.2 Solutions for cell culture applications

Table 8. Solutions for cell culture application

Name	Composition
Trypan blue	0.2% (m/v) Trypan blue (Fluka, # 23850) dissolved in PBS
Trypsin	0.05% trypsin/0.025% EDTA solution (Sigma, # 59417C)
TAC buffer	90% (v/v) NH ₄ Cl from 0.16 M stock 10% (v/v) Tris pH 7.65 from 0.17M stock
Collagenase solution	3mg/ml Collagenase (Worthington, Lakewood, NJ, # CLS 4) 1 mM CaCl ₂ 1 mM MgCl ₂ 5 µg/ml DNase I (Sigma, # DN-25)

3.1.4.3 Buffers for IF

Table 9. Buffers used for IF

Name	Composition and preparation
10x phosphate buffered saline (10x PBS)	<p>1.37 M Sodium chloride (NaCl from Merck, # 1.06404.5000)</p> <p>27 mM Potassium chloride (KCl from Sigma, # 7447-40-7)</p> <p>100 mM Sodium phosphate, dibasic (Na₂HPO₄ from Fluka, # 71650)</p> <p>18 mM Potassium phosphate, monobasic (K₂HPO₄, Sigma, # P5379)</p> <p>Reagents were dissolved in 800 ml of double distilled water (ddH₂O). pH was adjusted to 7.4 with hydrochloric acid or sodium hydroxide if necessary, and then ddH₂O was added to 1 l 10x PBS buffer was sterilized by autoclaving before stored at room temperature (RT). 1x PBS (PBS) was diluted with ddH₂O before use.</p>
Fixation buffer	<p>2% (w/v) Formaldehyde powder (Fluka, # 76240) was diluted in 1x PBS. Solution was heated up to 70 °C, allowing the paraformaldehyde completely dissolve. Buffer was stored at 4 °C in the dark.</p>
5% (w/v) Saponin	<p>Saponin (Sigma, # S-2149) was gently vortexed to be dissolved in ddH₂O and then stored at 4 °C in the dark.</p>
Blocking/permeabilization buffer:	<p>5% (v/v) Normal goat serum (Thermo scientific, #31873)</p> <p>0.1% (v/v) Saponin (Sigma, # S-2149)</p> <p>100% normal goat serum (Thermo scientific, 31873) and 5% saponin solution were diluted in PBS to the final concentration.</p>
Antibody dilution buffer	<p>1% (v/v) Normal goat serum (Thermo scientific, 31873)</p> <p>0.1% Saponin (Sigma, # S-2149)</p> <p>100% normal goat serum (Thermo scientific, # 31873) and 5% saponin solution were diluted in PBS to the final concentration</p>

3.1.4.4 Buffers and solutions for protein biochemistry

Table 10. Buffers and solutions used for protein biochemistry

Name	Composition and preparation
10 % APS	10 % (w/v) Ammonium persulphate (GE Health, # 17-1311-01) in ddH ₂ O
	10% (v/v) Glycerol (Sigma, # 49782-1L)
	20mM Tris-HCl pH7
	137mM NaCl (Merck, # 1.06404.5000)
	2mM EDTA (Sigma, # E5134-500G)
Lysis buffer	0.5% (v/v) Triton X-100 (Sigma, # 9002-93-1) in ddH ₂ O the following supplements were added freshly prior to use: 1 tablet of Mini complete protease inhibitor (Roche, # 11836153001) 1 tablet PhosSTOP phosphatase inhibitor (Roche, # 04906845001)
2 x Laemmli sample buffer	95 % (v/v) Bio-rad commercial product # 161-0737 5% (v/v) β-mercaptoethanol (Sigma, #M6250)
	60 mM Tris-HCl pH 6.8
	2% (w/v) Sodium dodecyl sulfate (SDS from Merck, # 8.2250.1000)
5 x Laemmli sample buffer	10% (v/v) Glycerol (Sigma, # 49782-1L) 5% (v/v) β-mercaptoethanol (Sigma, #M6250) 1% (w/v) Bromophenol blue (Sigma, # 263-653-2) in ddH ₂ O

10x PAGE buffer	<p>250 mM Tris-base (Merck, # 1.08382.2500)</p> <p>1.9 M Glycin (Sigma, #G8898-1KG)</p> <p>171 mM SDS (Merck, # 8.2250.1000)</p> <p>in ddH₂O</p> <p>Concentrated buffer was diluted with ddH₂O to 1x running buffer before use</p>
10x transfer buffer	<p>250 mM Tris-base (Merck, # 1.08382.2500)</p> <p>1.9 M Glycin (Sigma, #G8898-1KG)</p> <p>in ddH₂O</p>
1x transfer buffer	<p>10% (v/v) 10x transfer buffer</p> <p>20% (v/v) Ethanol absolute (EtOH, Merck, # 1.00983.2500)</p> <p>in ddH₂O</p>
10x Tris-buffered saline (10x TBST)	<p>0.1% (v/v) Tween-20 (GE Health # 17-13160-01)</p> <p>0.2 M Tris-base (Merck, # 1.08382.2500)</p> <p>1.5 M NaCl (Merck, # 1.06404.5000)</p> <p>in ddH₂O</p> <p>The 10x buffer was diluted with ddH₂O to 1x running buffer before use</p>
Blocking buffer	<p>5% (w/v) Bovine serum albumin (BSA from Biomol, Hamburg, # 67000.00) or skim milk powder (Fluka, # 70166-500G) in 1x TBST</p>

3.1.4.5 Buffers for Flow Activated Cell Sorting (FACS)

Table 11. Buffers for FACS analysis

Name	Composition
-------------	--------------------

FACS buffer	1% BSA (w/v) 0.02% NaN ₃ from 20% stock (w/v) in 1x PBS
Blocking buffer	1% (v/v) Fc block antibodies (anti-CD16/CD32) 0.1% (v/v) Ethidium monoazide (EMA) in FACS buffer
Fixation buffer	2% (w/v) Formaldehyde powder (Fluka, # 76240) in 1x PBS

3.2 Methods

3.2.1 Tissue culture

3.2.1.1 Cell lines

In general, all cell cultures were maintained at 37 °C in a humidified incubator with 5% CO₂ atmosphere using the media listed in Table 6, respectively. Cells were split every 3 to 5 days in a ratio ranging from 1:3 to 1:10 depending on the respective cell line. To passage cell lines that possess adherent growth properties, the medium was discarded, cells were washed with 1x PBS and subsequently detached from the culture surface by incubation with 1x trypsin/EDTA solution for 1 to 2 min at 37 °C. To inactivate the trypsin, cells were resuspended in the respective medium and plated at an appropriate density in new tissue culture ware.

In case of HaCaT cells, the culture medium was removed and cells were rinsed with 0.05% EDTA and incubated with 0.05% EDTA solution for 10 min at 37 °C. Thereafter, EDTA was replaced by 1x trypsin/EDTA solution until the cells started to detach. And then, cells were processed as described above for adherent cells.

To produce murine granulocyte macrophage colony-stimulating factor (mGM-CSF), the supernatant of the mGM-CSF secreting stably transfected murine melanoma cell line B16-F10 was harvested. Therefore, freshly thawed B16-F10 cells were cultured in a

T185 flask for one week before starting to collect the supernatant. Cells that reached 90% confluence were split every 3 days at ratio of 1:20 until 10 T185 flasks were seeded with cells. Supernatant was separately harvested on day 3, 4, 5, 6 post seeding, stored separately and then sterile filtrated through a 0.22 μm filter. Before aliquoting, the supernatants were first tested on chocolate agar plate for bacterial contamination. If uncontaminated, supernatants were further tested for the efficiency to generate BMDCs.

Cell lines were tested for mycoplasma contamination at regular intervals. Therefore, cell culture supernatant was subjected to either PCR or nucleic acid staining.

3.2.1.2 *Primary cells*

3.2.1.2.1 **Generation and culture of bone marrow derived DCs**

Bone marrow derived DCs (BMDCs) were generated from wild-type C57BL/6 mice and C3H mice or other mouse strains according to the respective experiments. Mice were euthanized by Isofluran inhalation and the body was disinfected with 70% EtOH. To obtain bone marrow cells, the femurs and tibias were removed and separated from fur and muscle tissue. Pre-cleared bones were rinsed with 70% EtOH and then immersed in fresh medium. Two edges of bones were cut open with sterilized scissors, and then the exposed bone marrow was flushed out with general medium into a 10 cm Petri dish by using a syringe with 30G needle under sterile conditions. After centrifugation at 1500 rpm at room temperature (RT) for 5 min, the cell pellet was resuspended in 3 ml TAC buffer to lyse red blood cells at 37 °C for 2 minutes. Red blood cell lysis was blocked by adding 37 ml fresh medium to the cells. Cells were filtered through a 100 μm sterile filter and centrifuged at 1500 rpm and RT for 5 min. The cell pellet was finally resuspended in fresh medium and cell numbers were determined using a hemacytometer.

5×10^6 bone marrow cells were seeded in 10 cm petri dishes in a total volume of 10 ml BMDCs medium and incubated at 37 °C for 7 days. On day 4, 10 ml fresh BMDC medium were added. On day 6, 10 ml of the cell suspension were centrifuged at 1500 rpm and RT for 5 min to remove the supernatant. Cell pellets were resuspended in 10 ml fresh BMDC medium and transferred back into the dishes.

3.2.1.2.2 **Isolation and culture of primary dermal fibroblasts**

Primary dermal fibroblasts were obtained from C57BL/6 mice. The hair on the belly and back of mice was removed by hair removal cream (Veet), and then washed away with ddH₂O. The exposed skin was air dried for 10 min at RT. Afterwards, mice were euthanized by Isofluran inhalation and the body was disinfected with 70% EtOH. The skin was dissected from the body, and then placed on the lid of a 10 cm petri dish with the epidermal side facing down by using sterile forceps. Fat and loose fascia were trimmed away by using disposable scalpels and scissors. To keep the tissue from drying, the tissue was rinsed with fresh medium every few minutes. After the trimming was complete, the tissue was cut into strips of approximately 0.5 cm x 1.5 cm and submerged into a 1.5 ml Eppendorf tube containing 700 µl collagenase solution. The tissue was completely shredded by cutting up and down using scissors, and then incubated at 37 °C for 2h for collagenase digestion.

At the end of the collagenase digestion, 10 mM EDTA was added to the tissue suspension to block the activity of Ca²⁺ and Mg²⁺. The suspension was thoroughly vortexed and then left at RT for 10 min before transferred into a 15 ml Falcon tube; 5 ml fresh medium was used to thoroughly flush the Eppendorf tube. The flushing medium was combined with the suspension afterwards. The entire mixture was filtered through a 100 µm filter. 20 ml medium was used to wash the Falcon tube again. The flushing medium together with the filtered mixture was centrifuged at 1500 rpm and RT for 5 min. The supernatant was carefully removed without touching the fat on the surface of the pellet. The wash step was repeated 1 to 2 times before the supernatant was completely clear. The cell pellet was resuspended in 5 ml fresh medium and the cell number was determined by using a hemacytometer. The cell suspension was diluted in medium to yield 8 x 10³ live cells/ cm² to be further cultured in a T 75 flask. After initial seeding of the primary culture, the medium was changed after 24 h, and then once every 48 h. Once the culture was around 90 % confluent, cells were subcultured at a ratio of 1:5 to 1:10 or cryopreserved.

3.2.1.3 Cultivation of C4H3 hybridoma and production of C4H3 antibodies

C4H3 hybridoma was shipped in freezing medium on dry ice. To take frozen cells into culture, the cryovial containing the frozen cells was removed from dry ice and immediately placed into a 37 °C water bath. Cells were quickly thawed by gently swirling the vial in the water bath. The cell suspension was then transferred into a 50ml Falcon tube

containing 10 ml of pre-cooled complete DMEM medium. Cells were centrifuged at 1500 rpm and 4 °C for 5 min. The supernatant was removed and the cell pellet was resuspended in 2 ml of fresh medium and seeded in one well of a 6-well plate. Cells were cultured at 37 °C and 5% CO₂ until the cell amount increased one fold. During log-phase growth, cells were subcultured at a ratio of 1:2 until there was enough amount to harvest the medium containing the C4H3 antibodies.

Total cell number and cell viability were determined in a hemacytometer using Trypan blue staining to discriminate live and dead cells. Cells were mixed with 0.2 % Trypan blue in PBS at a ratio of 1:1, and then the number of living (unstained) cells was counted. Afterwards, cells were seeded at a concentration of 2×10^4 cells/ml in a T75 flask and subcultured until the cells reached a density of 1×10^5 cells /ml.

Cells were seeded at a concentration of 1×10^7 cells/ml in a T25 flask for 3 to 4 days until the color of the medium turned yellow. The antibodies-containing supernatant was collected by centrifugation of the cells at 1700 rpm and 4 °C for 10 min. Prior to storage at 4 °C, the supernatant was filtered through a 0.22 µm filter.

3.2.1.4 Cryopreservation of cells

To keep a stock of cells with a low passage number, cells were frozen as permanent cultures in liquid nitrogen. Cells grown in log phase that have reached a confluence of 90 % were detached from the culture surface by either incubation with 1 x trypsin/EDTA solution (adherent cells) or flushing with culture medium (suspension cells). After counting and centrifugation at 1500 rpm and RT for 5 min, 1 to 3×10^6 cells were resuspended in 1 ml freezing medium, and then frozen down in a freezing container which provides a cooling rate of 1 °C/min for controlled cryopreservation of cells. After storing the frozen cells at -80 °C for one day, cells were transferred into liquid nitrogen for long-term storage.

3.2.1.5 Transient transfection of cell lines and BMDCs

Transient transfection of cell lines was performed using FuGENE® HD transfection reagent (Roche, #05 061 369 001) or X-tremeGene HP DNA transfection reagent (Roche, # 06366236001), together with serum-free RPMI 1640 medium. BMDCs were transfected using the Amaxa® mouse dendritic cell nucleofactor® kit (# VPA-1011) and the

respective electroporation device (Lonza, nucleofector™) according to the manufacturers instructions.

3.2.1.5.1 Transfection of cell lines

For the purpose of microscopy, 2×10^5 HeLa cells were plated in 2 ml culture medium and seeded in 35 mm dishes with glass bottom the day before transfection (to obtain about 70% confluency at the day of transfection). Transfection was carried out according to the protocol provided by the manufacturer. Briefly, FuGENE transfection reagent, DNA and diluent were adjusted to RT. DNA was diluted with serum-free medium to a concentration of 2 µg plasmid DNA/100 µl medium. 3 µl FuGENE transfection reagent or 6 µl XtremeGene transfection reagent (3:2 to 3:1 reagent to DNA ratio) was added into the medium containing DNA to form transfection complexes. The complex was vortexed for one to second seconds for mixing, and then it was incubated for 15 min at RT. Afterwards, the transfection complex was added to the cells in a drop-wise manner and then the plates were swirled to evenly distribute the transfection complexes over the entire culture plate surface. After 16 h of incubation at 37 °C and 5% CO₂ in a humidified incubator, the cells were subsequently subjected to viral infection or lysis for subsequent western blot analysis.

3.2.1.5.2 Transfection of BMDCs

On day 7, 1×10^6 immature BMDCs per sample were centrifuged at 1500 rpm and RT for 5 min. The supernatant was completely discarded so that no residual medium covered the cell pellet. The cell pellet was resuspended in 100 µl RT nucleofector solution per sample. 2 µg plasmid DNA or control vector expressing enhanced green fluorescent protein (EGFP) was added to the suspension. The cell/DNA suspension was transferred into a certified cuvette and then subjected to program Y-001 in the Nucleofector machine. 400 µl of the culture medium was added to the cuvette and then the whole mixture was transferred to the 35 mm dish with glass bottom. Afterwards, the cells were incubated in humidified incubator at 37 °C and 5% CO₂ for 16 h before they were subjected to virus infection.

3.2.2 Virological methods

3.2.2.1 *In vitro* infection of cells with MVA and VACV

For MVA and VACV infection of adherent cell lines (cells grown in log phase) and

suspension cells (e.g. BMDCs on day 7-10), desired cell populations were either detached from the culture plate by trypsin/ETDA or scraped off from the plate respectively, and then centrifuged at 1500 rpm and RT for 5 min. The supernatant was removed, only approximately 500 µl medium remained to cover the pellets. Virus (stored at -20 °C or -80 °C) was thawed at RT and sonified for 30 seconds in ice water to singularize viral particles. The desired multiplicity of infection (MOI) was added into the medium and gently mixed with the cell pellet. Cells were incubated with high concentration of virus at 37 °C for 30 min before diluted with fresh medium that cell density was adapted to a concentration of 2×10^6 cells/ml. Viral infection was carried out according to the respective experimental setup.

3.2.2.2 *Virus amplification and crude stock preparation*

For large scale MVA virus preparations primary CEFs were cultured in 10-40 T225 flasks at 37 °C. After 2-3 days, the 95 % confluent cell layer was infected at an MOI of 3 by adding the calculated volume of virus suspension diluted in 1 ml medium to each flask. CEFs were cultivated for another 2-3 days until a cytopathic effect without obvious cell death was recognizable. The cells were scraped off the plate and transferred into a 50ml Falcon tube. Cell suspension was centrifuged at 1700 rpm and 4 °C for 5 min. Cell pellets were resuspended in 4 ml of 10 mM Tris buffer (pH 9.0) and the Falcon tube was washed 2 times with 4 ml 10 mM Tris buffer (pH 9.0). Resuspended cells together with wash buffer were transferred into a fresh 50 ml Falcon tube. This crude stock virus preparation was either stored at -80 °C or further purified.

3.2.2.3 *Virus purification*

MVA crude stock preparations were purified from cellular debris and proteins by saccharose cushion ultra-centrifugation. To break down the cells and to separate virus particles, crude stock preparations were homogenized in ice water by 30 strokes in a 40-ml douncer with a pestle. Cellular debris was pelleted by centrifuging the suspension at 4000 rpm and 4 °C for 5 min. The virus containing supernatant was transferred to a fresh 50 ml Falcon tube and the pellet was resuspended in 25 ml of cold 10 mM Tris buffer (pH 9.0) and returned to the douncer. The procedure was repeated a total of three times and resulted in a maximum of 80 ml of virus suspension. Ultracentrifugation cups for the Beckman rotor SW28 were prepared with 25 ml of 36% sucrose (w/v) in 10 mM Tris buffer

(pH 9.0) and the virus suspension was carefully laid onto the cushion. Virus particles were pelleted by ultracentrifugation at 13500 rpm and 4 °C for 90 min (Optima LE 80K centrifuge, rotor: SW28). The supernatant was removed and the pellets resuspended in a maximum volume of 12 ml 1 mM Tris pH 9.0. For the second purification step, ultracentrifugation cups for Beckman rotor SW41 were prepared with 9.5 ml of sucrose 36% in 10 mM Tris buffer pH 9.0 and the purified virus suspension was again carefully laid onto the cushion. Virus particles were pelleted by ultracentrifugation for 90 min at 13.500 rpm and 4 °C (Optima LE 80K, rotor: SW41). The supernatant was removed carefully and the obtained virus pellet was resuspended in 3 to 6 ml 1 mM Tris pH 9.0 and stored at -80 °C.

3.2.2.4 Virus titration and growth kinetics

The infectivity of a MVA suspension was determined by titration and plaque formation frequency. Virus material was freeze-thawed thrice (-80° and 37° water bath) and sonicated three times for one minute in 50% ice water in a cup sonicator. The virus suspension was serially diluted in 2% RPMI medium to result in dilutions from 10^{-1} to 10^{-11} . Primary CEFs were harvested by trypsinization, split 1:10, and resuspended in a final volume of 10 ml 2% RPMI medium. 100 µl of cell suspension per well were plated into a flat bottom 96-well plate. Each time, 100 µl of the virus dilutions with different titration were added per well to a total of 16 wells/dilution. Cells were then incubated at 37 °C for 7 days, analyzed for cytopathic effect by microscopy and the virus titer was calculated based on the number of CPE per dilution.

To test whether recombinant viruses had similar growth kinetics as wild-type virus CEFs were infected at MOI 0.01 and harvested at different time points (whereas t=0 is harvested immediately to control the viral input). Titration was carried out for each time point.

3.2.3 Confocal laser scanning microscopy (CLSM)

3.2.3.1 Intracellular IF

Briefly, cells were grown on Cell ViewTM – cell culture dishes with glass bottom (Greiner Bio-one, 627975) until they reached 80% confluency before staining. Usually, BMDCs were seeded on Cell View® dishes at a concentration of $2.5 \times 10^5 / \text{cm}^2$ one day before

infection. If cells were infected in advance, virus at the indicated MOI was administered to the cells with the 200 μ l medium only covering the cell surface, to allow for virus attachment for 0.5 h. Afterwards, 300 μ l fresh medium were supplemented to optimize growth condition. To terminate the infection, the medium were decanted and cells were washed twice with ice cold 1x PBS. For fixation, cells were covered with 2% formaldehyde (200 μ l) for 15 min at RT. Afterwards, the cells were rinsed 3x in cold PBS. Specimen were permeablized and blocked for unspecific binding together in blocking buffer for 60 min at RT, followed by primary antibodies incubation overnight at 4 °C or 1h in the dark at RT. Cells were washed 3x in cold PBS for 5 min before being probed with fluorochrome-conjugated secondary antibodies diluted in antibody dilution buffer for 60 minutes at RT in the dark. Cells were gently washed again 3x in cold PBS for 5 minutes each. DAPI containing mounting medium was added to the samples. Samples were examined using appropriate excitation/emission wavelength under a confocal laser scanning microscope (Olympus, Fluoview FV10i)⁹.

3.2.3.2 *Live cell imaging and co-localization analysis*

First, cells were seeded in Cell ViewTM – cell culture dishes with glass bottom at a concentration of $1-2.5 \times 10^5$ cells/cm² one day before imaging. Before starting to observe, cells should be checked for the presence of the respective fluorescence signals under a normal fluorescence microscope. Then the incubator in the Fluoview FV10i confocal microscope was turned on and the temperature was set to 37 °C and 5% CO₂ 30 min before putting the dishes inside. Dishes were kept in the incubator for at least 30 min to allow the cells to adjust to the environment before the images were taken. Next, the depth of the lens and the time frame of observation were set up and taking pictures was started. Normally, to insure the quality of images, test shooting should be performed in the first two cycles.

To analyze the co-localization of two or more channels of images, Olympus FV10-ASW 2.0 was used for analysis. First, the intense value was adjusted according to the photo quality by the 2D “auto change” function. Then the positive regions of each channel were exported individually and counted by blind counting for quantification. In each sample, at least 10 cells were taken into analysis and the experiment was repeated for 3 times. Alternatively, the merge image was exported and co-localization was indicated by double or triple color.

3.2.4 Protein biochemistry

3.2.4.1 *Preparation of cell lysates*

Cells were grown in 10 cm tissue culture dishes until the cell density reached 80% confluency. Lysates were collected at the indicated conditions and time points under each experimental setup. In brief, the culture medium was removed and cells were washed twice with ice cold PBS and then lysed with 500 μ l complete lysis buffer. Afterwards, the dish was placed on ice for 5 min for lysis of the cells. Cells were then scraped off and transferred into 1.5 ml Eppendorf tubes to be sonified in ice water for 30 seconds to promote complete release of cytoplasmic proteins into the lysis buffer. The lysates were further incubated on ice for 15 min. To remove cell debris, the lysates were centrifuged at 13000 rpm and 4 °C for 20 min. The cleared cell lysate was transferred into a fresh pre-cooled 1.5 ml Eppendorf tube and used for further analysis. For long-term storage, the lysates were immediately stored at -20 °C.

3.2.4.2 *Determination of protein concentration*

To determine the protein concentration of the cell lysates, a protein standard using different dilutions of bovine serum albumin stock solution was prepared. Bradford reagent was obtained from Bio-Rad (Cat. No. 500-0006) and used according to the manufacturer's instructions. The protein concentration was determined at 595 nm using the SmartSpec Plus Spectrophotometer (Bio-Rad, 170-2525).

3.2.4.3 *Immunoprecipitation (IP)*

For IP experiments, Protein G sepharose beads (PGS, GE healthcare life science, 17-0618-01) were used. Prior to IP, the protein concentration was determined by Bradford assay. 2-4 mg of the protein lysates were subjected to IP. A pre-clear step was performed to reduce unspecific binding between sepharose beads and proteins. Therefore, 100 μ l of PGS per sample were washed with 500 μ l lysis buffer, and centrifuged at 6000 rpm and 4 °C for 5 min. The washing step was repeated for two more times and then the PGS was resuspended in the cell lysates. After incubation for 1h at 4 °C on a roller shaker, pre-cleared lysates were centrifuged at 6000 rpm at 4 °C for 5 min to separate the PGS beads from the pre-cleared supernatant which is subsequently used for IP. The pre-cleared lysate was then transferred into a fresh 1.5 ml Eppendorf tube and the antibodies used for

IP was added at a concentration of 1:100 to form protein-antibody complexes. After overnight incubation at 4 °C on the roller shaker, PGS beads which have been washed three times with IP lysis buffer were added to the protein-antibody mixture. After incubation for 1 h at 4 °C on a roller shaker, the PGS-antibody-protein mixture was centrifuged at 6000 rpm at 4 °C for 5 min to collect the proteins of interest which have been bound to the beads. The supernatant was removed and stored for subsequent analysis of IP efficiency. After washing the bead-complex 5x with lysis buffer, 2x Laemmli loading buffer was added to the IP product. The initial cell lysate and the supernatant after IP together with the IP product were boiled at 95 °C for 5 min followed by centrifugation to recover the proteins for subsequent analysis by 12 % SDS-PAGE.

3.2.4.4 Polyacrylamide gel electrophoresis

Proteins were separated by sodium dodecyl sulfate (SDS)-polyacrylamide gel electrophoresis (PAGE) under denaturing conditions. SDS-PAGE was performed using gels of 1.5 mm thickness or precast commercial gels (Bio-Rad/Thermo Scientific). First, a 12 % or a 15 % resolving gel was poured and immediately covered with 1 ml Butanol in the casting stand. After polymerization, the Butanol was decanted and the gels were rinsed several times with ddH₂O. Afterwards, the stacking gel (5 %) was poured and inserted with 10-well comb to allow the gel polymerize.

Before running the gel, the running cassette was assembled and the gel was completely immersed in 1x running buffer. After the comb was removed, wells were flushed with running buffer to remove residual acrylamide. Generally, 40 µg or maximum 60 µl/well sample (for a gel of 1.5 mm thickness using a 10 well comb) can be loaded onto the gel. For estimation of the molecular weight of the proteins to be analyzed, 8 µl of a protein standard (Bio-Rad) were loaded onto the gel. In the Mini Protean Tetra system, constant 20-25 mA/gel were applied until the bromophenol frontier reached the end of the gel.

Table 12. Composition of SDS-PAGE gels

The indicted amounts were sufficient to prepare 1 gel (size 6 x 9 cm) that is used in the Mini Protean II vertical electrophoresis system.

Volume (ml)	Resolving gel (12%)	Resolving gel (15 %)	Stacking gel (4 %)
-------------	---------------------	----------------------	--------------------

30% Acrylamide	2.0	2.5	0.33
ddH₂O	1.6	1.1	1.4
1.5 M Tris-HCl (pH8.8)	1.3	1.3	–
1.0 M Tris-HCl (pH6.8)	–	–	0.25
10% SDS	0.05	0.05	0.02
10% APS	0.05	0.05	0.02
TEMED	0.002	0.002	0.002
Total	5	5	2

3.2.4.5 Immunoblotting (IB)

After SDS-PAGE was complete, proteins were transferred from the gel to a nitrocellulose membrane (Whatman, #10401196) by tank blotting. The Whatman gel blotting paper (GB005, Z613916) and the nitrocellulose membrane of the same size as the gel were soaked in the blotting buffer in advance. From the negative electrode side, place one fiber pad, one piece of Whatman paper, the gel, the membrane, one piece of Whatman paper, one fiber pad in turn to assemble the gel-membrane sandwich protein transfer. The membrane was exactly aligned on the top of the gel, and a roller was used to remove any air bubbles trapped between the gel and membrane. Once the cassette was closed and locked, it was inserted in the tank and transfer buffer was added to the tank until it reached the filling line. Transfer was performed overnight (16-20 h) at constant voltage of 25 V at 4 °C using the Mini-Trans blot system (Bio-Rad, #170-3930). For protein detection, the membranes were subsequently incubated in blocking buffer for 1h at 4 °C to avoid unspecific antibody binding. Then the membrane was incubated with the respective primary antibodies diluted in TBST overnight at 4 °C or 2h at RT. Afterwards, the membrane was extensively washed 4x with TBST for 5 min each before probed with peroxidase-conjugated secondary antibodies for 30 min at RT. Finally, the proteins of interest as well as β -Actin as loading control were detected using SuperSignal West Dura

Chemiluminescent Substrate (Thermo Scientific, #34075). Band intensities were quantified using the Image Lab software (Bio-Rad, ChemiDoc MP Imaging System) and statistically analyzed with GraphPad Prism 5.

If it was necessary to incubate the membrane with a secondary different antibodies, the previous antibodies was removed by stripping. Briefly, the membrane was rinsed in TBST for 10 min, followed by incubation with Restore Western Blot Stripping Buffer (Bio-Rad, #5000006) at RT for 15 min with gentle agitation. After washing in TBST 3 x at RT for 5 min, the stripped membrane was blocked for 0.5-1 h in blocking buffer and then subjected to a second round of protein detection.

3.2.5 Flow chemistry

For intracellular cytokine staining, 200 μ l cell suspension contained 5×10^5 cells per sample were transferred to V-bottomed 96-well plates. Cells were centrifuged at 1400 rpm at 4 °C and then washed one time with 150 μ l FACS buffer. To discriminate dead/live cells and prevent binding of antibodies to Fc receptors, cells were incubated with 50 μ l blocking buffer contains EMA (1:1000) and Fc blocking antibodies (1:100) for 20 min under light. Afterwards, cells were washed twice with 150 μ l FACS buffer. For surface marker staining, cells were stained with 50 μ l FACS buffer contained the respective antibodies for 20 min on ice in the dark. For intracellular cytokine staining, cells were treated with 100 μ l Cytofix/Cytoperm to fix and permeabilize cell membranes for 15 min on ice. And then cells were washed 3 x PermWash buffer before they were stained with 50 μ l FACS buffer contained the respective antibodies for 20 min. After staining, cells were washed again 3 x 150 μ l FACS buffer, resuspended in 300 μ l FACS buffer plus 60 μ l fixation buffer and store at 4 °C in dark until analysis. FACS data were analyzed with FlowJo software.

4. Results

4.1 MVA induced autophagy and the molecular mechanisms behind

Autophagy controls and shapes the quality and extent of viral antigen presentation, especially by MHC II molecules. In order to characterize the molecular and cellular mechanisms, which impact autophagy during acute poxviral infection, this dynamic and multi-step process from its signaling initiation to functional maturation was investigated.

4.1.1 MVA accumulates LC3 to induce autophagosome formation

4.1.1.1 *LC3 is increased in BMDCs, BMDMs, and HeLa cells after MVA infection*

As mentioned in the Introduction, cytosolic LC3-I conjugates with PE and converts to lipidated autophagosome-associated LC3-II upon induction of autophagy. Up to now, LC3-II is the only protein marker that is reliably associated with completion on the double-membrane of functional autophagosomes.⁶⁸ The amount of LC3-II is closely correlated with the number of autophagosomes.⁶⁹ Therefore, monitoring the conversion of LC3-I to LC3-II is widely accepted to measure autophagosome formation.⁷⁰

The first experiment aimed to detect quantitative changes of the two LC3 isoforms in BMDCs during the first 8h of MVA infection. As shown in Fig. 6A, kinetic analysis of LC3 expression by western blot exhibited an increasing amount of both LC3 isoforms up to 8h post infection (pi) in a time-dependent manner. Particularly, LC3-I showed a prominent upregulation, while enhanced LC3-II production revealed an increased autophagosome formation upon viral infection.

To distinguish the source of LC3-II upregulation, the lysosomotropic agent chloroquine was applied to prevent endosomal acidification. After that, the amount of LC3-II was measured in the presence and absence of virus (Fig. 6B). As shown by immunoblotting, chloroquine was able to increase LC3-II protein levels by inhibiting its autophagic degradation within the lysosome. In BMDCs, an obvious increase of LC3-II at 8h of MVA

infection was found, which, importantly, was further enhanced in the presence of chloroquine, demonstrating that the increased LC3 lipidation was caused by autophagosome accumulation induced by MVA, but not due to the interruption of LC3 degradation.

To extend the results from BMDCs to the other cell types, two other cell types: bone marrow-derived macrophages (BMDMs) and HeLa cells were chosen for analysis in the LC3 turnover assay. In HeLa cells, autophagosome-associated LC3-II strongly accumulated upon MVA infection and further increased in the presence of chloroquine, though this phenomenon was not so strong in BMDMs. Taken together, these experiments confirm that MVA-induced autophagy is a constitutively active process in the cell types analyzed.

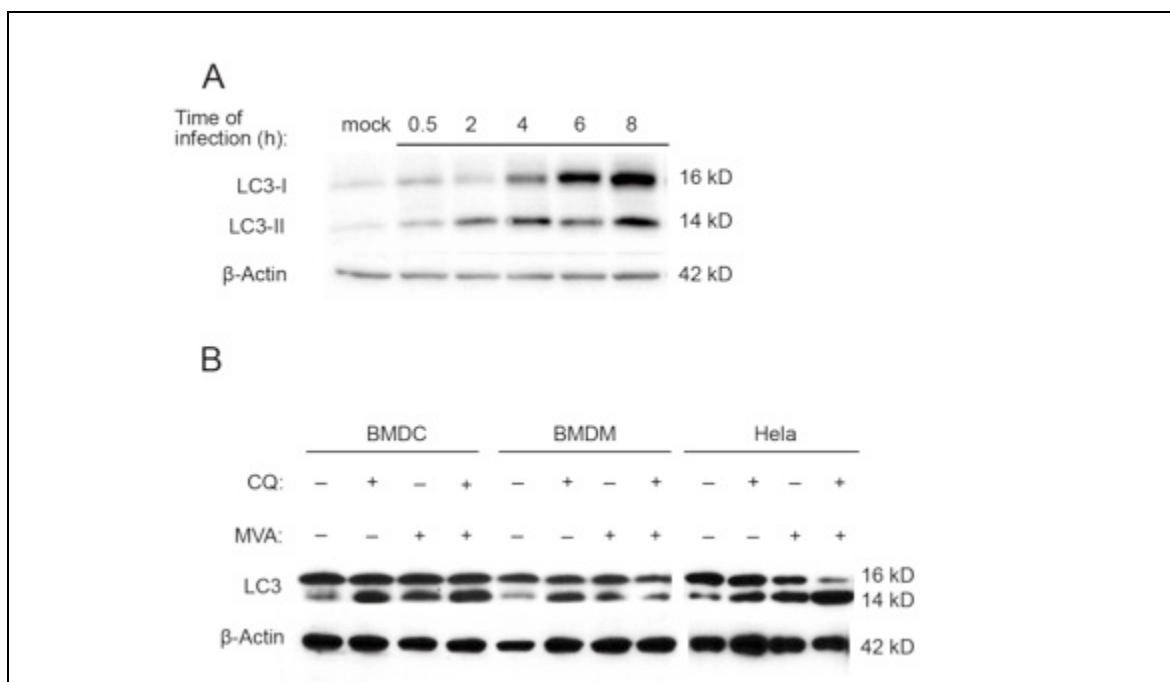


Figure 6. Kinetic expression of LC3 in MVA infected BMDCs, BMDMs and HeLa cells

A. Kinetics of LC3 expression in MVA-EGFP P7.5 infected BMDCs. **B.** BMDCs, BMDMs and HeLa cells were either mock-treated or infected with MVA-EGFP-P7.5 for 8h in the presence or absence of chloroquine (CQ, 50 μ M) for 2 hours before the cells were lysed. Cell lysates were analyzed by SDS-PAGE and immunoblotting within 24h or aliquoted to store at -20 $^{\circ}$ C. ($n \geq 3$. If not mentioned, one representative experiment is shown)

4.1.1.2 VACV enhances LC3 lipidation

When the VACV strain CVA was attenuated to MVA, 15% of the viral genome was lost, restraining the virulence and enhancing immunogenicity. Therefore, it was interesting to investigate if the VACV was capable of inducing autophagy. Furthermore, the efficiency of LC3-II induction between VACV and MVA was compared.

As shown in Fig. 7, VACV infection also led to an increase in LC3-II levels, and the increment was further enhanced in the presence of the lysosomal inhibitor chloroquine, suggesting that VACV could also induce autophagosome formation. However, in the comparison to MVA, VACV was less efficient (around 30%, Fig. 7B) in the induction of LC3 lipidation. It could be speculated that due to attenuation, some viral genes that suppress the induction of autophagy in the host were removed, as it is believed that autophagy can improve the capacity of APCs to stimulate helper T cells (Thiele, unpublished data). This result may also support the view that compared to VACV, MVA may be a better activator of cellular immune response.³¹

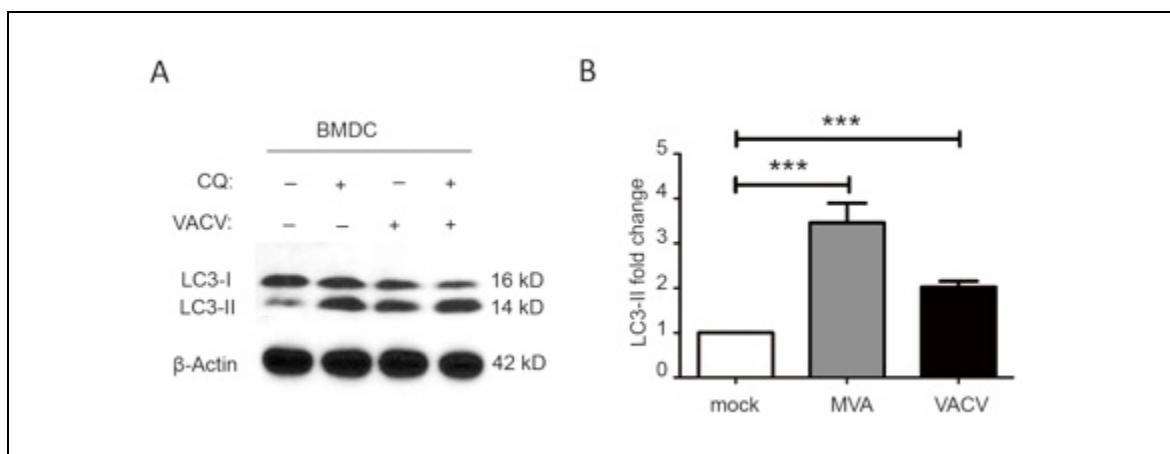


Figure 7. The expression of LC3 in VACV infected BMDCs

A. Same procedure as in Fig. 6B was performed on BMDCs with VACV. **B.** Quantification of the LC3-II fold change (ratio of LC3-II to β -actin) in VACV or MVA infected BMDCs compared to mock-treated BMDCs. ($n \geq 3$, *** $P < 0.005$. If not mentioned, the P value was calculated by using t-test in this thesis.)

4.1.1.3 LC3-II conversion is abolished in Atg7-deficient BMDCs

In response to starvation, eukaryotic cells recover nutrients through autophagy by recycling of long-lived proteins, organelles and other components of the cytoplasm for degradation, gaining an internal reservoir of nutrients.⁷¹ Thus, starvation was used

experimentally as a common method to induce autophagy. To investigate whether MVA induced LC3 augmentation is dependent on Atg7 expression, the LC3-II conversion in BMDCs derived from mice with conditional knockout of Atg7 (Fig. 8) after MVA infection and starvation was examined.

As shown in Fig. 8A, MVA infection and starvation were both able to induce LC3-II conversion in wild-type BMDCs. However, MVA induced much stronger LC3-II levels than starvation, suggesting that MVA infection might be a more efficient stimulus as compared to starvation. As expected, in Atg7-deficient BMDCs (*Atg7* loxP/loxP x *Cre*^{+/-}), LC3-II was almost abolished associated with decreased LC3-I in the MVA infected and nutrient depleted groups. Quantifying analysis revealed that the LC3-II was decreased in Atg7-deficient BMDCs with MVA infection (Fig. 8B), suggesting that the deletion of *Atg7* results in the blockade of LC3-I to LC3-II transformation. Our data proved those of former reports showing that *Atg7* is essential for a functional ATG conjugation system and for autophagosome biogenesis.⁷² Of note, the conversion of LC3 was also completely suppressed in *Atg5*^{-/-} cells under the serum free condition,⁷⁰ demonstrating that *Atg5* and *Atg7* are essential proteins for mammalian autophagy. On the other hand, MVA infection failed to induce LC3-II in Atg7-deficient cells, demonstrating that LC3-II is also a specific marker for MVA stimulated-autophagy. Since LC3-II was absent in Atg7-deficient BMDCs, the cells may be useful tools for investigating the contribution of autophagy on endogenous antigen presentation during MVA infection.

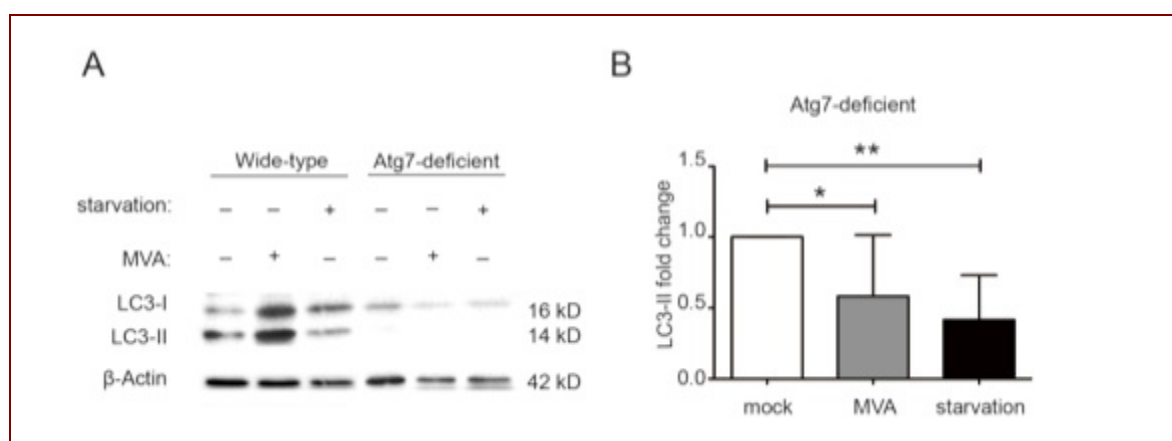


Figure 8. The expression of LC3 in Atg7-deficient BMDCs

A. BMDCs derived from Atg7-deficient (*Atg7* loxP/loxP x *Cre*^{+/-}) or wild-type mice cultured until day 7, were sorted by FACS for CD11c⁺ and MHC II⁺ surface markers and then infected with MVA for 8h or starved for 4h respectively. Cell lysates were subjected to SDS-PAGE and subsequently analyzed by immunoblotting. **B.** Quantification of LC3-II fold change (ratio of LC3-

II to β -actin) in Atg7-deficient BMDCs. ($n \geq 3$, * $p < 0.05$, ** $p < 0.01$)

4.1.2 Autophagic flux is enhanced by MVA

4.1.2.1 *Autophagosomes and autolysosomes are detectable by immunofluorescence after transfecting mRFP-EGFP-LC3 plasmids*

To quantify the autophagic flux and to visualize the intracellular flow of viral antigens into autophagic and/or degradative compartments, it is necessary to monitor the autophagy morphology intracellularly. To obtain a better image on the cellular level, endogenous LC3 was analyzed by using anti-LC3 antibodies for immunofluorescence staining in HeLa cells, as this cell line allows for a strong MVA-induced autophagy (Fig. 6) and preserves a largely unchanged cell shape during infection. However, the amount of endogenous LC3 protein was inefficient for intracellular staining, thus the staining was not satisfying (data not shown). To overcome this limitation, LC3 bearing a fluorescent protein tag such as EGFP or/and monomeric RFP (mRFP) at its N-terminus was expressed from a mammalian expression vector and used for detection. The working model of this system is depicted in Fig. 9A, showing that both mRFP-LC3 and EGFP-LC3 can be incorporated on the outer and inner membranes of the autophagosome. EGFP-tagged LC3 is sensitive to the acidic environment, so that the green fluorescence signals due to increasing instability are self-quenched when they have been delivered to the lysosome. In contrast, mRFP exhibits a more stable fluorescence in low pH compartments. Therefore, more mRFP-LC3 in contrast to EGFP-LC3 can be detected in the autolysosome (red signal),⁷³ whereas the autophagosome is visualized by both fluorochromes presented as yellow signals as a result of the overlay of mRFP and EGFP when co-expressed.⁷⁴

Due to transient transfection of the LC3 expression plasmid, it is worthwhile to perform a screening to identify the observation frame that gives the best signal to noise ratio. As shown in Fig. 9B, HeLa cells were analyzed at 8h, 16h and 24h after transfection with mRFP-EGFP-LC3. Obviously, at 8h post transfection (p.t.), strong expression of the cytosolic form of LC3 was observed since mRFP and EGFP were detected spreading over the entire cytoplasm. However, at 16h p.t., dot-like mRFP and EGFP accumulation was overlapping, indicating that cytosolic LC3-I was transformed to LC3-II, which accumulated on the double-membrane of the autophagosome. At 24h p.t., green

fluorescence signals declined and a few mRFP positive dots were separately found from EGFP. Concluding from the pictures, mRFP-EGFP LC3 expression plasmids are successfully expressed in HeLa cells, allowing the characterization of the continuous autophagic flux. Based on the given results, the optimal observation frame to analyze the autophagic compartment should be between 16h and 24h after transfection of the LC3 expression plasmid.

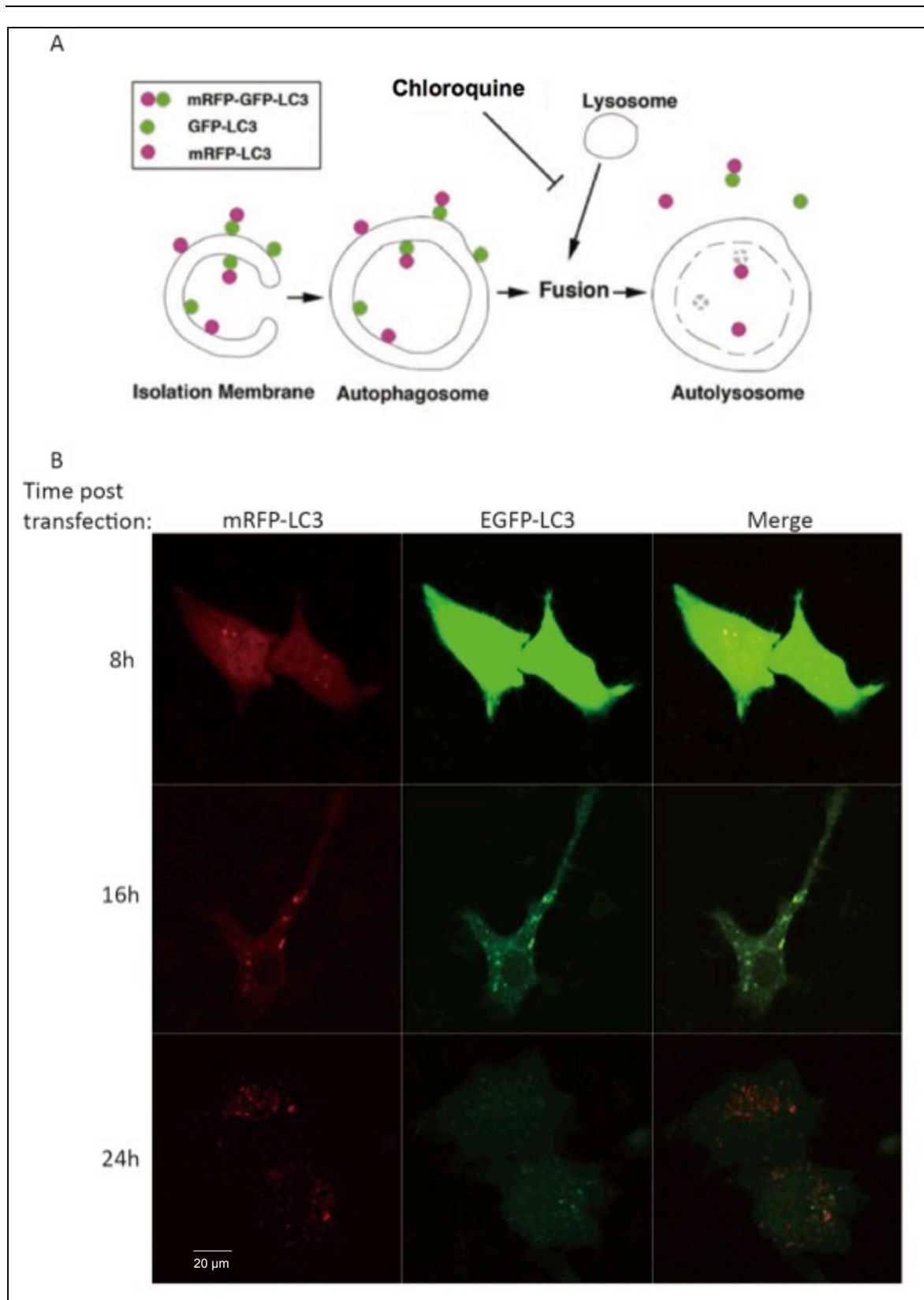


Figure 9. Transient transfection of HeLa cells with the mRFP-EGFP-LC3 expression plasmid

A. Schematic diagram of the maturation steps of autophagic flux (modified from Autophagy, 2007⁷⁴). **B.** HeLa cells were transfected with mRFP-EGFP-LC3 for 8h, 16h and 24h respectively,

and then specimens were fixed and mounted to be analyzed using CLSM.

In EGFP-LC3 transfected HeLa cells, the presence of lysosomal acidification inhibitor chloroquine blocked lysosomal proteolysis and thereby increased the number of EGFP-LC3 when autophagy was induced. However, the absence of such an effect on the total number of EGFP-LC3 positive punctae or increasing percentage of cells displaying numerous punctae indicates a defect in autophagic flux. Therefore, to investigate the functional autophagic flux in MVA infected cell lines, HeLa cells were transfected with the mRFP-EGFP-LC3 plasmids and then screened for the effective concentration of chloroquine on the autophagic flux that does not influence the cell viability and morphology (Fig. 10).

Fig.10 indicates that the accumulation of EGFP quenching was not obvious when treated with 25 μ M chloroquine, while 100 μ M chloroquine caused severe cytotoxicity leading to cell shrinkage. In comparison, 50 μ M chloroquine induced a prominent increase of EGFP and mRFP signals without impact on the cell viability. Thus, the optimal concentration of chloroquine is 50 μ M, which was used in the next experiment.

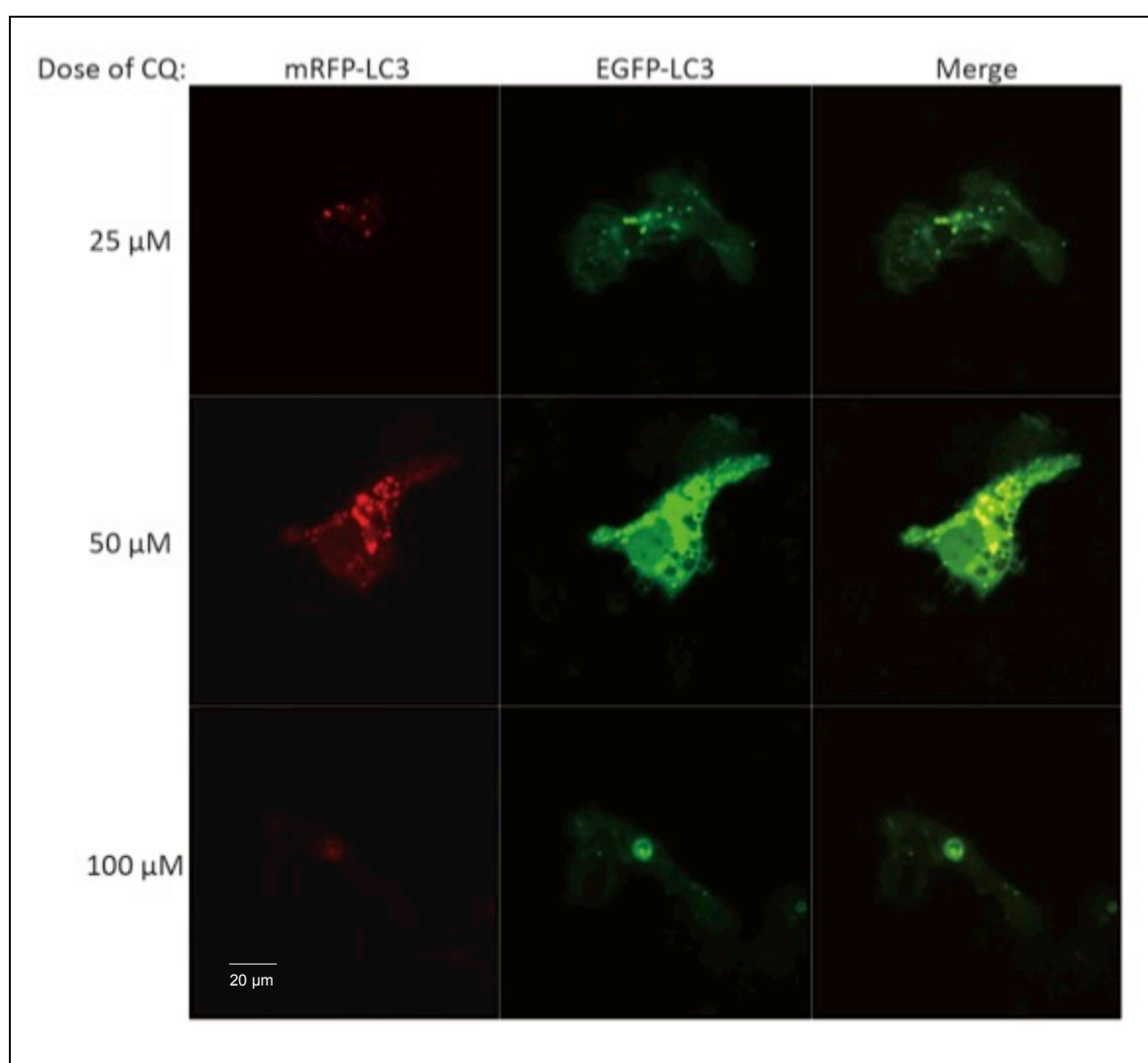


Figure 10. Optimization of chloroquine concentration in mRFP-EGFP-LC3 transfected HeLa cells

HeLa cells were transfected with mRFP-EGFP-LC3 for 16h, and then treated with chloroquine (CQ) for 2h at the concentration of 25 μM , 50 μM and 100 μM respectively. Specimens were fixed and mounted to preserve the fluorescence before CLSM observation.

4.1.2.2 *EGFP-LC3 is degraded in the lysosome upon MVA infection*

To monitor the autophagic flux during MVA infection, HeLa cells were transfected with mRFP-EGFP-LC3 for 16h and subsequently infected with MVA in the absence or presence of chloroquine from 2h to 8h (Fig. 11). The number of co-localization punctae between mRFP-LC3 and mRFP/EGFP-LC3 was calculated to quantitate the process.

As shown in Fig. 11, the amount of EGFP and mRFP punctae remained nearly unchanged

from 2h to 4h p.i. in the absence of lysosomal inhibitor, indicating that autophagosome formation had not been initiated yet. The green and red signals were overlapping in almost all punctae, suggesting that the autophagosomes had not yet merged with the lysosome. Then, the two fluorophores were separately detected in the cytoplasm from 6h p.i. on, while at the same time a decreased number of yellow dots was observed due to the quenching of EGFP in the acidic environment of the lysosome. At 8h p.i., the EGFP punctae markedly decreased, leaving only the mRFP localized in the autolysosome. In comparison, due to the inhibition of the autophagic flux by chloroquine treatment, the individual mRFP positive signals could not be detected, demonstrating that the inhibition of lysosomal acidification is able to prevent the degradation of EGFP. Furthermore, the increasing number of double-positive signals (EGFP and mRFP) in chloroquine treated cells and increased mRFP dots in only MVA infected cells indicated that autophagosome biogenesis was induced upon viral infection.

The statistical analysis of the percentage of co-localized of mRFP/EGFP double-positive to total mRFP positive dots clearly showed that the co-localization rate dropped from around 80% (2h p.i.) to 50% (8h p.i.) caused by MVA infection. However, the percentage of that had not significant changed during MVA infection, when chloroquine had been added (Fig. 11B). Therefore, this result for the first time demonstrates the existence of a functional-active autophagic flux in MVA infected HeLa cells. More importantly, that the enhanced autophagic flux delivers the cargo to lysosome and leading to degradation.

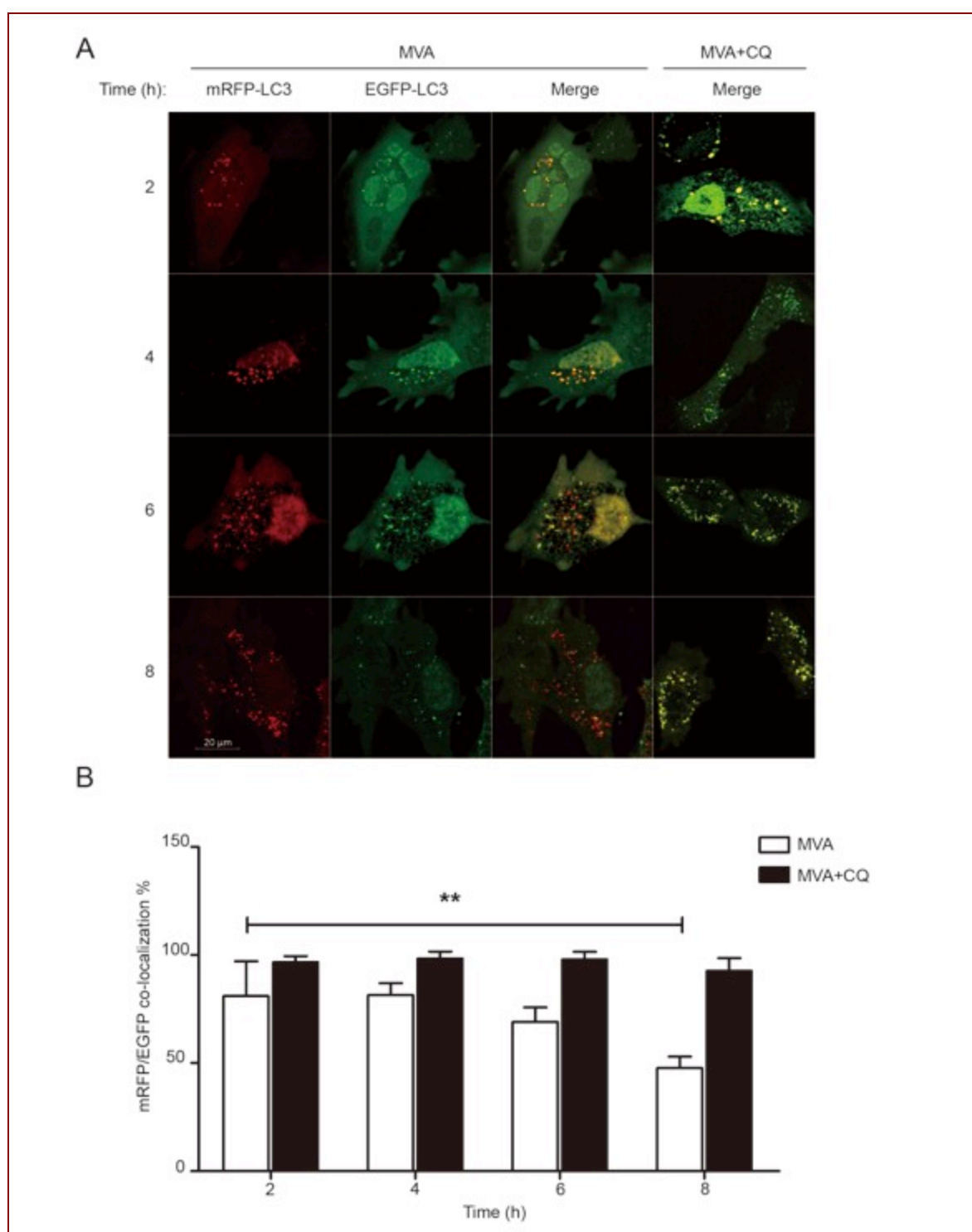


Figure 11. mRFP-EGFP-LC3 quenching assay in HeLa cells

A. HeLa cells were transfected with mRFP-EGFP-LC3 for 16h and then infected with MVA for 2h, 4h, 6h or 8h respectively. On the most right panel, MVA infected cells were treated with Chloroquine (CQ, 50 μ M) for 2h. **B.** Quantification of the ratio of mRFP-EGFP double positive signals to single mRFP positive signals. ($n \geq 3$, over 10 cells were counted in each sample per experiment, ** $P < 0.01$.)

4.1.2.3 *Fusion of autophagosome with lysosomes is increased*

Autophagy is one of the main catabolic pathways for degradation of cytosolic contents despite of viral infection. The average infection rate of MVA in HeLa cells was around 80% (MOI 10, data not shown). Hence, it was not guaranteed that the transfected cells observed in the above experiment were infected. To draw the conclusion that MVA is inducing autophagy, it is essential to demonstrate that the respective cells were infected. Since mRFP-LC3 has proven to be stable in autophagic compartments, a co-staining assay of autophagosome/lysosome-lysosome was performed in HeLa cells infected with EGFP expressing MVA. Lysosome associated membrane protein 2 (LAMP-2), acting in the protection, maintenance, and adhesion of lysosomes, is a specific marker for lysosome.⁷⁵ Therefore, in this set up the co-localization of mRFP-LC3 and LAMP-2 was analyzed only in EGFP expressing cells.

Under the confocal microscope, mRFP began to co-localize with LAMP-2 signals between 4h and 6h p.i.. Together with the increased number of mRFP-LC3 punctae, the mRFP-LC3/LAMP-2 co-localization was enhanced until 8h p.i. (Fig. 12), thus supporting the finding depicted in Fig.11 that MVA infection induced autophagosomes fusion with lysosomes. Quantification of the mRFP/LAMP-2 double positive punctae per cell showed that at 8h p.i. the number was 1.6 fold increased compared to that at 2h p.i.. Therefore, in HeLa cells, MVA promoted not only initiation but also maturation of autophagosomes as evidenced by an increase in cellular compartments with the co-localization of the mRFP-LC3 and LAMP-2. Taken the results obtained from mRFP-EGFP-LC3 quenching assay and the analysis of LC3 expression by western blot together, it could be demonstrated that MVA infection not only augments the assembly of autophagosomes, but also induces the formation of downstream product-autolysosomes. As a result, the contents engulfed in the autophagosome may be degraded within the lysosomal compartments.

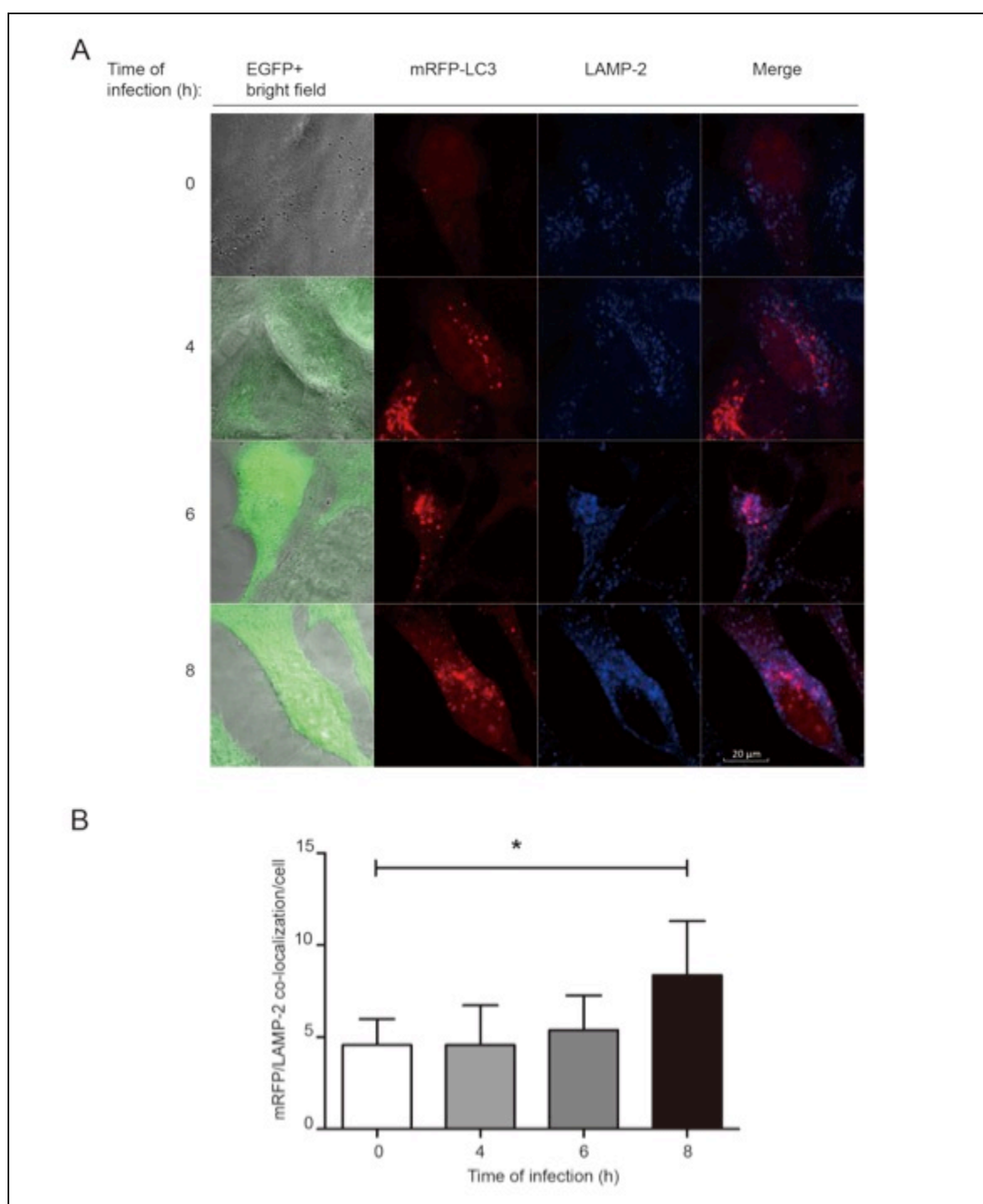


Figure 12. Autophagic flux in MVA-EGFP P7.5 infected HeLa cells

A. HeLa cells were transfected with mRFP-LC3 for 16h and then infected with MVA-EGFP P7.5 for 0h, 4h, 6h or 8h respectively. **B.** Quantification of the mRFP/LAMP2 double positive dots per cell. ($n \geq 3$, over 10 cells were counted in each sample per experiment, $*P < 0.05$)

4.1.3 MVA-induced autophagy requires the TLRs adaptor protein MyD88

4.1.3.1 *MyD88 and Beclin-1 levels are upregulated*

The results presented above demonstrate that MVA infection induced functional autophagy. However, the molecular mechanisms and the signaling pathways responsible for viral-induced autophagy remain elusive. TLRs are an important family member of PRRs that also play a role in sensing MVA infection in dendritic cells. Published data suggest that the TLRs adaptor protein MyD88 is an essential factor for the induction of autophagy by interacting with Beclin-1.^{55,61-63} Beclin-1, the homologue of Atg6 in mammalian cells, is targeted by viruses like influenza A, HSV-1 and HIV to subvert the autophagy pathway for their own benefits, resulting in an increased viral replication and/or control over apoptosis of their host cells.⁷⁶ Therefore, it seems worthwhile to investigate the role of these two proteins in MVA-induced autophagy.

First, the protein levels of MyD88 and Beclin-1 were examined by western blot in BMDCs during MVA infection. It was observed that the amounts of both proteins were gradually increased upon infection (Fig. 13). At 8h p.i., MyD88 was significantly more abundant (3.5 fold) compared to the mock control. The expression of Beclin-1 was also mildly increased, though not as strong as MyD88 (about 1.6 fold at 8h p.i. compared to the to the mock control).

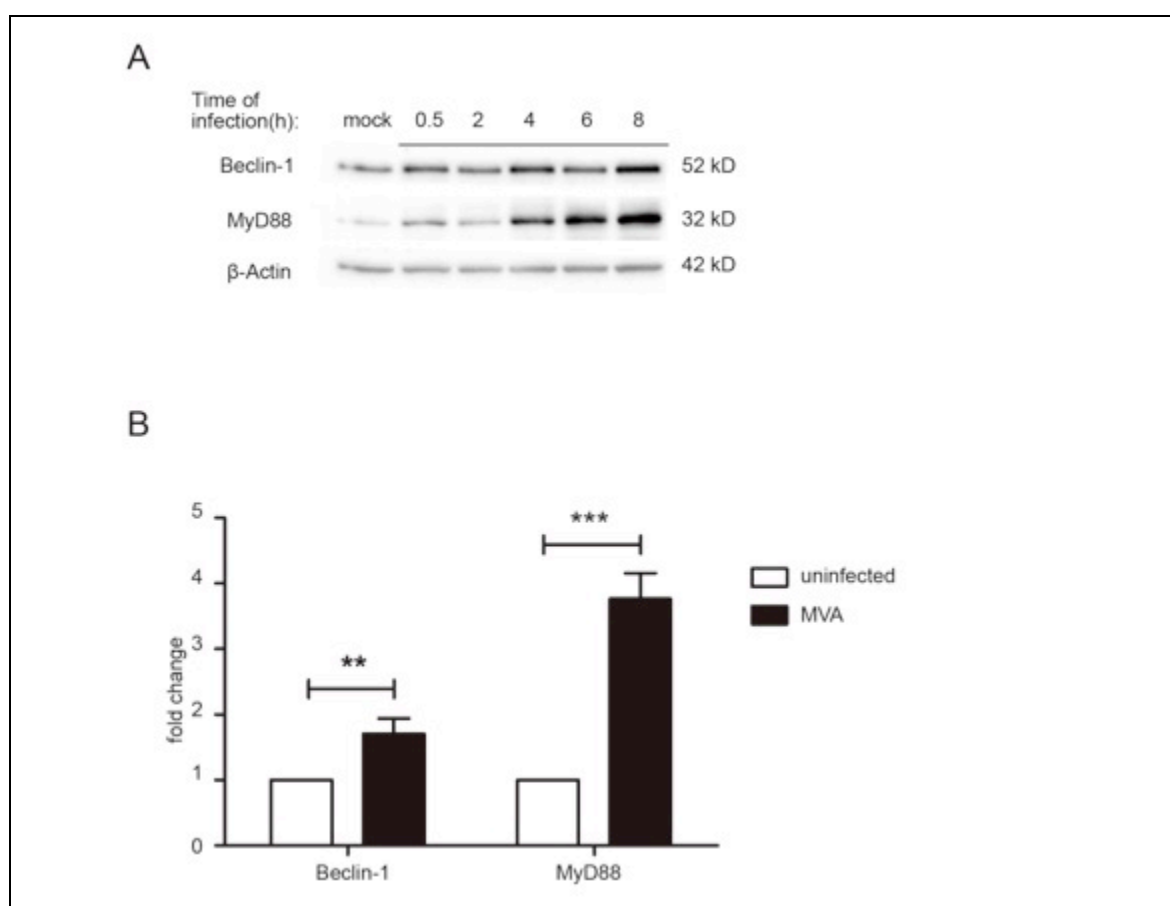


Figure 13. Kinetic analysis of Beclin-1 and MyD88 expression in MVA infected BMDCs

A. Kinetics of MyD88 and Beclin-1 expression in mock treated and MVA-EGFP P7.5 infected BMDCs at 0.5h, 2h, 4h, 6h and 8h p.i. respectively. Cell lysates were subjected to SDS-PAGE and analyzed by western blot within 24h. **B.** Quantification of Beclin-1 and MyD88 protein levels (fold change compared to the mock control at 8h p.i.). ($n \geq 3$, ** $P < 0.01$, *** $P < 0.005$)

4.1.3.2 MVA infection fails to induce autophagy in *MyD88*^{-/-} BMDCs

It is comprehensible that Beclin-1 was increased as autophagy was activated by viral infection, but the reason for MyD88 upregulation was not clear. To determine the role of MyD88 in MVA induced autophagy, the expression levels of Beclin-1 and LC3 were monitored by kinetic western blot analysis in BMDCs derived from *MyD88* homozygous knockout mice (Fig. 14).

During infection, both LC3-I and LC3-II levels did not significantly change compared to that of the mock control, suggesting autophagy was not induced by MVA infection. Strikingly, a prominent decrease of Beclin-1 expression was found depending on the time

of infection, which revealed a close relationship of Beclin-1 levels with the initiation of autophagy. Furthermore, the analysis of LC3-II conversion was also additionally performed in MyD88^{-/-} BMDCs upon infection with replication-competent VACV to comparatively analyze possible changes related to autophagy for MVA and VACV. In this setup, LC3-II levels in VACV infection seemed comparable to mock or MVA, and were even a bit reduced. These data are in line with those shown in Fig.7, proving that VACV has a weaker impact on the induction of autophagy than MVA. For both viruses, the induction of autophagy might depend on the presence of MyD88. Possibly, MyD88 through Beclin-1 controls the stimulation of autophagy. However, further experiments are needed to characterize the detailed mechanism, i.e. if there is a direct protein-protein binding of MyD88 to Beclin-1 or indirect interactions between the two proteins via a third party.

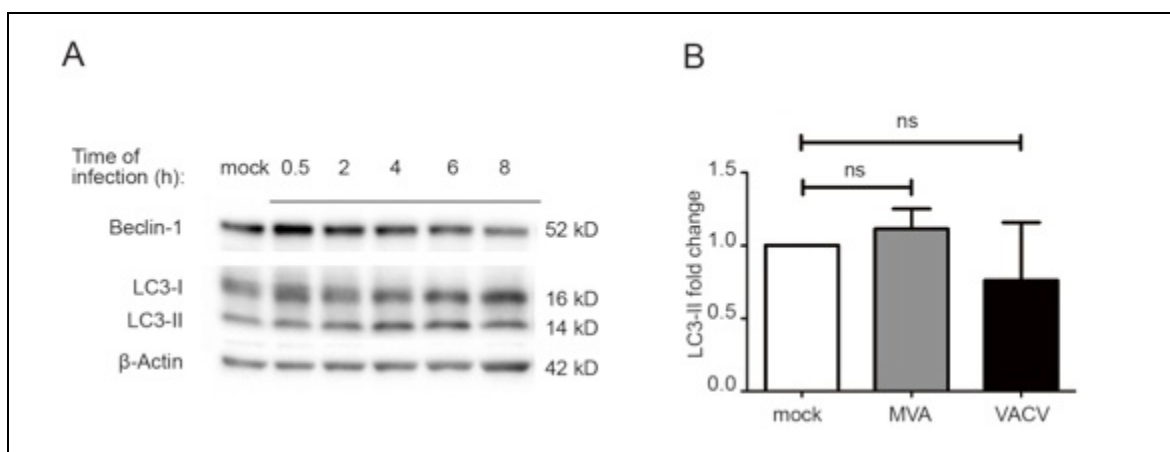


Figure 14. Analysis of Beclin-1 and LC3 in MVA or VACV infected BMDCs

A. Kinetics of LC3 and Beclin-1 expression in MVA-EGFP P7.5 infected BMDCs derived from MyD88^{-/-} mice. Cells were harvested at the indicated time points and cell lysates were subjected to SDS-PAGE and subsequent western blot analysis. **B.** Quantification of LC3-II expression level changes in MVA or VACV infected MyD88^{-/-} BMDCs as fold change (ratio of LC3-II to beta-actin) compared to mock treated cells at 8h p.i.. ($n \geq 3$, ns=no significant change)

4.1.3.3 Starvation-induced autophagy is functional in MyD88^{-/-} BMDCs

To prove that MyD88 was required for viral induced autophagy, it was necessary to analyze whether deletion of MyD88 would also result in a general autophagy deficiency. Therefore, BMDCs derived from MyD88^{-/-} mice were cultured under starvation conditions

to examine, if LC3 lipidation was defective.

Fig.15 shows that starvation could efficiently increase the level of LC3-I as well as the transformation from LC3-I to LC3-II when the nutrients were depleted for 4h, demonstrating that induction of autophagy under starving conditions was not hampered in BMDCs lacking MyD88. Furthermore, chloroquine treatment in MVA or VACV infected MyD88^{-/-} BMDCs resulted in accumulation of LC3-II, indicating that the autophagic flux was functional. From the data shown in Fig.14 and Fig.15, it may be concluded that autophagy is functional at basal levels in MyD88-deficient BMDCs. Of note, the absence of MyD88 in MVA or VACV-infected BMDCs resulted in the abrogation of MVA-induced autophagy, which also leads to the degradation of Beclin-1.

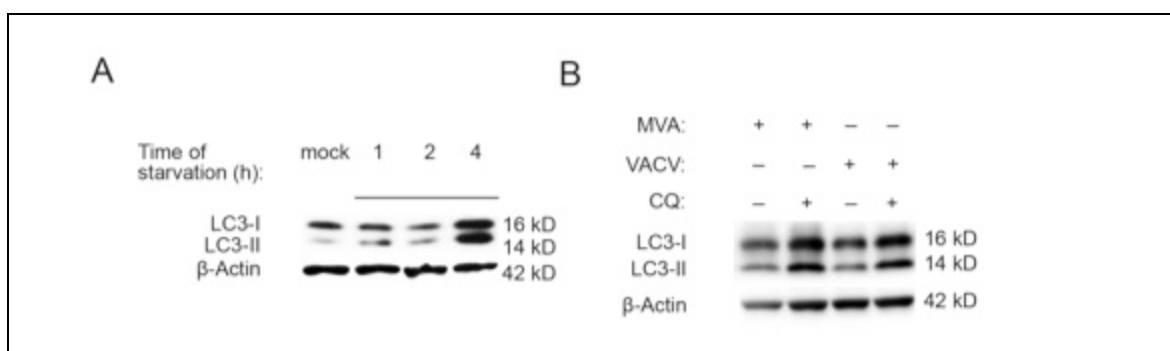


Figure 15. Expression of LC3 in MVA or VACV-infected MyD88 deficient BMDCs

A. BMDCs were washed 2 times with amino acids-deprived medium before they were cultured under starvation condition for the indicated time points. Cell lysates were subjected to SDS-PAGE and subsequent western blot analysis. **B.** BMDCs were infected with MVA or VACV for 8h. Additionally, infected cells were incubated with chloroquine (CQ, 50 μ M) for 2h before harvesting. The expression of LC3-I/LC3-II was analyzed and β -actin was used as loading control.

4.1.3.4 Autophagy induction requires viral replication intermediates

Each individual TLR consists of an ectodomain containing leucine-rich repeats that mediate recognition of PAMPs. Upon recognition of the respective ligand, the TLR downstream signal is transmitted via an adapter protein to finally induce the production of type I interferon and proinflammatory cytokines as first line of defense against the pathogen that has been sensed. Except for TLR3, which utilizes TRIF as adapter protein, all other TLRs transmit their signals via the adaptor protein MyD88. It might be possible that MVA-induced autophagy through a TLR signaling pathway. Therefore, it was important to decipher which TLR-MyD88 pathway is triggered by the virus and what are

the cognate ligands recognized by the receptor.

To investigate this, DNA replication was inhibited by Ara-C, thus only allowing the entry of MVA cores into the cytoplasm, and the subsequent activation of viral transcription factors such as RNA polymerase, capping enzyme and methylating enzymes to allow for early viral gene transcription in infected BMDCs. MVA-infected BMDCs were treated by Ara-C and the level of autophagy was determined by the expression level of LC3. 3-Methyladenine (3-MA) was used to inhibit autophagy by blocking autophagosomes formation via the inhibition of PI3K. It is shown in Fig.16 that 3-MA efficiently decreased LC3 lipidation in the presence of MVA that served as a positive control. Ara-C also diminished LC3-II in MVA infected cells. Thus inhibition of viral DNA replication prevented the virus-induced autophagy. However, Ara-C was diluted when it was co-incubated with the cells ahead of infection applied, which might not be sufficient to inhibit viral DNA replication. Furthermore, Ara-C can cause a blockage of DNA replication in host cells as well, leading to a generally impaired protein synthesis of infected cells.

To overcome this limitation, the virus stock was pretreated with psoralen in combination with ultraviolet (UVA) radiation (so-called PUVA treatment), to directly break viral DNA double-strands, resulting in replication-deficient viruses. It was observed that LC3 lipidation was blocked by PUVA treatment in a time-dependent manner (Fig.16). When MVA was treated with PUVA for 3 min, the inhibition of LC3-II conversion was not prominent, while after 20 min PUVA treatment, the level of LC3-II was comparable to that of the mock control, suggesting that prevention of viral DNA replication cascade decreased the capability of MVA to trigger autophagy. This data reveals that MVA-induced autophagy requires viral DNA replicates or subsequent intermediate/late viral gene products.

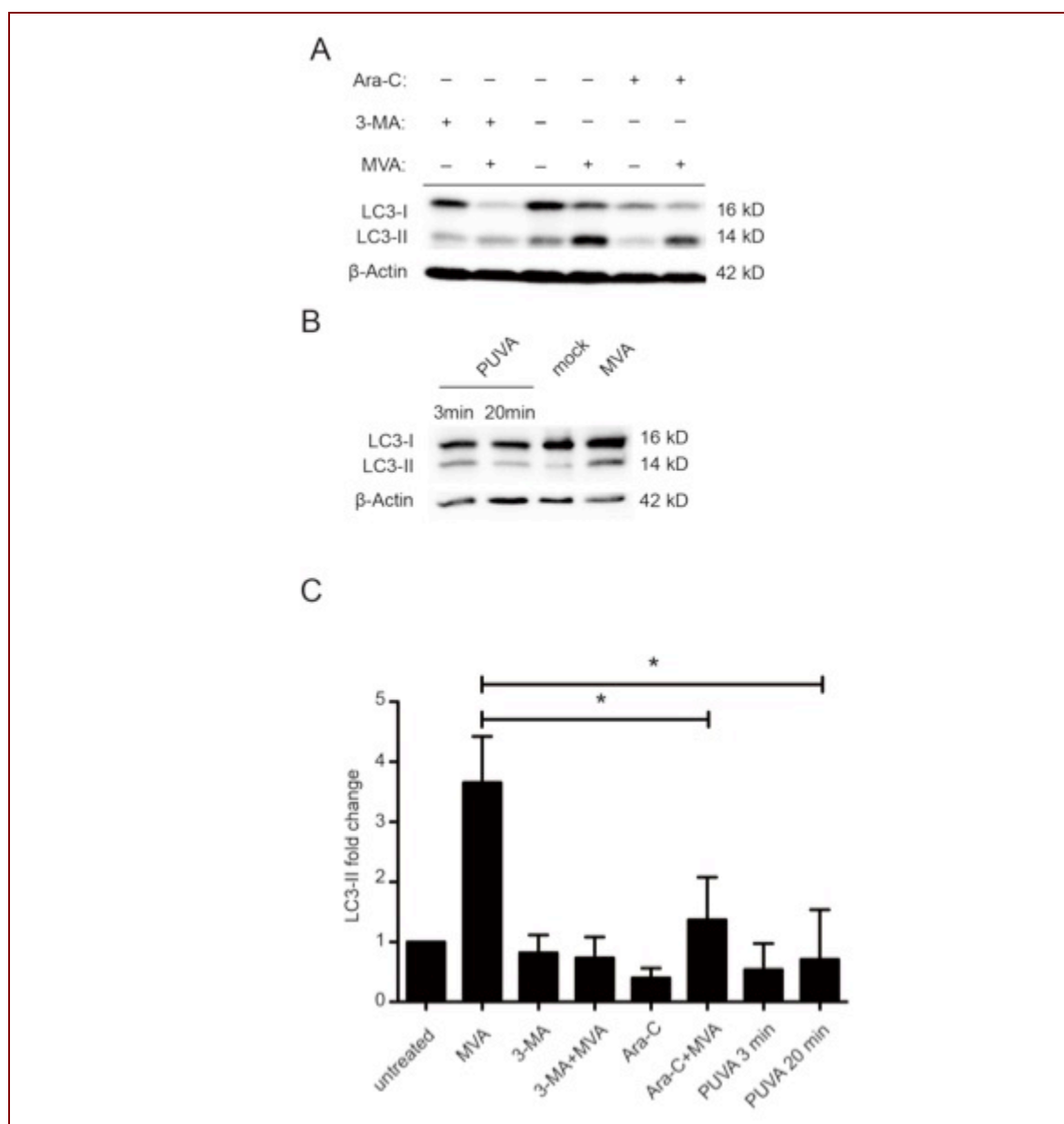


Figure 16. The expression of LC3 under conditions that block viral DNA replication

A. BMDCs were infected with MVA-EGFP P7.5 for 8h or left uninfected. To block DNA replication, Ara-C (1:1000) was added to cell culture 0.5h before virus infection. Autophagy inhibitor 3-MA (500 μ M) was used as a control. **B.** To inhibit viral DNA replication, MVA was first incubated with psoralen (0.3 μ g/ml, sigma # P8399) at 37 $^{\circ}$ C for 10min, and then exposed to UVA light (0.6 Joule/cm²) for 3 min or 20 min, respectively. Inactivated virus was added and co-incubated with the cells for 8h. **C.** Quantification of LC3-II fold change (ratio of LC3-II to β -actin) in samples from A and B. ($n \geq 3$, * $P < 0.05$)

4.2 Endogenous MHC II presentation of MVA-produced HEL

As it is described in the above chapter, autophagosome formation as well as the autophagic flux was induced in MVA- and to a lesser degree in VACV-infected BMDCs. Since autophagy is a main catabolic pathway for degradation of cytosolic constituents, induced autophagy upon infection might promote the elimination of viral pathogens in the lysosome. As a result, this pathway is able to provide antigenic peptides to MHC II loading compartment (MIIC), which may lead to the induction of stronger CD4⁺ T cell responses. The following chapter will show evidences that upon MVA infection, MHC II restricted endogenous antigen processing and presentation is occurring in BMDCs, which might depend on autophagy.

4.2.1 Infected BMDCs fail to endocytose exogenous apoptotic cell debris

To investigate the MHC II endogenous presentation pathway, it is necessary to demonstrate first that the endogenous antigens bind to MHC II. Secondly, it has to be shown that endogenous peptide-MHC II complexes can be presented on the cell surface and consequently activate CD4⁺ T cells. To prove that endogenous antigens bind to MHC II, it was necessary to exclude that the exogenous antigen-MHC II pathway may contribute. In order to fulfill this prerequisite, endocytosis experiments explained schematically in Fig. 17A were designed. Briefly, intracellular antigens from infected BMDCs or soluble proteins were co-incubated with MVA infected cells respectively. The co-localization of extracellular antigens/proteins within the cytoplasm of the infected cells revealed the capacity of endocytosis for infected BMDCs.

As shown in Fig.17B, EGFP derived from infected cells could only be detected outside of MVA-mCherry infected BMDCs (red mCherry expression) through the whole course of observation, whereas in the control group (uninfected BMDCs), EGFP was found to enter these cells. Furthermore, to a low extend soluble ovalbumin (PE-OVA) was taken up by infected BMDCs (37% BMDCs contained PE), while more than 90% of uninfected BMDCs efficiently endocytosed PE-OVA. From the endocytosis experiments with cell-derived and soluble protein, it may be concluded that the endocytosis ability of MVA

infected BMDCs is severely damaged for cell-derived proteins.

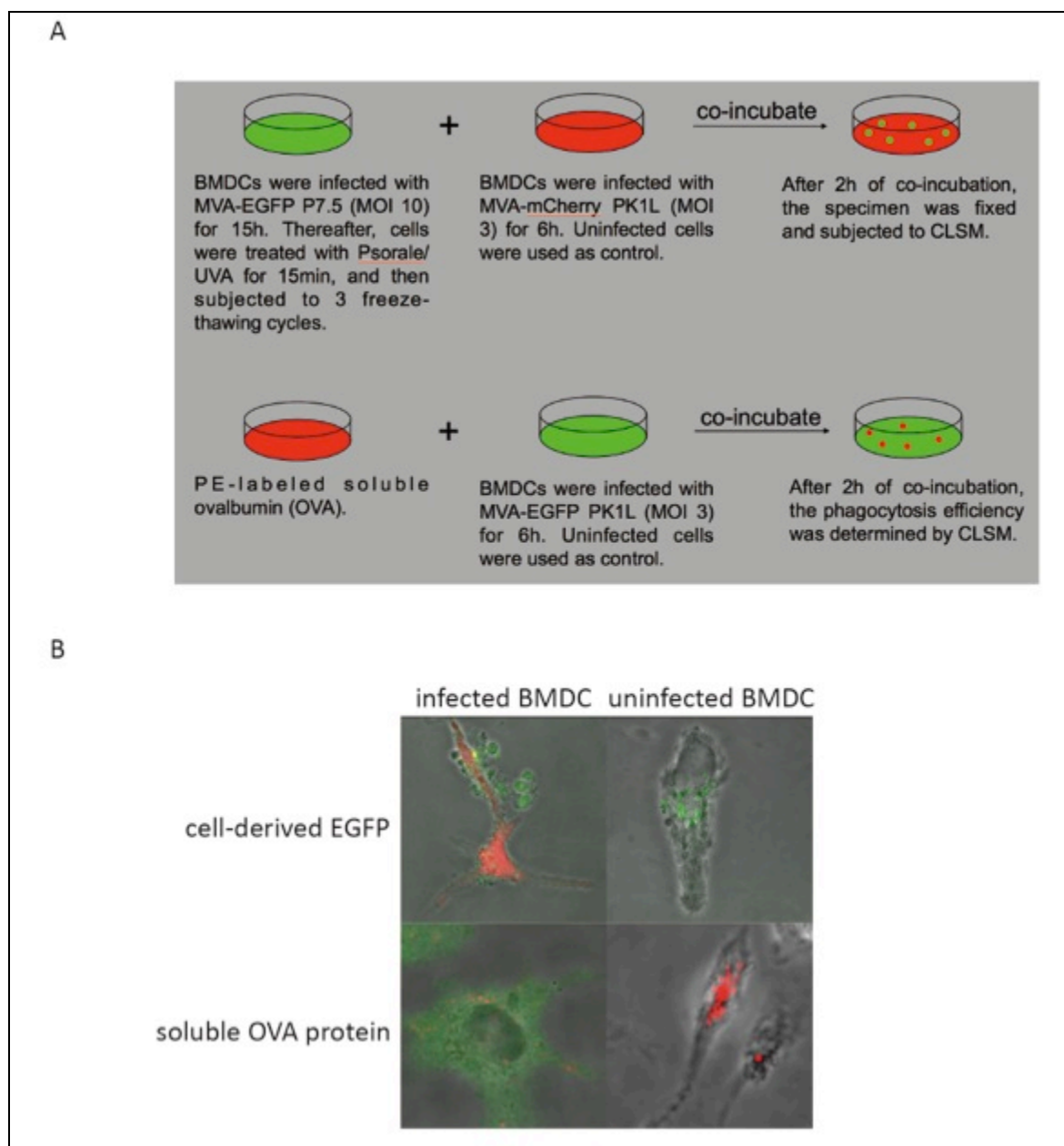


Figure 17. Schematic presentation of endocytosis assay methods

A. Upper row: BMDCs were infected with MVA-EGFP P7.5 at a high MOI to produce large amounts of endogenous EGFP. To inactivate residual virus on cell membranes, psoralen ($0.3 \mu\text{g/ml}$) was added to cells at 37°C for 10 min and then cells were exposed to UVA 0.6 Joule/cm^2 for 30 min. To induce the formation of cell debris, cells were fast frozen at -80°C and then thawed to RT. This freeze-thaw cycle was repeated for 2 more times and then debris was collected in 1 ml fresh medium. BMDCs were infected with MVA-mCherry PK1L for 6h, allowing mCherry expressed in the cytoplasm and then co-incubated with 1 ml cell debris prepared as described above for 2 h before fixation and observation. Lower row: BMDCs were infected with MVA-EGFP PK1L for 6h to express EGFP in the cytoplasm and then co-incubated with soluble PE-OVA for 2h before fixation and observation. **B.** BMDCs endocytosis assay by CLSM.

4.2.2 Endogenous viral antigens are presented to CD4⁺ T cells

Since the infected BMDCs are not able to endocytose exogenous proteins or antigens, the capability of infected BMDCs to present viral antigens to CD4⁺ T cells is likely due to an intrinsic ability of infected BMDCs to present the endogenous viral antigens. Thus, to determine if MHC II can recognize viral antigens produced in the cytoplasm of infected APCs, CD4⁺ T cells specifically recognizing OVA-derived epitopes OVA₂₆₅₋₂₈₀ (CD4^{OVA} T cells) were used. CD4^{OVA} T cells were incubated with uninfected BMDCs that were pulsed with OVA peptide or MVA-OVA PK1L infected BMDCs, respectively. To determine the CD4⁺ T cell response, interferon-gamma (IFN- γ) secretion was measured by fluorescence-activated cell sorting (FACS, Fig. 18). The data showed that both exogenous OVA and MVA-derived OVA presented by BMDCs equally induced around 90% CD4^{OVA} T cells expressing IFN- γ , indicating the high efficacy presentation of MVA derived antigens. Since infected BMDCs showed poor uptake of cell-associated antigens as demonstrated using EGFP containing apoptotic bodies, furthermore uninfected cells in this assay don't take up and present antigens (Fig.17 and data not shown), this finding may indicate that the CD4^{OVA} T cells were likely activated by endogenous OVA presentation via MHC II from MVA-OVA PK1L infected BMDCs. Thus, it is suggested that the endogenous MHC II antigen presentation pathway exists and is active in MVA infected BMDCs.

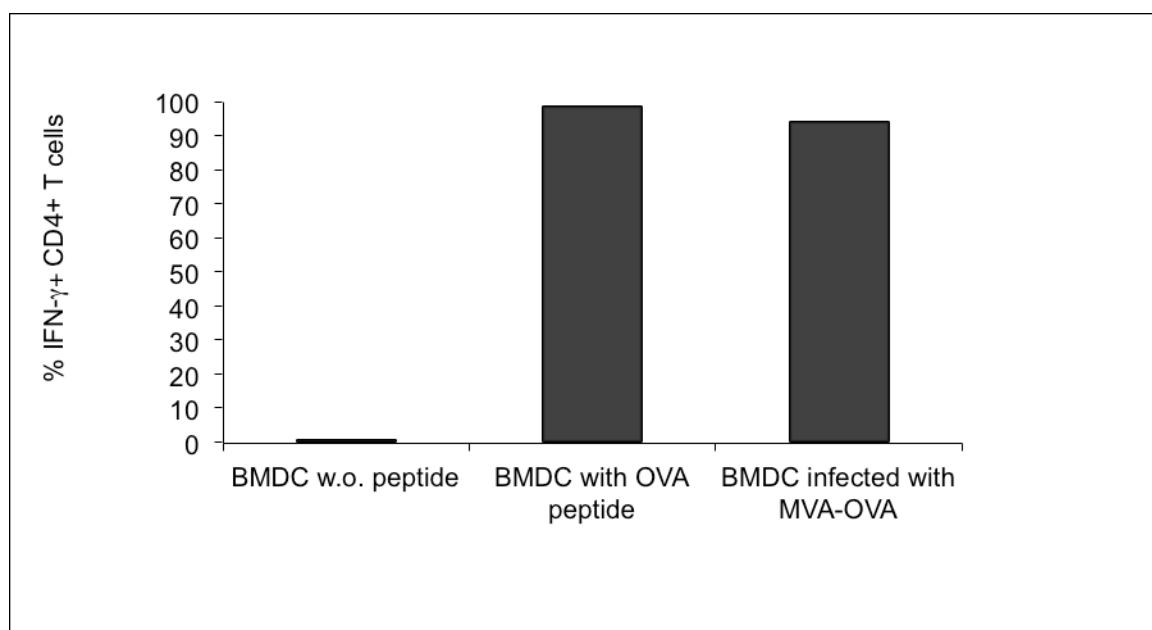


Figure 18. Stimulation of CD4^{OVA} T cells by OVA peptide or MVA-OVA PK1L infected

BMDCs

BMDCs were incubated either with or w/o OVA peptide (2 µg/ml) or infected with MVA-OVA PK1L (MOI 10) overnight. Infected BMDCs were sorted for double positive signals of MHC II and CD86, and then incubated with CD4⁺ T cells. The cultures were incubated for 14h at 37 °C and the stimulation of the T cells was analyzed by subsequent intracellular cytokine staining (ICS). (Experimental data as a courtesy of Frank Thiele)

4.2.3 HEL-MHC II complexes are detected in the cytoplasm and on the cell membrane**4.2.3.1 Aw3.18 mAb only recognizes surface antigen-MHC II complexes**

It has been shown that endogenous-presentation of viral antigens by MHC II exist in MVA infected BMDCs. But how does this pathway deliver endogenous MVA antigens to be loaded on MHC II molecules and which cellular organelles contribute to this pathway? To investigate that, the Aw3.18 monoclonal antibodies (Aw3.18 mAbs; biotinylated), which specifically recognizes the peptide/MHC II complex of hen egg lysozyme peptide 48-62 (pHEL48-62) and the MHC II molecule I-A^k (pHEL/I-A^k) was used. Aw3.18 mAb has been successfully used to detect the pHEL48-62/I-A^k on the surface of splenocytes.⁷⁷ To test whether Aw3.18 mAb could recognize the complex on BMDCs generated from C3H mouse, presenting MHC II (I-A^k), were applied in the following experiments in the chapter if not specified. Cells pulsed exogenously with different amounts of HEL protein for 6h or 16h, respectively, to screen for the appropriate protein amount and optimal time point after pulsing to detect the complexes on cellular membranes. The pHEL/I-A^k expression was determined by surface staining with Aw3.18 mAb by FACS.

As was shown in Fig. 19, 80% of BMDCs presented pHEL/I-A^k when 5000 µg/ml HEL were incubated with the cells for 6h. Until 16h, 80% of BMDCs pulsed with 500 µg/ml HEL presented pHEL/I-A^k, indicating that HEL antigens were presented in a time dependent manner. However, a relatively high background staining was observed when the cells were not pulsed with any HEL protein.

A Amount	6h	16h
-------------	----	-----

Figure 19. Presentation of HEL antigens was detected by FACS using Aw3.18 mAb

A. Zero to 5000 $\mu\text{g/ml}$ HEL protein was co-incubated with BMDCs derived for 6h or 16h, respectively. Surface staining was performed using a biotinylated Aw3.18 mAbs and anti-biotin secondary antibodies, subsequently analyzed by FACS. **B.** Statistical analysis of the percentage of Aw3.18 positive BMDCs to all BMDCs. (Experimental data as a courtesy from Jacob Loschoko. BMDCs derived from C3H mouse were used in Figure 19 to 23 if not specified.)

4.2.3.2 C4H3 monoclonal antibodies recognize intracellular pHEL/I-A^k

Next, to test whether Aw3.18 was able to stain intracellular pHEL/I-A^k, BMDCs were co-incubated with 500 $\mu\text{g/ml}$ HEL protein for 16h. Afterwards, the cells were subjected to surface staining or fixed and permeabilized for the intracellular IF staining using Aw3.18 mAb. The CLSM images obtained revealed that the pHEL/I-A^k could be detected by surface staining. However, the pHEL/I-A^k signals were lost when intracellular staining was performed due to the staining protocol (Fig. 20). To optimize the intracellular staining protocol, different reagents for fixation, permeabilization and blocking were tested. Unfortunately, despite all efforts signals for pHEL/I-A^k were still poor and unspecific (data not shown).

To solve this problem, the C4H3 mAb was tested. C4H3 mAb has been reported to recognize the complex of HEL peptide 46-61 and MHC II molecule I-A^k (pHEL46-61/I-A^k) and was successfully used for IF staining of intracellular antigens in individual APCs.^{78, 79} Thus, surface and intracellular staining was performed by C4H3 mAb. As shown in Fig. 20, C4H3 mAb accumulated on the cell surface when the cells were not fixed, indicating that this mAb recognized the pHEL46-61/I-A^k presented on the cell membrane. When the specimens were fixed and permeabilized with 0.1 % saponin, the C4H3 signals appeared in the cytoplasm with a clear dot-like pattern, demonstrating that the C4H3 mAb can be used for intracellular staining of the pHEL46-61/I-A^k in C3H mouse derived BMDCs.

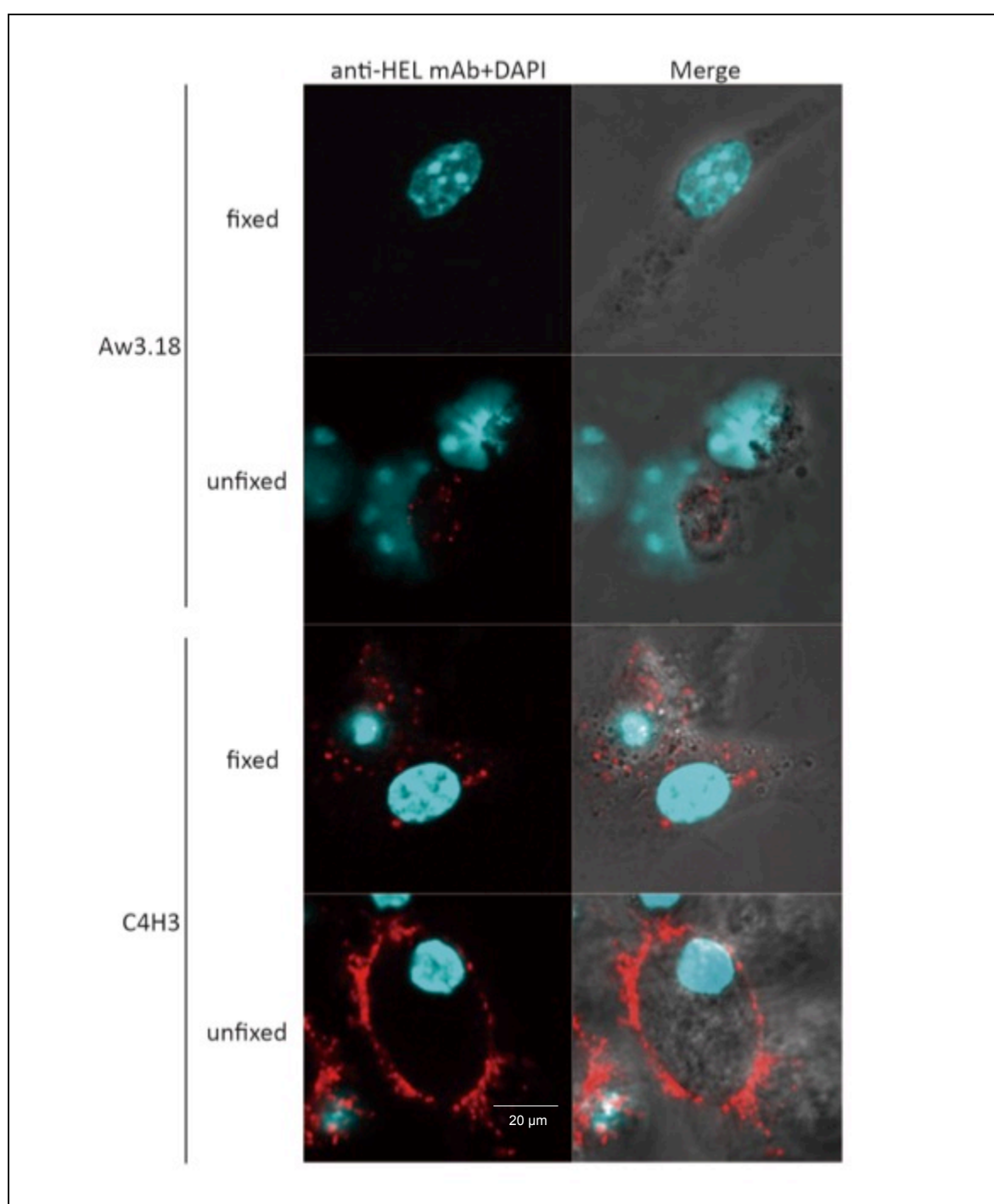


Figure 20. Comparison of pHEL/MHC II immunofluorescence by using Aw3.18 mAb and C4H3 mAb

BMDCs were co-incubated with 500 $\mu\text{g/ml}$ HEL protein at 37 $^{\circ}\text{C}$ for 16h and then cells were either washed twice with cold PBS and then stained with PE-Aw3.18 mAb or C4H3 mAb (1:200 dilution), or were fixed and then intracellularly stained with the two antibodies respectively. Alexa Fluor[®] 594 anti-rat antibodies were used as secondary antibodies for the detection of C4H3 mAbs staining. For unfixed samples, BMDCs were treated with 5 $\mu\text{g/ml}$ LPS when HEL protein was added to the cells, allowing a stronger presentation of pHEL-MHC II on the cell surface. Before observation, cells were mounted with DAPI containing mounting medium to stain the nuclei.

4.2.3.3 Self-produced C4H3 mAb additionally recognizes the pHEL46-61/I-A^k complexes

Next, a C4H3 mAbs producing hybridoma cell line was cultured and the antibodies containing culture supernatant was harvested. The freshly prepared and unpurified antibodies were tested for the capacity of intracellular staining. According to the publication by Zhong *et al.*, 3mg/ml instead of 500 µg/ml HEL protein were incubated with BMDCs from C3H mouse over night.⁷⁸ As shown in Fig. 21, using the unpurified antibodies (hybridoma supernatant), strong fluorescence signals that were similar to the pattern observed with purified C4H3 mAb could be detected. Therefore, the self-produced C4H3 mAb was used for intracellular staining in the following.

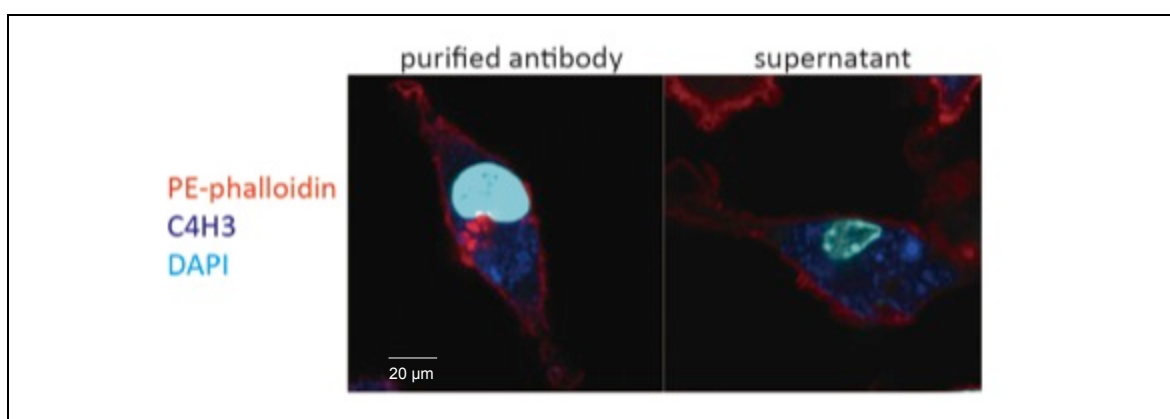


Figure 21. Intracellular staining of pHEL46-61/I-A^k by using purified C4H3 mAb or hybridoma supernatant

Three mg/ml HEL protein were co-incubated with BMDCs for 16h and then cells were fixed and stained with either purified C4H3 mAb (1:200) or hybridoma supernatant (1:1). After the primary antibodies staining were complete, samples were stained with Alexa Fluor® 647 anti-rat antibodies and PE-phalloidin (1:800 dilution) as a cell membrane marker. Before observation, cells were mounted with DAPI containing mounting medium to stain the nuclei.

4.2.4 Endogenously loaded pHEL46-61/I-A^k are present in BMDCs infected with MVA-HEL

From the above experiments, it has been proven that exogenous HEL proteins were endocytosed in BMDCs, and subsequently degraded into peptides. The epitope pHEL46-61 was loaded on MHC II molecules, which could be detected intracellularly by staining with the C4H3 mAb. To address the question if endogenous HEL antigens can be processed and presented by MHC II molecules, a recombinant MVA expressing HEL under promoter P7.5 (MVA-HEL P7.5) was generated and served as a vector to produce

endogenous HEL protein in infected cells. Therefore, the MVA-HEL P7.5 provides a tool to investigate the endogenous HEL presentation pathway.

A kinetic IF to detect pHEL46-61/I-A^k by using C4H3 supernatant was applied on BMDCs that were infected with MVA-HEL P7.5 from 2h to 8h (Fig. 22). At 2h p.i., the complexes were detected close to the nuclei in dots-like structures. Then as the infection lasted until 4h, the C4H3 signals became very strong and started to spread out in the cytoplasm. At 8h p.i., most of the pHEL46-61/I-A^k were detected on the cell surface. The dynamic observation showed that the complexes were transported from intracellular location where near the nuclei to cell membrane waiting to be recognized by T cells. These imaging results substantiate our hypothesis that the endogenous HEL antigen processing and presentation pathways exist in MVA infected APCs.

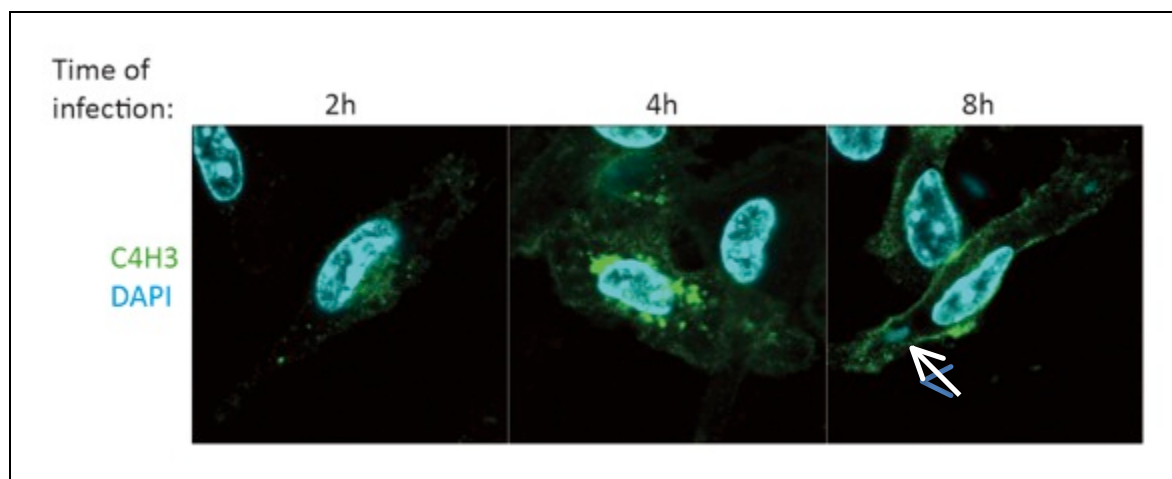


Figure 22. Kinetics of pHEL46-61/I-A^k expression in MVA-HEL P7.5 infected BMDCs

BMDCs infected with MVA-HEL P7.5 were analyzed at 2h, 4h and 8h p.i.. pHEL46-61/I-A^k were detected with C4H3 antibodies containing supernatant and then Alexa Fluor® 488 anti-rat secondary antibodies to show localization within the cells. DAPI was added to indicate the nuclei and viral factory (white arrow).

4.2.5 The presentation of pHEL46-61/I-A^k associates with MHC II

Additionally, the binding of HEL peptides to MHC II was examined by co-staining with the C4H3 mAbs containing supernatant and anti-MHC II antibodies. As depicted in Fig. 23, the C4H3 signals co-localized with MHC II in the cytoplasm that after 2h p.i.. Similar to the presentation process of pHEL46-61/I-A^k, MHC II was mainly visible on the cell surface at 8h p.i.. This co-localization pattern between the two signals strongly supported

the previous result that the pHEL46-61/I-A^k endogenous presentation was associated with MHC II.

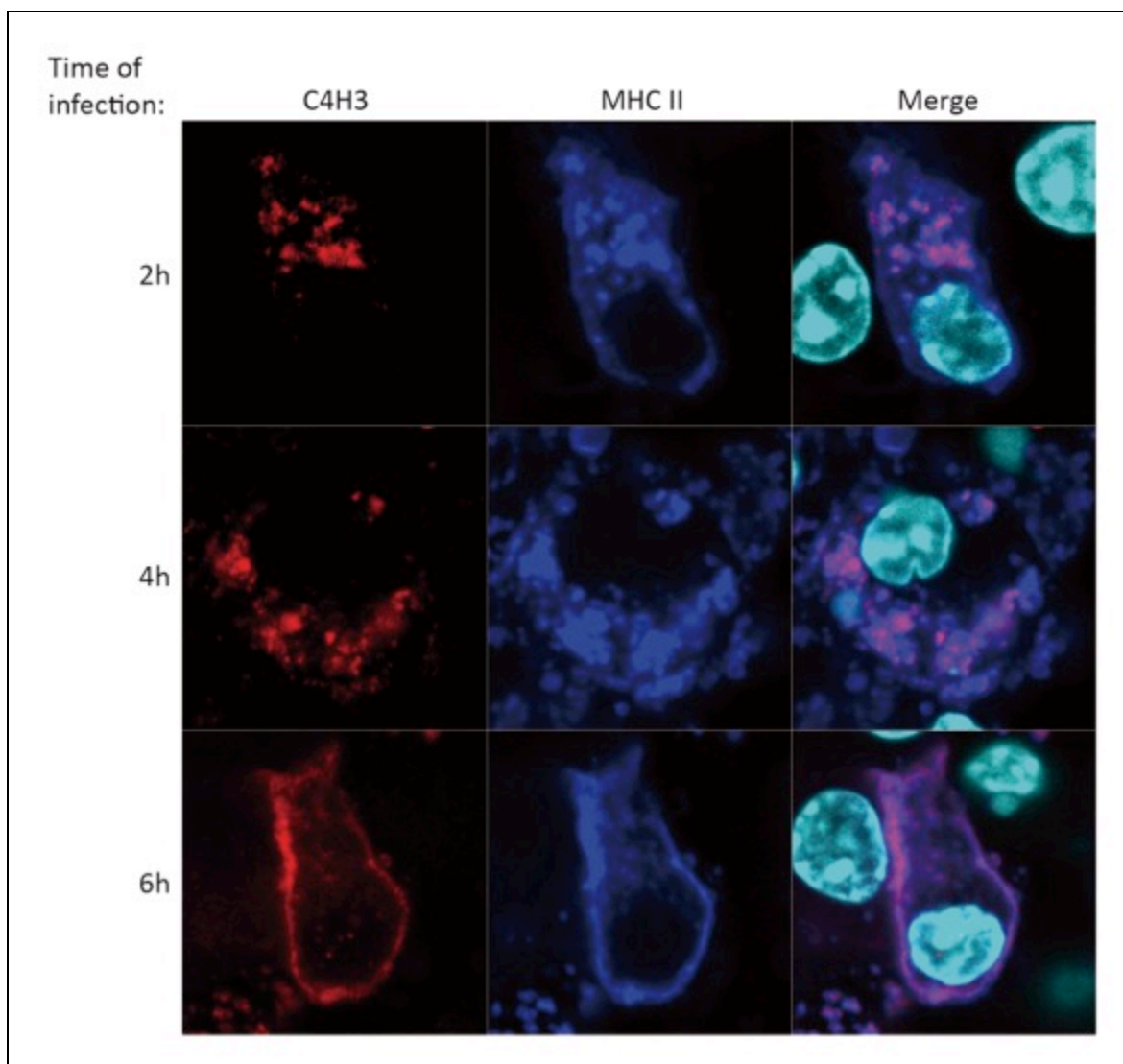


Figure 23. Co-localization of C4H3 and MHC II in MVA-HEL P7.5 infected BMDCs

BMDCs infected with MVA-HEL P7.5 were analyzed at 2h, 4h and 6h p.i., respectively. pHEL46-61/I-A^k were detected with C4H3 antibodies containing supernatant and then Alexa Fluor® 594 anti-rat secondary antibodies to show the localization within the cell. MHC II was stained by anti-MHC II antibodies and then Alexa Fluor® 647 anti-mouse secondary antibodies. DAPI was added to indicate the nuclei.

4.3 Detection of viral antigens and intracellular organelles by confocal laser scanning microscopy

The third aim of the study was to investigate the processing and presentation of viral antigens as well as to determine the cellular organelles that are likely to interact with these antigens during viral infection. To achieve these goals, fluorescence labeled antibodies, reporter gene plasmids, recombinant viral vectors and other tools were used in the relevant experiments. To monitor the dynamic process, kinetics was performed. The results obtained by CLSM for viral antigen transportation and the co-localization of antigens and organelles are presented in the following chapter.

4.3.1 Spatiotemporal distribution pattern of foreign gene expression under control of early or late promoters by recombinant MVA

4.3.1.1 EGFP expression pattern

In the recently described experimental setup, EGFP was used as a reporter gene to prove successful MVA infection by the expression of EGFP in the cytoplasm. However, it has not been examined what is the subcellular localization in the cytoplasm of EGFP when it is expressed under the MVA early or late promoter. Therefore, to investigate the spatiotemporal differences in EGFP under PK1L (early) or P11 (late) promoter, the semi-adherent-DC 2.4-a dendritic cell line, were infected with the two viral constructs, respectively, and analyzed at 3h, 5h, 9h and 15h p.i. (Fig. 24).

At 3h p.i., clear EGFP signals started to appear in the cytoplasm and in the nuclei of DC 2.4 cells infected with early promoter recombinant MVA, whereas only a focal EGFP signal could be detected with the late promoter recombinant virus. For EGFP expressed under the control of late promoter, the signal started to increase at 5h p.i., with increasing infection rate and fluorescence intensity up to 9h p.i. In general, both viruses were able to infect 50%-64% of the cells at 9h p.i. in this experimental condition (data not shown). The infection with the late promoter recombinant virus resulted in stronger EGFP signals compared to the early promoter recombinant virus at 9h and 15h p.i.. In addition, there was no particular spatiotemporal pattern of EGFP expression restricted to certain cellular compartments as EGFP was spread through out the entire cytoplasm. According to this result, it may be concluded that within 8h p.i., EGFP expression is expected to be

detected in the entire cytoplasm with no particular localization.

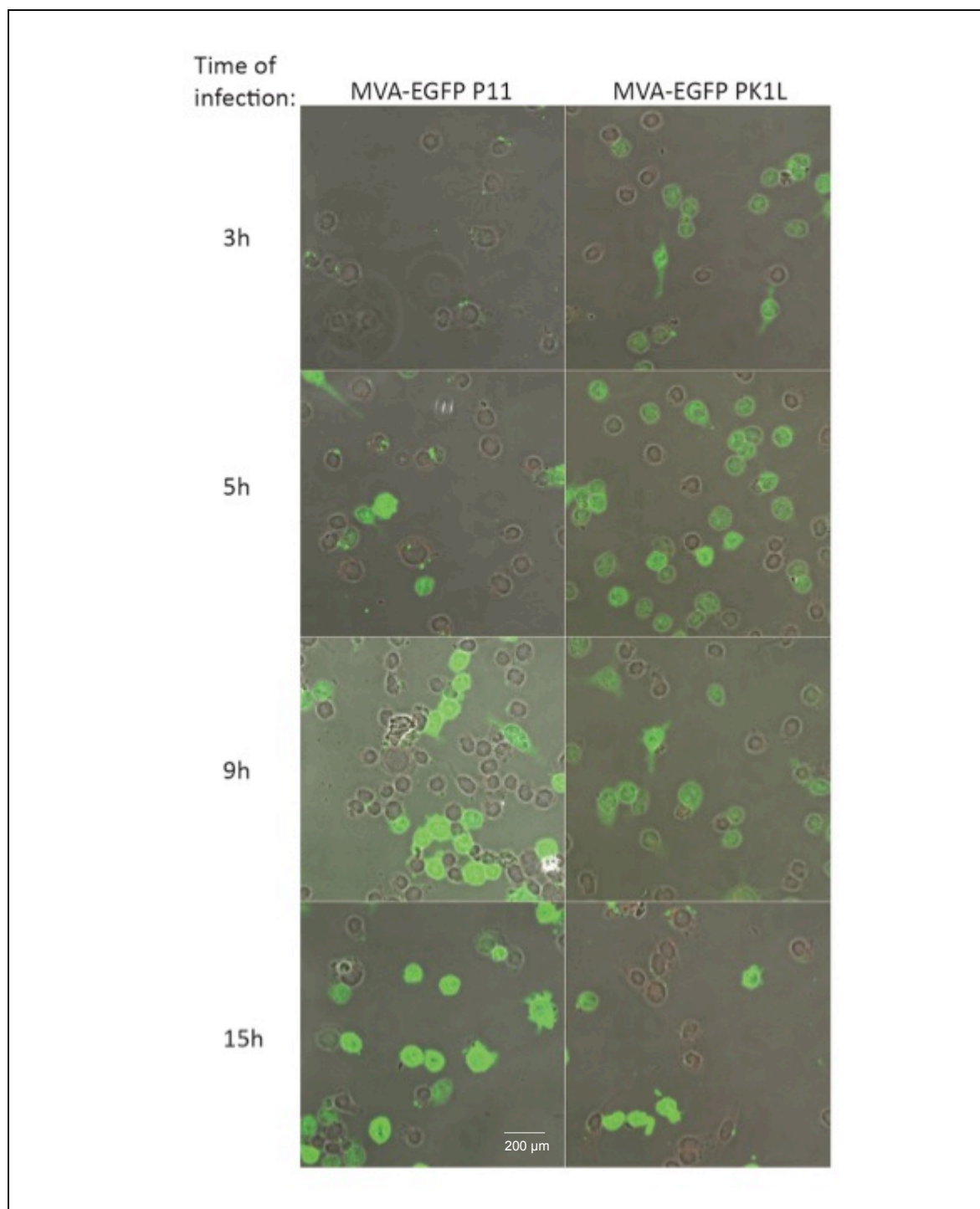


Figure 24. Detection of EGFP expression under the control of MVA early (PK1L) or late (P11) promoters

DC 2.4 cells were infected with MVA-EGFP PK1L or MVA-EGFP P11 (MOI 10 for both viruses) for the indicated time. Cells were fixed and analyzed by CLSM. To gain information on the general infection pattern, images were taken with low magnification.

4.3.1.2 OVA expression pattern

Another well established model antigen is full-length ovalbumin (OVA). OVA was expressed under the control of the early and late promoter P7.5 (MVA-OVA P7.5) in DC 2.4 cells (Fig. 25). To optimize the detection, anti-OVA primary antibodies concentrations were tested. Images indicated that a 1:200 dilution worked the best, showing a strong staining with low background. OVA fusion protein was detected spreading out in the entire cytoplasm. Additionally, no OVA co-localization with viral factory was found at 8h p.i., indicating no exclusive regions of OVA expression in the cytoplasm.

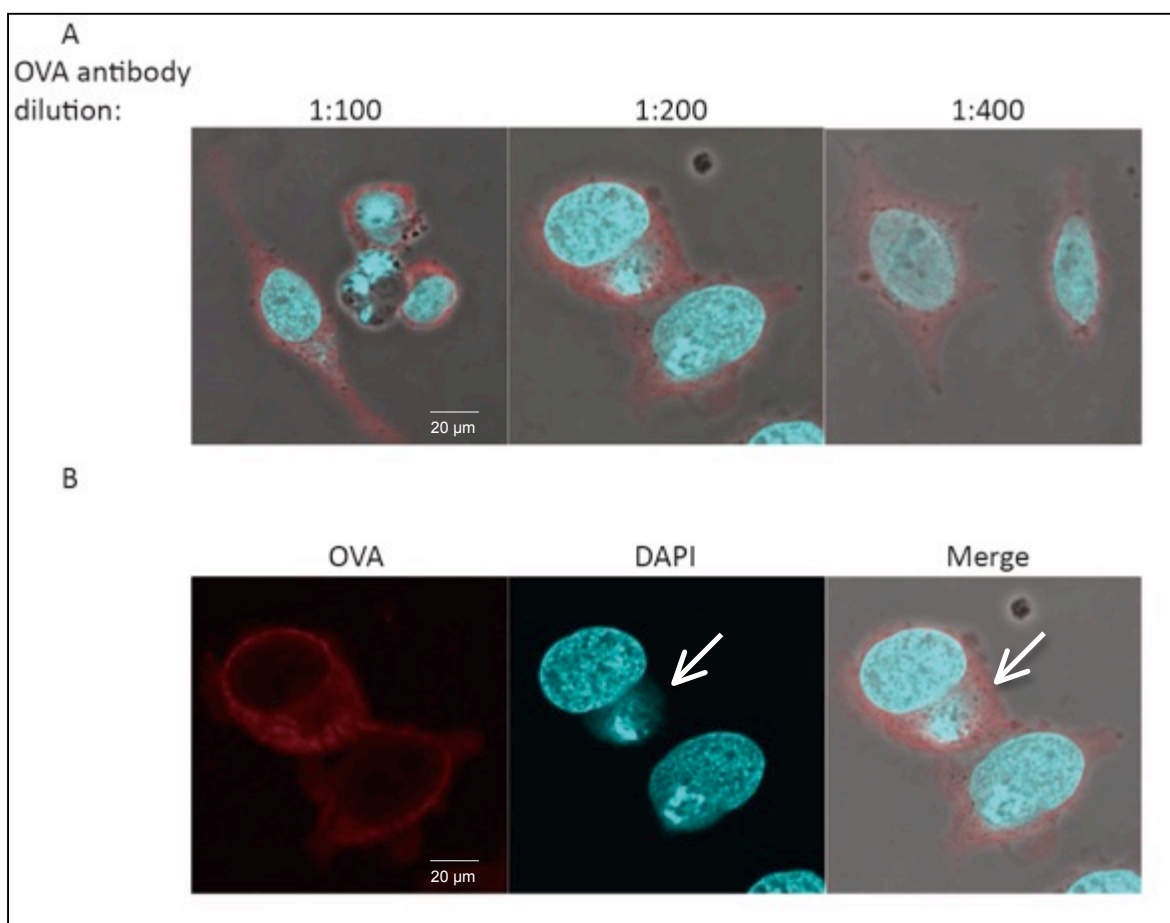


Figure 25. Characterization of recombinant OVA expression in the cytoplasm

A. DC 2.4 cells were infected with MVA-OVA P7.5 (MOI 10) for 8h. Specimens were incubated with anti-OVA primary antibodies diluted 1:100, 1:200 and 1:400 respectively. After washing, samples were stained with Alex Fluor® 594 anti-rabbit secondary antibodies. **B.** A sample stained with anti-OVA antibodies diluted 1:200 was analyzed for subcellular localization of OVA. DAPI stained for nuclei and viral factory (white arrow points to viral factory).

4.3.2 Spatiotemporal distribution pattern of viral antigens during infection

4.3.2.1 *H3 is present around viral factories and then transported to the cell membrane*

Since both foreign antigens EGFP and OVA were widely distributed in the cytoplasm, it is worthwhile to identify whether the viral backbone antigens have different localization patterns. H3, the envelope protein that binds to heparin sulfate on the cell surface, might be responsible to facilitate virion attachment to target cells. Previous data in our lab have shown that H3L₁₈₄-specific T cells were not able to recognize infected cells before 8h after infection.¹⁸ To determine the intracellular localization of H3, HeLa cells were infected with MVA-EGFP P 7.5 (Fig. 26).

H3 was first found around viral factories in MVA infected HeLa cells at 3h p.i.. The kinetics of H3 expression exhibited that this viral antigen was transported from viral factories to the cell periphery at 7h p.i.. This spatiotemporal district localization pattern of H3 may explain its function in the maturation of virion membranes and subsequent release of virions by cell lysis.



Figure 26. Spatiotemporal distribution of H3 in MVA-infected HeLa cells

HeLa cells infected with MVA-EGFP P7.5 (MOI 10) were observed at 3h, 5h, and 7h p.i., respectively. H3 was detected with anti-H3 primary antibodies and then Alexa Fluor® 594 anti-rabbit secondary antibodies to show the localization of H3 within the cells. DAPI was applied to stain the nuclei and viral factories (white arrow).

4.3.2.2 *A27 is present around viral factories only*

The structural protein A27, which is involved in the development of mature virions (MV) to form the wrapped virions (WV), was found to be mainly located around viral factories in MVA infected HeLa cells (Fig. 27). The kinetics of A27 expression revealed that unlike H3, no further transport of A27 to other cellular compartments took place. It has been reported that A27 protein binds to cell surface heparin sulfate and provides an anchor for A26 protein packaging into mature virions (MV), which plays an indirect role in MV-cell fusion.⁸⁰ However, MVA assembly is blocked at a late stage of infection in HeLa cells and immature virions (IV) accumulate,⁸¹ which could have resulted in A27 resting at the DNA replication site. From the above data, viral factories seem to have a central role for intermediate and late viral antigen synthesis and may represent the start line of distribution. Therefore, the following experiments focused on the location of viral factories within the cell and a possible connection with other antigens or organelles.

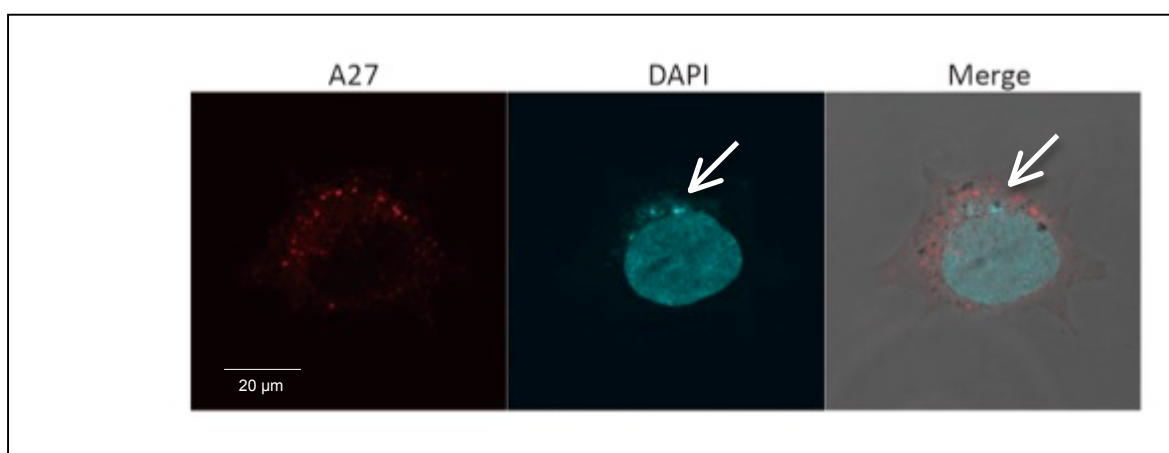


Figure 27. Characterization of viral antigen A27 localization in the cytoplasm

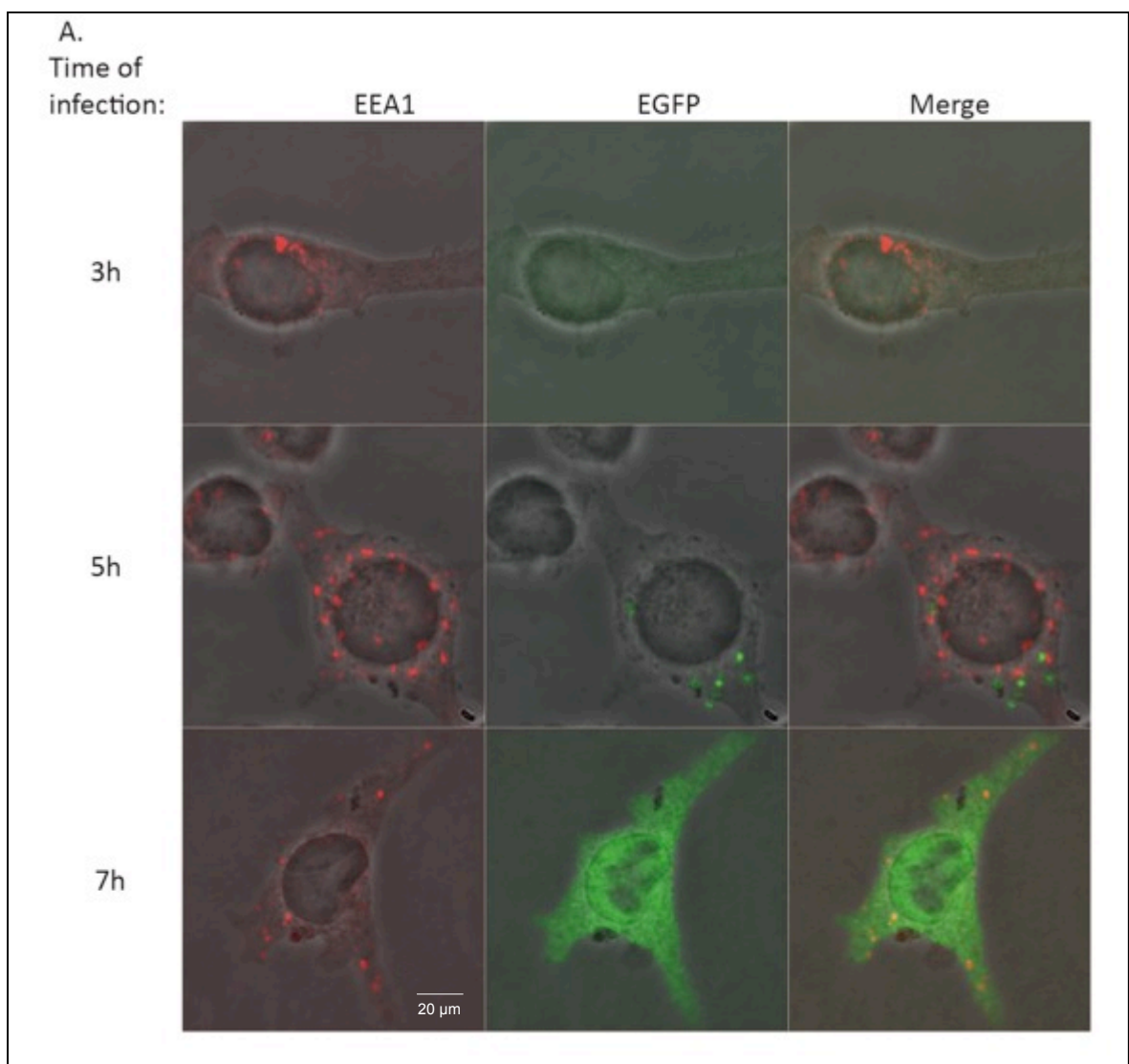
HeLa cells were infected with MVA (MOI 10) for 9h before observation. A27 was stained with anti-A27 primary antibodies and Alexa Fluor® 594 anti-rabbit secondary antibodies. DAPI was applied to stain the nuclei and viral factories (white arrow).

4.3.3 Cellular organelles undergo morphological changes upon infection

4.3.3.1 *Early endosomes do not co-localize with viral factories*

One of the most important antigen transport pathways from the plasma membrane to the MHC II containing compartment is via endosomes. Early endosomes receive endocytosed material and sort them for vesicular transport to late endosomes and lysosomes or for recycling to the plasma membrane.⁸² Exogenous antigens can be processed through this pathway and then be loaded onto MHC II, e.g. exogenous HEL protein was internalized in BMDCs and the pHEL-46-61 was detected in the cytoplasm as well as on the cell surface (see Fig. 20 and Fig. 21). Therefore, it is interesting to investigate if (early) endosomes are involved in the formation of endogenous viral peptide-MHC II complexes. DC 2.4 and HeLa cells were infected with MVA-EGFP P11 and then stained with the early endosome marker (EEA1). EEA1 localizes exclusively to early endosomes and has an important role in endosomal trafficking.

As shown in Fig. 27A, it was observed that EEA1 was distributed in dots-like pattern in the cytoplasm at all the time points. When EGFP started to be expressed at 5h p.i., there was no co-localization with endosomes (EEA1) and EGFP. At 7h p.i., the EEA1 signals located in the cytoplasm without significant location changes, while EGFP was spread out in the infected DC 2.4. HeLa cells were then co-stained with DAPI and EEA1 to investigate the connection between early endosomes and viral factories (Fig. 27B). During the infection (from 3h to 7h p.i.), no clear co-localization of the two compartments was detected. From the above data, it may be concluded that there is no direct contact of early endosomes with viral factories.



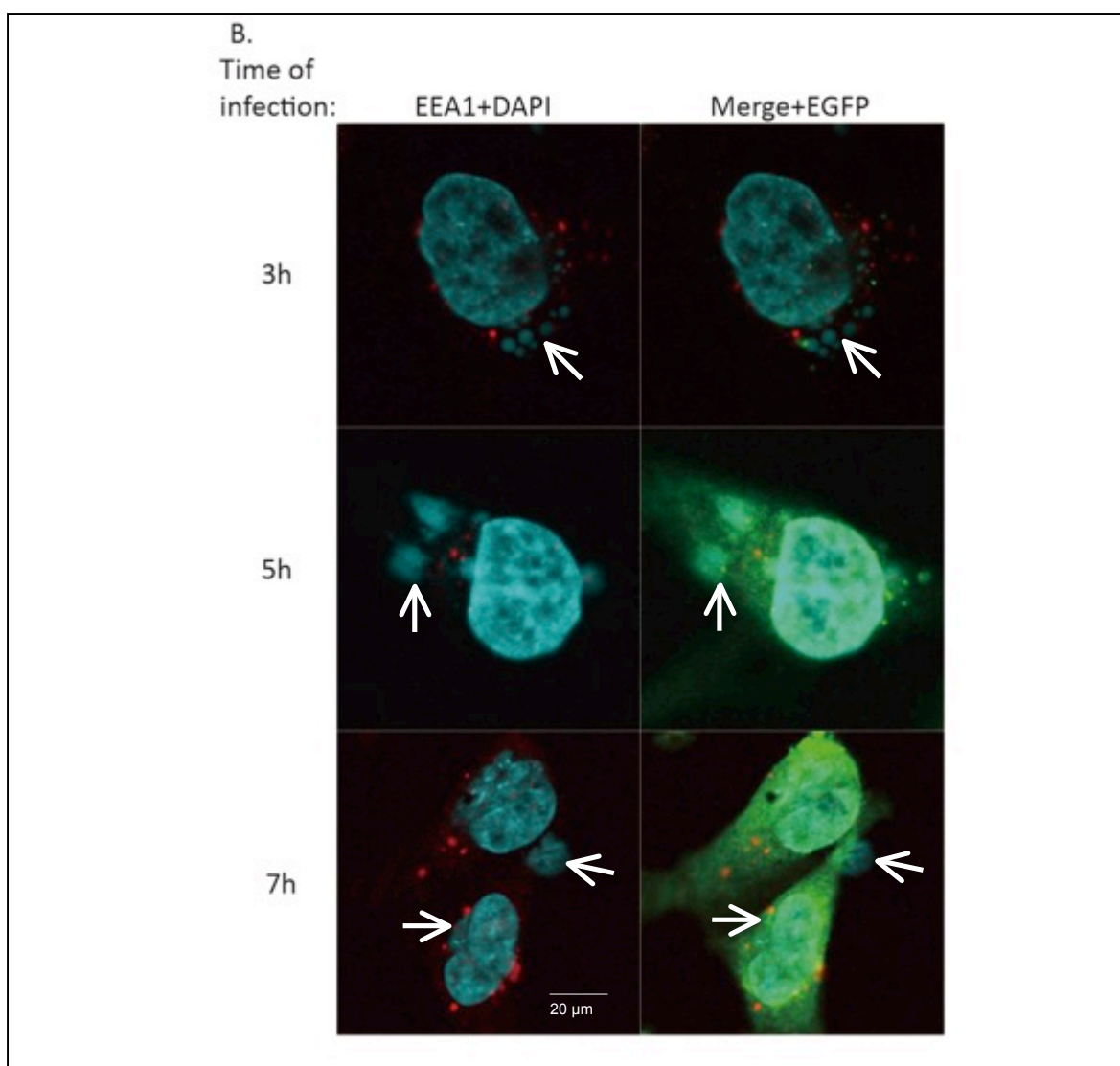


Figure 28. Kinetics of recombinant gene expression and localization of early endosomes in MVA infected DC 2.4 or HeLa cells

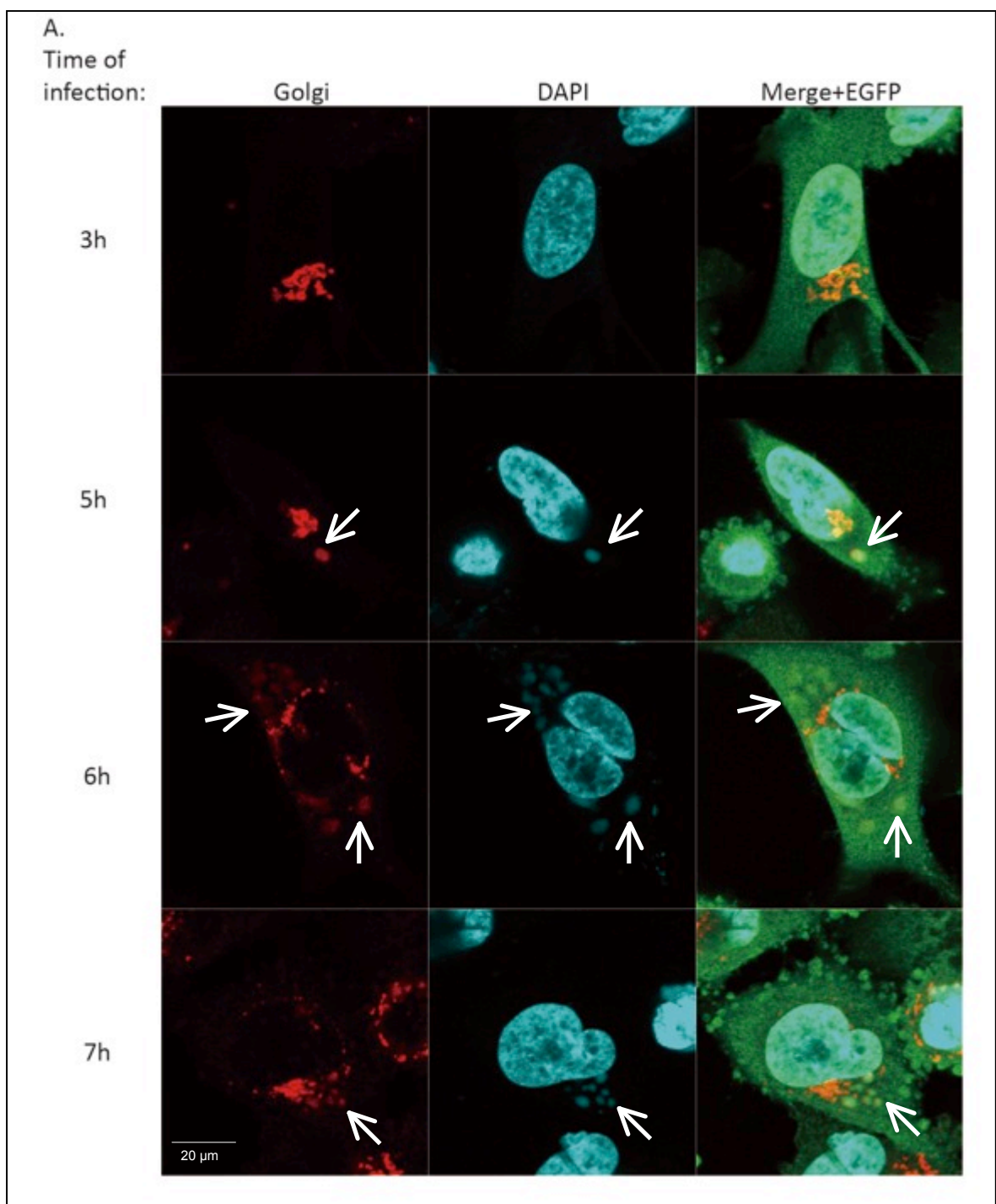
DC 2.4 (A) and HeLa cells (B) were infected with MVA-EGFP P11 (MOI 10). Early endosomes were stained with anti-EEA1 primary antibodies, followed by Alexa Fluor® 594 anti-rabbit secondary antibodies. Cells were observed at 3h, 5h, and 7h p.i., respectively. DAPI was applied to stain the nuclei and viral factories (white arrows).

4.3.3.2 *The Golgi complexes co-localize with viral factories*

The Golgi is integral in modifying, sorting and packaging cell synthesized macromolecules. Intracellular mature vaccinia virus virions are wrapped in cisternae derived from virus-modified trans-Golgi or endosomal membranes, and then transported via microtubules to the cell periphery.^{83, 84} To investigate the potential relation of Golgi complexes with viral

factories during MVA infection, the localization of Golgi complexes was monitored in MVA-EGFP P7.5 infected HeLa cells or BMDCs from 3h to 7h p.i..

In all the pictures taken, Golgi was found to be close to or to surround the nuclei. In the infected HeLa cells (6h and 7h p.i., Fig. 29A), more Golgi bodies were formed compared to 3h and 5h p.i., suggesting that Golgi was required for viral products genesis. The first co-localization (white arrow) of Golgi and viral factories in HeLa cells was detectable at 5h p.i., while in BMDCs this overlapping was already seen at 3h p.i. (Fig. 29B), suggesting that the virus has an earlier DNA replication behavior in APCs. As infection was going on, the observed co-localization was more prominent in both cell types. At 7h p.i., viral factories almost completely overlapped with Golgi in BMDCs. Of note, it was observed that viral factories expanded in the size during the infection process in BMDCs.



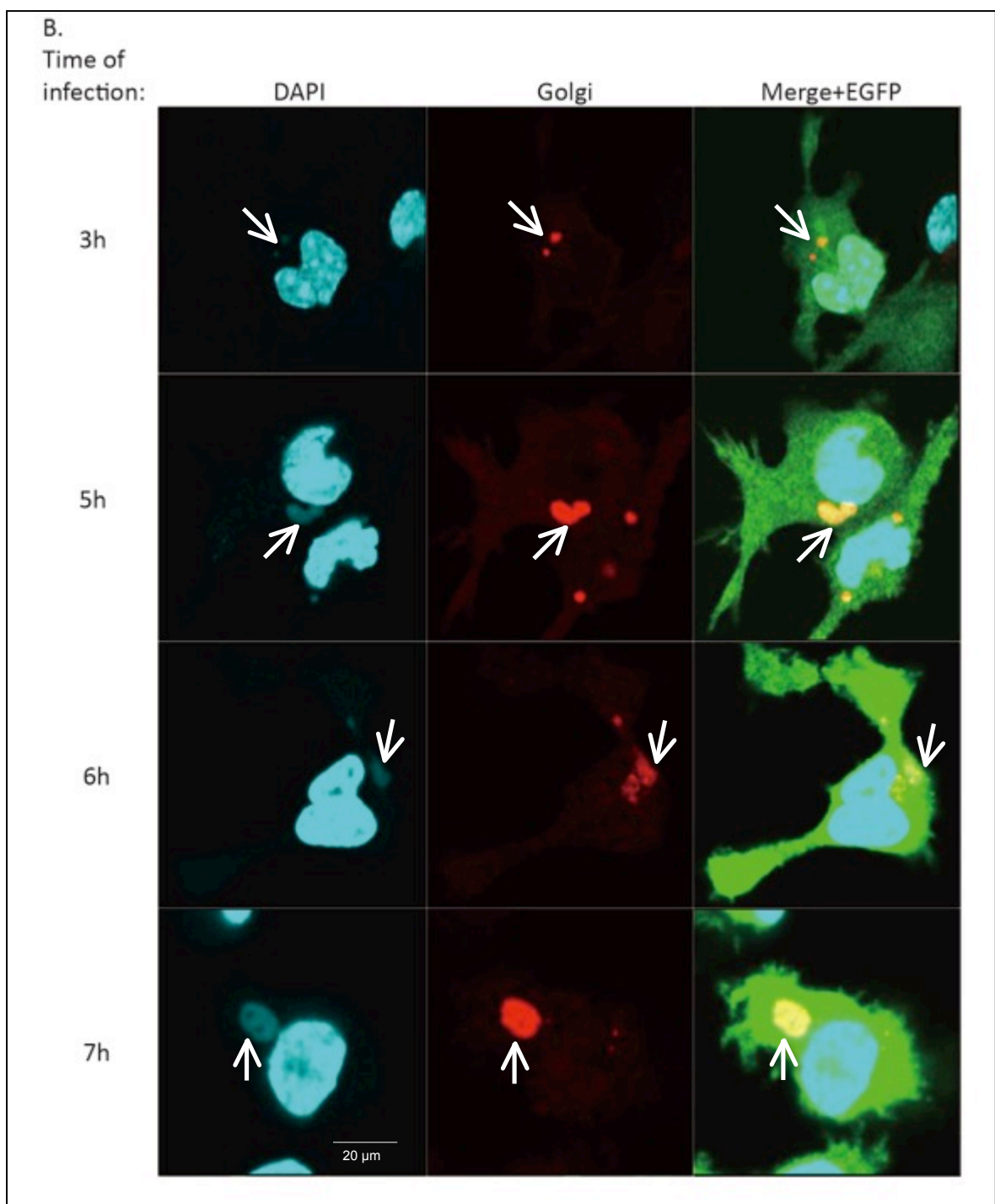


Figure 29. Temporal distribution of Golgi complexes and viral factories in infected HeLa cells or BMDCs

HeLa cells (A) and BMDCs (B) were infected with MVA-EGFP P7.5 (MOI 10) from 3h to 7h p.i.. GOLGH 4 was used as a Golgi marker and subsequently detected by staining with Alexa Fluor® 594 anti-rabbit secondary antibodies. Viral factories (white arrow) and nucleus were stained with DAPI.

4.3.3.3 *Detection of the MHC II containing compartment (MIIC)*

4.3.3.3.1 **MIIC transforms into a large tubular structure only upon MVA infection**

To form peptide/MHC II complex, Ii occupies the groove of MHC II molecules until they arrive in MIIC, where in the presence of HLA-DM, CLIP is released, allowing appropriate length of peptides to bind MHC II. Therefore, MIIC is a very important cellular compartment to investigate peptide/MHC II complex formation throughout MVA infection. To detect the localization of MIIC, HLA-DM was used as a specific marker in immunofluorescence.

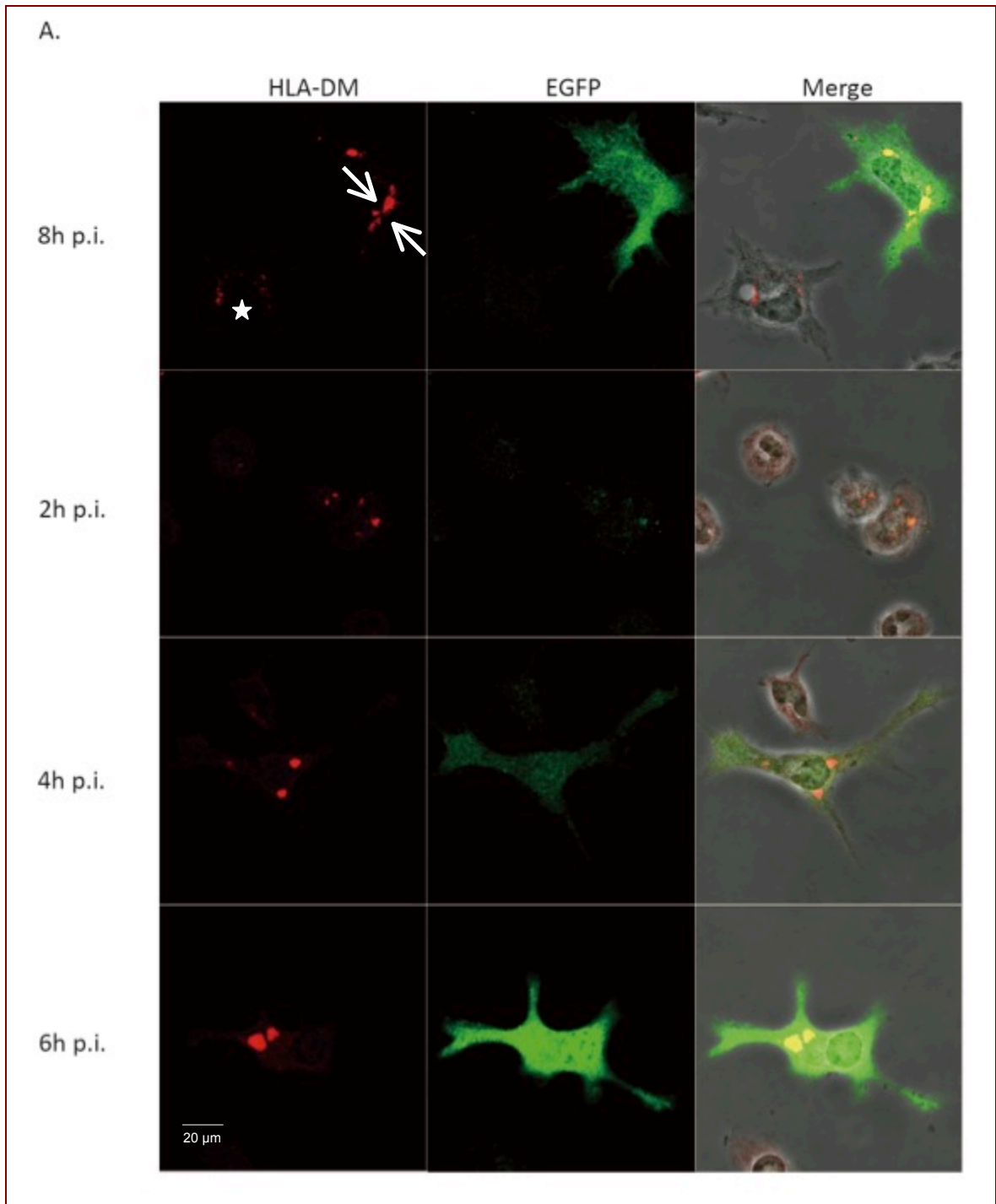
In MVA-EGFP P11 infected BMDCs, it was found that MIIC transforms from dots-like structures in uninfected cells (Fig. 30A, white asterisk) into large tubular structures in infected cells (Fig. 30A, 8h p.i. and C, white arrow). Furthermore, the dynamic process of MIIC transformation was monitored. In cells infected for 2h (no EGFP), only few and small sized MIIC was seen. After 4h p.i., EGFP expression in the cytoplasm started and the size of MIIC became bigger and the distance between individual MIIC was decreased. Whereas at 6h p.i., the enlarged MIIC was not only 2 to 3 fold the size of that in 2h p.i. cells, and also exhibited a trend to fuse, indicating that the MIIC gradually transform into reticular network in response to MVA infection. (Fig. 30A).

Next, the cause of the enlarged and tubular structure of MIIC was investigated. To analyze if this transformation is the byproduct of the maturation process of BMDCs, the cells were treated with LPS for 6h to trigger the maturation (Fig. 30B). Interestingly, disconnected and spherical MIIC were found in LPS stimulated cells, which was similar to the pattern observed in mock-treated cells. These results indicated that the change of MIIC from dots-like/spherical formations to large tubular structures are unique for MVA infection.

4.3.3.3.2 **MIIC co-localize with viral factories**

To investigate the relationship between MIIC and viral factories, co-staining of HLA-DM and DAPI was performed in MVA-EGFP P7.5-infected BMDCs (Fig. 30C). Strikingly, viral factories were nicely co-localized with the enlarged tubular structures of MIIC at 8h p.i.. Considering the observation that the Golgi complex overlapped with virus factories and the fact that processing of MHC II molecules and HLA-DM synthesis also require the

function of Golgi complex, it may be anticipated that MIIC-viral factories-Golgi complex triple co-localization was a consequence of the viral infection.



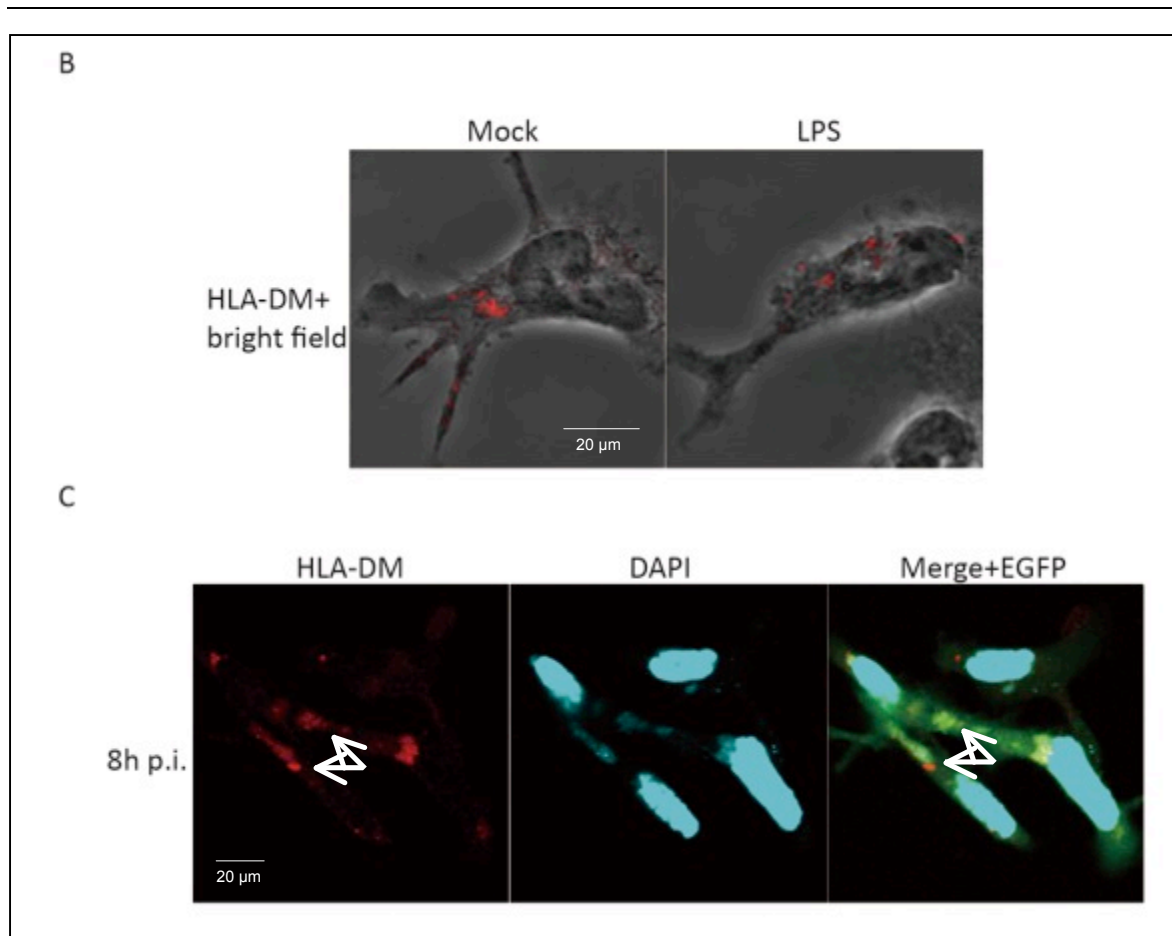


Figure 30. Monitoring the MIIC transformation upon MVA infection or LPS stimulation

A. BMDCs were infected with MVA-EGFP P7.5 (MOI 10) for 2h, 4h, 6h and 8h, respectively. **B.** BMDCs were either treated with 10 μg/ml LPS for 6h or mock treated. **C.** BMDCs were infected with MVA-EGFP P7.5 (MOI 10) for 8h. MIIC was stained with the specific marker HLA-DM and subsequently detected with Alexa Fluor® 594 anti-rabbit secondary antibodies. DAPI was applied to stain the nuclei and viral factories. Viral infection was represented by EGFP expression. White arrows point out the location of tubular MIIC. The white asterisk indicates normal MIIC in uninfected cells.

4.3.3.4 *MHC II co-localize with MIIC and then move on to the cell surface during cell maturation*

When investigating the cellular distribution of MHC II, it was observed that both LPS treatment and MVA infection induced the maturation of BMDCs, leading to the translocation of MHC II to the cell surface (Fig. 31A). In immature cells, MHC II localized in cytoplasm as well as on the cell surface. When cells received a bacterial or viral stimulus, the majority of MHC II presented to the cell membrane. During MHC II transport, MHC II was found to be located close to or partially co-localized with MIIC (Fig.

31B). This result might suggest that viral peptides replace Ii to bind on MHC II in the MIIC, leading to presentation of the peptide/MHC II complexes on the cell surface waiting for the recognition by CD4⁺ T cells.

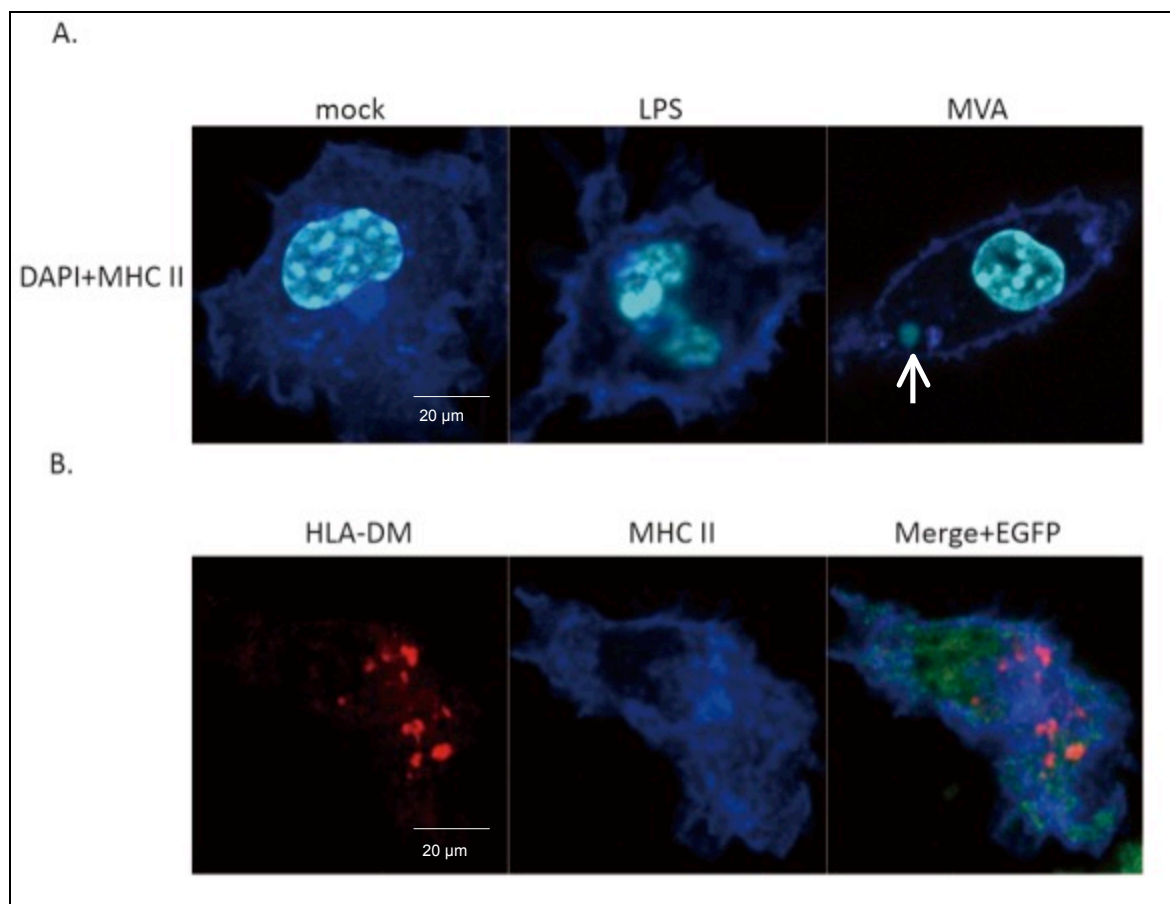


Figure 31. Transport of MHC II during the maturation of BMDCs

A. BMDCs were either mock-treated or incubated with LPS (10 μg/ml) for 6h, or infected with MVA-EGFP P7.5 (MOI 10) for 8h. MHC II was stained with anti-MHC II primary antibodies and then Alexa Fluor® 647 anti-mouse secondary antibodies. DAPI was used to stain the nuclei and viral factory (white arrow). **B.** BMDCs were infected with MVA-EGFP P7.5, MHC II was stained with the anti-MHC II primary antibodies and subsequently detected with Alexa Fluor® 647 anti-mouse secondary antibodies. Viral infection was represented by EGFP expression.

4.3.3.5 MHC II co-localizes with lysosomes

The above experiments have already shown that the MIIC have specific spatial organization which is transforming during MVA transfection. MHC II was also observed to co-localize with MIIC and then to be rapidly distributed to the cell surface in infected BMDCs. To gain a better understanding of this process, C57BL/6 mouse primary dermal

fibroblasts were generated. These primary cells may be regarded as APCs under inflammatory conditions. They possess expanded amounts of cell plasma that BMDCs are lacking, thus giving better cellular structure images. MHC II and LAMP-2 were co-stained in MVA-EGFP P7.5 infected fibroblasts to observe the interaction between MHC II and lysosomes.

As shown in Fig. 32, large amounts of MHC II and lysosomes were detected in the cytoplasm, which were intensively overlapping with each other when EGFP had not yet spread in cytoplasm. In chapter 4.1.2, it has already been demonstrated that the autophagosomes fuse with lysosomes. Therefore, the co-localization of MHC II-lysosomes-autophagosomes powerfully supports our previous finding that MVA-induced autophagy can facilitate the processing and presentation of endogenous viral peptides by MHC II.

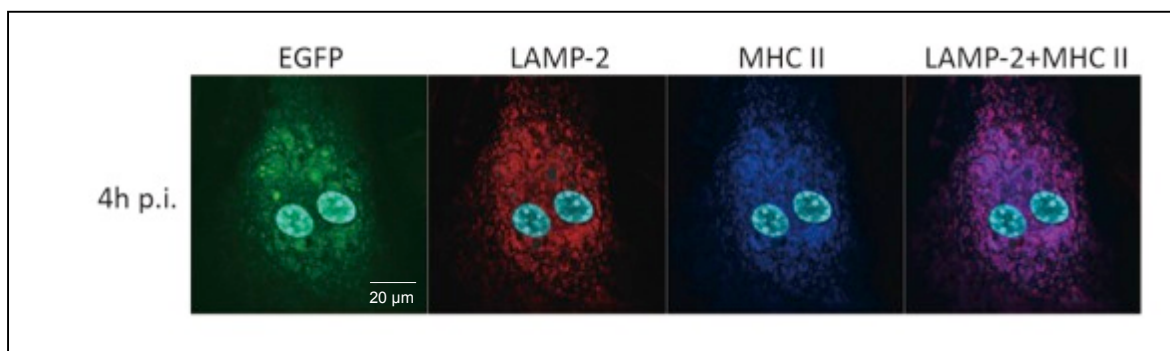


Figure 32. MHC II co-localizes with LAMP-2

Murine primary dermal fibroblasts were cultured for 7 days until they reached 80% confluency. Cells were infected with MVA-EGFP P7.5 (MOI 10) for 4h. Lysosomes and MHC II were detected with the anti-LAMP-2 and anti-MHC II primary antibodies respectively, and subsequently stained with Alexa Fluor® 594 anti-rabbit secondary antibodies against LAMP-2 and Alexa Fluor® 647 anti-mouse antibodies against MHC II. DAPI was used to stain the nuclei and viral factories.

5. Discussion

5.1 Autophagy is important for MVA-related MHC class II antigen processing and presentation

Recent *in vitro* data in our group showed that activation of CD4⁺ T cells stimulated by MVA antigens from MVA infected BMDCs was hampered by the inhibition of autophagy in those APCs. Particularly, the decreased T cell response was more prominent against the late viral antigens than against the early ones (Thiele, unpublished data). These findings suggest that autophagy may be involved in MVA antigen presentation by MHC II, though the underlying mechanism remains elusive. As autophagy delivers cytosolic material to lysosomes for degradation, it can be assumed that APCs (e.g. BMDCs) direct the autophagy machinery against viral infection by promoting the survival rate of infected cells through activation of the innate immune system (e.g. delivery of the respective TLR ligands to endosomes), or by feeding MHC II the peptides to induce a T cell response for the adaptive immunity.⁸⁵ Of note, the function of autophagy aiming to clear cytosol-invading microbes is referred to as “xenophagy”, which is considered as an important component of the innate immune system.⁸⁶ Thus, investigating the mechanisms of autophagy-mediated viral antigen presentation, especially for endogenous antigens presented by MHC II, might highlight new aspects of this essential pathway.

5.1.1 Methods and limitations to monitor autophagy in BMDCs

To demonstrate the status quo of autophagy within a cell, it is essential to identify the criteria, which determine the occurrence of an autophagic process. Unfortunately, it is a “moving target” as the field evolves very quickly and there are no generally applicable criteria that fit in every experimental setup to address particular cells, tissues or organisms. Accordingly, several independent methods should be combined to allow for a more reliable interpretation of this dynamic process.^{68 54, 87}

5.1.1.1 Interpretation of LC3-turnover analysis by immunoblotting

Western blot analysis of LC3 expression is the most widely used method to determine autophagosome formation.⁵⁴ This method detects a rather early step in this process and to some extent reflects the initiation of autophagy. LC3-I is an ubiquitin-like protein that can be conjugated to phosphatidylethanolamine (PE) to become LC3-II. Although the molecular weight of LC3-II (18kD) is larger than that of LC3-I (16kD) because of PE conjugation, the apparent size of LC3-II on an SDS-PAGE is around 14 kD, which is smaller than that of LC3-I with a size of around 16 kD. This contradictory phenomenon is due to the extreme hydrophobicity of the PE molecule so that LC3-II runs faster than LC3-I.⁶⁹ Caution should be raised that LC3 conversion from LC3-I to LC3-II only represents the protein lipidation, which is only the primary step of autophagosome formation. LC3 processing actually defines a functional autophagy.⁶⁹ Inhibition of autophagosomes' fusion with lysosomes or loss of degradative function of lysosomes can also result in a similar high level of LC3-II, because it inhibits LC3-II degradation or its recycling from the membrane of autophagosomes.⁶⁹ Hence, the measurement of the LC3-II turnover by western blot analysis needs to include experimental control in the presence or absence of lysosomal protease inhibitors or lysosomotropic agents, such as chloroquine or bafilomycin A1. Only when the LC3-II further accumulates in the presence of a suitable inhibitor, the conclusion of the upregulation of autophagy can be drawn. In line with this, when chloroquine was applied in MVA or VACV infected cells (Fig. 6B and Fig. 7), it could be demonstrated that the increase of LC3-II is not because of a halted degradation.

In yeast, the amounts of Atg8, the homologue of LC3, increases at least 10 fold upon the induction of autophagy.⁸⁸ However, in mammalian cells the total amount of LC3 may remain unchanged under the same condition because of increased conversion from LC3-I to LC3-II or fast degradation of LC3-II being delivered to lysosomes. Hence, determine the kinetics of the LC3 turnover is necessary to monitor the autophagosome formation during MVA infection. Since the VACV/MVA replication cycle is completed within 8h p.i., the kinetics of LC3 turnover was chosen within the first 8h p.i. accordingly in Fig. 6. LC3 expression increased gradually during the time of infection, clearly demonstrating that MVA-induced autophagy is a constitutively active process. It is possible that LC3-II will increase relative to LC3-I after 8h p.i., because MVA infection interferes with host cellular translation machinery which would selectively inhibit the host protein synthesis (Thiele, unpublished data), which might leading to a rapid shut down of newly synthesized LC3-I.

In comparison, actin as a long-life protein is required by VACV to induce actin-based viral motility, has a general half-life of 48h.^{89,90} Thus, it is more accurate to calculate the ratio of LC3-II to β -actin than LC3-II to LC3-I if LC3-I is not abundant in the cells or tissues analyzed.

5.1.1.2 *Dissection of autophagy maturation by EGFP/mRFP-LC3 lysosomal delivery and proteolysis*

Autophagic activity does not just include the increased synthesis or lipidation of LC3-II, or an increase in the formation of autophagosomes, but most importantly the enhanced autophagic flux. Only if the entire system is functional, the engulfed materials can be finally delivered to lysosomes for degradation. Moloughney *et al.* found that VACV infection led to massive LC3 lipidation, but devoid of autophagosome formation and autophagic flux in the virus infected cells.⁹¹ Hence, autophagic substrates need to be monitored to verify that they have reached the autolysosomes and become degraded. This process is also referred to as autophagy maturation.

Due to different stability in the lysosomal environment, mRFP-LC3 and EGFP-LC3 exhibit distinct detection patterns when autophagosomes undergo maturation, which can be utilized for dissecting the status of the autophagic flux.⁷⁴ However, it may be problematic to only count the number of EGFP-LC3 punctae, as in infected cells new EGFP-LC3 is being synthesized when earlier produced EGFP-LC3 is degraded within autolysosomes. This probably explains the prominent increase of LC3-II at 4h p.i., which was detected by western blot (Fig. 6), while no corresponding increase in EGFP-LC3 punctae was observed by microscope analysis (Fig. 11). A possible solution to circumvent this effect is the application of chloroquine in cells transfected with EGFP-LC3 expression plasmids. In this case, EGFP-LC3 cannot be degraded because the access to lysosomes is blocked. As a result, the number of the green fluorescent punctae was markedly increased in MVA-infected cells, which had been treated with chloroquine (Fig. 11 6h and 8h p.i.). In contrast, the metabolism of EGFP-LC3 in MVA infected samples revealed the increased amount of LC3 proteins at 6h p.i., while decreased LC3 at 8h p.i. as they were delivered to autolysosomes for subsequent degradation.

Another alternative is co-localizing the mRFP-LC3 with a lysosomal marker, such as LAMP-2. It is known that GFP has a relatively higher pKa value (pKa=6.2) than mRFP

(pKa=4.8), suggesting that mRFP is resistant to the acidic lysosomal environment.^{74, 92} Although, co-localization between mRFP-LC3 with LAMP-2 is not sufficient to demonstrate the proteolysis of autophagic substrates in autolysosomes, it directly proves the fusion between autophagosome and lysosome. In Fig. 12, an obvious increase in mRFP-LC3 punctae co-localized with LAMP-2 was seen, supporting two previous results: 1) mRFP-LC3 accumulation induced by viral infection is in line with the increase of LC3 lipidation detected by western blot analysis. 2) mRFP-LC3 delivery to lysosomes corresponds to the decreased amount of EGFP-LC3 punctae during autophagy maturation.

One should be careful that when EGFP-LC3 was overexpressed by transient transfection, large amounts of fluorescent dots were observed without any relation to autophagy, indicating that EGFP-LC3 can form aggregates independently of autophagy.⁷⁰ Thus, to circumvent this experimental drawback, the use of EGFP-LC3 transgenic mice or cell lines either stably expressing EGFP-LC3 or mutated EGFP-LC3, which lacks the capacity to form these artificial aggregates is recommended.⁷⁴ To generate transgenic mice that express EGFP-LC3 in dendritic cells might fulfill our experimental requirements, but it is a time-consuming work. Therefore, to exclude or minimize the false positive signals derived from artificial aggregates due to over expression, the time point after transfection for analysis (Fig. 9) as well as the amount of the plasmid used for transfection (data not shown) were carefully determined in time and dose-dependent experimental evaluation. It was shown that the aggregation effect can be diminished by a low amount of plasmid DNA and also the time of analysis after transfection was important. A strong background was observed when the samples were analyzed earlier than 16h post transfection, while after 24h, the fluorescence signals were below the detection limit.

In addition, the effective chloroquine concentration that was not toxic to BMDCs and HeLa cells was determined, because this chemical inhibitor which has been used for an anti-malarial drug has broad biological effects.⁹³ The well-known effects of chloroquine include radiosensitizing through lysosome permeabilization⁹⁴ and chemosensitization by inhibition of ATP-binding cassette transporters.⁹³ Fan *et al.* reported that chloroquine increased the volume of lysosomes at low concentration (from 0.25 to 32 μ M), and induced cell apoptosis and necrosis at higher concentration (64 to 128 μ M), exerting an anti-tumor effect in A549 lung cancer cells.⁹⁵ In line with this, as shown in Fig. 11 that application of 100 μ M of chloroquine lead to strong cytotoxicity, while the accumulation of LC3 is not

clear when chloroquine was used at a lower concentration of 25 μ M. In conclusion, in order to establish the transient transfection of fluorescence-tagged LC3 plasmids as a reliable method in the research of autophagic flux, the dose of plasmid DNA and the time frame of observation as well as the concentration of chloroquine should be carefully optimized. Secondly, this system works well in the experimental setup described here and the microscope data nicely support the immunoblotting results.

5.1.2 Both MVA and VACV infection activate autophagy in BMDCs

5.1.2.1 *Atg7 is required for MVA induced autophagy in BMDCs*

It is thought that the E1 enzymatic activity encoded by *Atg7* is essential for autophagy involving the ubiquitin-like protein *Atg8*.⁹⁶ However, Chang *et al.* provide evidence that an *Atg7*- or *Atg3* independent autophagy pathway exists that facilitates programmed reduction of cell size during intestine cell death.⁹⁷ Nishida *et al.* showed that mouse embryo fibroblasts (MEFs) lacking *Atg5* or *Atg7* are able to form autophagosomes/autolysosomes, though the conversion of LC3-II cannot occur, suggesting an *Atg5/Atg7* independent alternative mechanism of autophagy.⁹⁸ These reports show that autophagy can occur independently of certain *Atg* proteins. Whether VACV, the wild-type virus strain, can induce autophagy or if autophagosome formation requires the expression of *Atg7* in VACV/MVA infected cells remains controversial. It was reported that VACV infected ovarian cancer cells induce marked lipidation of LC3 proteins, but there is no general activation of the autophagic process.⁹⁹ Massive LC3 lipidation was observed in mouse fibroblast cells upon VACV infection but this was independent of *Atg5* and *Atg7*, which suggested an incomplete autophagy.⁹¹ Deng's group showed that the infection of macrophages and conventional DCs with MVA but not VACV triggers autophagy formation and that the LC3 turnover is dependent on *Atg5* (information taken from XIX Poxvirus, Asfarvirus & Iridovirus Conference, Salamanca 2012).

In the present study, the immunoblotting analysis showed that the LC3-II bands were almost absent in BMDCs derived from *Atg7* conditional deficient mice, which were infected with MVA or subjected to nutrient starvation (Fig. 8). Furthermore, VACV induced LC3-II upregulation was also devoid in *Atg7* deficient BMDCs. These results demonstrated that *Atg7* is required for LC3 turnover induced by VACV or MVA infection in BMDCs. These controversial data can be reasoned with different cell types used in

the respective experimental settings, because autophagy is a conserved protective cell function that affects many cell types. For example, apparent induction of LC3-II in MEFs is detected after 30 min starvation,⁶⁹ whereas in the comparable condition it takes 4h in BMDCs to induce LC3-II lipidation (Fig. 10). Therefore, it is reasonable to assume that there is another unknown factor assisting LC3-II lipidation in a very short time in MEFs, which are reported to have an Atg5-/7- independent autophagy pathway.⁹⁸ In further, the investigation of the role of Atg7 in MVA-induced autophagy can be extended to the analysis of antigen presentation ability, such as comparison of the CD4⁺ T cell responses against the MVA infected Atg7-deficient and wild-type BMDCs.

5.1.2.2 *MVA infection induces stronger autophagy than VACV infection*

In this study, it has been found that VACV was able to induce LC3-I conversion to LC3-II, though it was less efficient than MVA (Fig. 7). Moreover, LC3 lipidation is aborted in both VACV and MVA-infected MyD88-deficient BMDCs, indicating that both viruses may use the same machinery to activate autophagy. However, the ancestor VACV was much attenuated to generate MVA, thus the host range gene in VACV that may suppress autophagy induction could be lost in the MVA genome. MVA induces apoptosis in human DCs earlier than VACV due to the earlier downregulation of Bcl-2 and Bcl-xL in MVA-infected cells than VACV.³⁴ The anti-apoptotic family members Bcl-2, Bcl-xL and Bcl-w, are known as cell death regulators controlling the intrinsic apoptotic pathway in mitochondria by inhibiting mitochondrial depolarization in order to prevent the release of apoptogenic factors.¹⁰⁰ Additionally, the Bcl-2 homology (BH) domain 3 (named BH3 domain) of Beclin-1 can bind to the BH3-binding groove present in the Bcl-2 protein, so that Bcl-2 blocks the formation of the Beclin-1/PIK3C3 complex to inhibit autophagosome formation.¹⁰¹ In the therapeutic design for Alzheimer's disease, small molecule drugs which can prevent the binding of Bcl-2 to Beclin-1 are considered as promising candidates because they can promote autophagy.¹⁰² Hence, differences in the genomic background between MVA and VACV as well as the finding discussed above that the earlier downregulation of anti-apoptotic proteins in MVA-infected cells occurs earlier, could provide some explanations of why MVA induces stronger autophagy than VACV.

5.1.3 **MVA induces autophagy through a TLRs adaptor protein**

Autophagy has been considered to be an innate defense mechanism to eliminate bacterial pathogens including group A *Streptococcus* and *Shigella flexneri*.^{103, 104} There is growing evidence that PRRs play a role in the activation of autophagy upon detection of pathogen-derived molecules. It has been reported that upon engagement with the respective ligands, TLRs trigger Beclin-1 to be recruited to the phagosome. Subsequently, other autophagy associated proteins, such as Atg5, Atg7 and LC3 were upregulated to facilitate the fusion of phagosomes with lysosomes, leading to rapid acidification and enhanced killing of the ingested organisms in the phagosome-autophagy system.⁵⁹ Additionally, by screening a panel of PAMPs for the capability to induce autophagy, it was found that ligands for TLR7 (ssRNA), TLR3 (Poly (I:C)) and TLR4 (LPS) are able to evoke GFP-LC3 punctae.⁶² Thereafter, the TLR adaptor proteins involve MyD88, MyD88-adaptor like (MAL), TRIF, TRIF-related adaptor molecule (TRAM) and sterile α - and armadillo motif-containing protein (SARM) were investigated for their role in TLR signaling-induced autophagy. Xu *et al.* suggested that autophagy is regulated through a TRIF-dependent, MyD88-independent TLR4 signaling pathway.¹⁰⁵ Delgado and colleagues reported that the induction of autophagy is abrogated specifically in response to TLR7 ligands but not starvation in cells subjected to MyD88 knockdown.⁶² In line with this, it was also found that MVA-induced autophagy was dependent on MyD88, while starvation induced autophagy was not hampered in MyD88 knockout BMDCs (Fig. 15). Since MyD88 is one of the two key adaptor proteins that initiates all TLR signaling pathways except TLR3 that utilizes TRIF, MyD88 provides a good target to investigate a potential link for MVA-dependent TLR signaling to control autophagy.

To elucidate how the TLR signaling pathway impacts autophagy, Shi and colleagues revealed that LPS-mediated activation of TLR4 triggers the interaction of Beclin-1 with MyD88 and TRIF, thereby reducing the binding of Beclin1 to Bcl-2. These adaptor proteins consequently activate TRAF6, which induce the Lys63-linked ubiquitination of Beclin-1 at Lys117 in the BH3 domain. The ubiquitination of Beclin-1 then provokes its oligomerization and stimulates autophagy.^{56, 64} Therefore, it is proven that Beclin-1 is a molecular platform assembling an interactome with stimulating components from TLR adaptor proteins (e.g. MyD88), which regulate the initiation of autophagosome formation. On the other hand, Lysakova-Devine *et al.* identified that an 11-aa-long peptide from VACV protein A46 fused to a cell-penetrating delivery sequence, which potently inhibits

TLR4 through MAL and TRAM,¹⁰⁶ suggesting that VACV tries to escape from immune recognition by inhibiting TLRs. This finding may indicate that MVA, which also expresses A46, activate autophagy by manipulating TLR4. However, in this thesis it was found that when BMDCs were treated with the TLR4 ligand LPS, the upregulation of autophagy was not prominent (data not shown). When the double-stranded viral DNA was disrupted by PUVA treatment leading to replication-deficient viruses, the MVA-induced LC3-II turnover was consequently inhibited in a time-dependent manner (Fig. 16B). Moreover, chemical reagent Ara-C which interferes with DNA synthesis showed a comparable inhibition of LC3-II lipidation, though the reasons for severe variation on LC3-I level need to be further elucidated (Fig. 16A). These results strongly suggest that viral replicates or subsequent intermediate/late viral gene products are necessary to stimulate LC3-II conversion. Therefore, MVA-induced autophagy may not depend on TLRs on the cell surface but on the ones located on the endosomal membrane, such as TLR7/8, TLR9 and TLR3, which recognize ssRNA, ssDNA and dsRNA, respectively. In line with this, it was found that MyD88 is significantly upregulated upon MVA infection, raising the level of MyD88 to 3.5 fold at 8h p.i. compared to mock treated cells. Besides, the level of Beclin-1 was also increased in wild-type BMDCs upon MVA infection, while decreased in MyD88-deficient BMDCs, suggesting a close link between MyD88 and Beclin-1 in the induction of autophagy. Therefore, further research should be carried out to identify whether there is a direct interaction between MyD88 and Beclin-1. Particularly with regard to the current data that the increased levels of MyD88 and Beclin-1 are associated with autophagy induction, it can be speculated that MVA infection activates the TLR signaling pathways via adaptor protein MyD88 to induce autophagy.

5.2 Endogenous antigen presentation of HEL peptides

5.2.1 Endocytotic ability of MVA-infected BMDCs is impaired

Vaccinia virus utilizes multiple mechanisms to penetrate the cell membrane, among which the most productive entry is reported to be dominated by low pH-dependent endocytosis into large uncoated vacuoles that occurs in cell-to-cell spread of extracellular enveloped virions (EEV).¹⁰⁷ When EEV is endocytosed into host cells, its outer membrane is disrupted in the low-pH condition and by fusion the endosomal membrane with the exposed intracellular matured virions (IMV), the core is released into the cytoplasm.¹⁰⁸ A recent study suggests that both IMV and EEV are taken up mainly via macropinocytosis, which is a regulated form of endocytosis that mediates the non-sensitive uptake of soluble antigens, but does not rely on low pH-fusion to allow for entering the cytoplasm.^{109, 110} VACV may use macropinocytosis to enter the cells because their large size is comparable to the apoptotic bodies that are macropinocytosed by phagocytes or other cell types. Additionally, macropinocytosis of apoptotic debris is triggered by surface-exposed phosphatidylserine (PS), which is enriched on the IMV virion membrane, so that the IMV can mimic the apoptotic bodies to enter cells by macropinocytosis.¹⁰⁷ The advantage of this entry is that by mimicking apoptotic bodies, virions can avoid being detected by the immune system, because this process does not require receptor-specific interaction. On the other side, since APCs like macrophages and DCs possess very strong endocytosis ability, they are preferentially targeted by VACV *in vivo*.⁴⁹ The viruses, commonly used for infection in this thesis are IMV, because the purification of MVA is based on material gained from lysates of infected chicken embryo fibroblasts (CEF). As a result, the infection rates of VACV or MVA in DCs are quite high. For example, around 50% to 64% of DC 2.4 cells expressed EGFP when MVA-EGFP P7.5 was applied to these cells for 9h (Fig. 24). The infection rate of BMDCs was close to 70% using the same experimental setup (data not shown), demonstrating DCs seems to be easily infected by MVA.

An accepted hallmark of DC maturation is the eventual down-regulation of the endocytic capacity in these cells.¹¹¹ Wilson and others have shown that upon malaria infection, mature DCs downregulate their capacity to cross-present newly encountered antigens *in vivo* while maintaining the ability to present endogenous antigens. They argued that this impairment was due to the downregulation of endocytosis that accompanies DC

maturation.¹¹² Usually, studies employed the activation of T lymphocyte as a marker for the endocytotic ability of DCs or electron microscope techniques to track artificial particles, reflecting the endocytosis process in APCs.^{113, 114} Unlike others, by using recombinant MVA containing fluorescent reporter proteins such as EGFP or mCherry, we were able to observe endocytosis of viral gene products in BMDCs using confocal microscopy. By analyzing the co-localization of exogenous proteins with cellular compartments in BMDCs, the data clearly demonstrates that within 8h after MVA infection, infected BMDCs were not able to endocytose cell-derived protein (from MVA-EGFP P7.5 infected cells) as well as soluble protein (exogenously pulsed OVA protein) into the cytoplasm (Fig. 17). In comparison, uninfected BMDCs have strong endocytotic activity so that the large amounts of co-localization of EGFP or PE-OVA were detected in the cells, which is in line with the reports described above.

5.2.2 Infected BMDCs can present endogenous antigens to CD4⁺ T cells on MHC II

As described above MVA infection strongly impairs the endocytosis capacity of BMDCs. Furthermore, it was reported that apoptotic cell death was detected from 14h p.i. on in MVA-infected DCs.^{34, 107} Therefore, uptake of apoptotic cell debris by BMDCs from neighboring MVA-infected cells within 14h p.i. should be very limited. Consequently, it is assumed that the presentation of viral antigens by MHC II molecules to CD4⁺ T cells is hampered. However, when BMDCs were incubated with MVA-OVA PK1L for 16h and sorted thereby allowing only infected BMDCs to contact antigen-specific CD4⁺ T cells (CD4^{OVA} T cells), nearly 90% of CD4^{OVA} T cells were stimulated by OVA antigens as indicated by IFN- γ secretion (Fig. 18). Based on this result, it is reasonable to argue that the CD4^{OVA} T cell activation exclusively reflects the efficacy of endogenous antigen presentation in infected BMDCs. In addition, the comparison of exogenous soluble OVA protein with the MVA-OVA PK1L derived endogenous antigen surprisingly showed that although both proteins were processed via different presentation pathways, they stimulated similar levels of IFN- γ secretion in CD4^{OVA}, suggesting a high efficiency of the endogenous pathway in BMDCs.

However, this *in vitro* experimental read out is relatively artificial compared to the *in vivo* situation because only infected BMDCs were picked up to incubated with T cells. *In vivo*,

Gasteiger *et al.* demonstrated that CTL responses against MVA-produced antigens are dominated by cross-priming in DCs,¹⁷ which suggests that large portion of DCs remains uninfected *in vivo* thus endocytose extracellular antigens and presented to CTLs. Although the direct presentation of endogenous antigen by MHC II to CD4⁺ T cells has not been investigated *in vivo* yet, it is speculated that this mechanism maybe not relevant for primary MVA vaccination, rather important to stimulate CD4⁺ T cells after MVA infection of DCs in secondary responses because the direct presentation could process and present antigens much faster. Additionally, DCs generated from bone marrow precursors *in vitro* are great tool to study and understand antigen presentation properties, but the cultured BMDCs resemble a somewhat homogenous population compared to the actual *in vivo* situation. Distinct DC subpopulations with diverse antigen-presentation abilities exert their immunological function in different lymphoid organs *in vivo*. Hence, this natural heterogeneity has to be taken into account when analyzing and interpreting antigen presentation experiments performed with DCs differentiated *in vitro*.

5.2.3 Endogenous HEL peptides are processed and presented by MHC II

So far, it has been shown that endogenous viral antigen presentation by MHC II is occurring in MVA-infected DCs. However, the intracellular events such as the initial transport of peptides from the cytoplasm to MIIC, the peptide loading on MHC II molecules as well as the subsequent trafficking of the peptide/MHC class II complex to the cell surface, are poorly understood. The conventional experimental read out of DC-T cell interaction is T cell proliferation and activation, which relies on the secretion of different patterns of cytokines, including IFN- γ and IL-2. This method is suitable to analyze the efficiency of T cells stimulation by specific peptides as well as to determine the amount of peptide/MHC class II complex on the cell surface, but it is not eligible to characterize the intracellular antigen processing, neither can it be used to address the questions mentioned above. Therefore, model protein antigens such as HEL or OVA constitute a very elegant tool to examine the intracellular antigen presentation pathways. APCs process HEL into four major peptide families, which were identified biochemically by analyzing the peptide/MHC class II complex using mass spectrometry.¹¹⁵ Among these peptides, peptide 46-61 of HEL (NTDGSTDYGILQINSR) was abundantly selected for a strong binding motif.¹¹⁵ Monoclonal antibodies (mAbs) recognizing HEL peptides bound to the

MHC II molecule I-A^k and have been intensively reported to provide a tool to better understand the peptide/MHC II intracellular interactions.^{26, 116} By staining the complexes with the C4H3 mAbs, Inaba and colleagues reported that in MIICs of immature DCs, the formation of pHEL/MHC II is inhibited, suggesting an arrest of antigen presentation at the peptide-loading step in the absence of DC maturation stimuli.⁷⁹ In this thesis, the C4H3 mAbs enriched in a hybridoma supernatant proved to be sufficient for intracellular staining of pHEL/I-A^k complexes (Fig. 20 and 21). Compared to the Aw3.18 mAbs, which recognize the same epitope, the C4H3 mAbs have stronger affinity as well as cell viability after staining the complexes. The staining exhibited a dot-like structure in the cytoplasm and on the cell membrane, which was similar to previous published images.⁷⁸

A recombinant MVA expressing the entire HEL protein under the early and late promoter P7.5 was constructed, allowing us to characterize endogenous processing of viral gene products in APCs on a single cell basis by immunofluorescence using confocal microscopy. Using the C4H3 mAbs, a detailed spatiotemporal analysis of when and where MHC II molecules are loaded with HEL peptides was revealed (Fig. 22 and Fig. 23). For the first time, direct proof of endogenous HEL antigen processing and presentation in MVA infected APCs was provided. When HEL was expressed under the control of the P7.5 promoter, pHEL/I-A^k was formed after 2h infection in BMDCs and was localized near the nuclei. The complexes appeared on the cell membrane at 6h to 8h p.i.. pHEL/I-A^k was strongly co-localized with MHC II, demonstrating that the efficiency of this antigen processing and presentation pathway was quite high. The MVA-HEL P7.5 virus provides an excellent tool to characterize the cellular mechanisms that may control this pathway. For example, it can be used to investigate whether MVA-induced autophagy impacts the quality and extent of HEL antigen presentation.

5.3 Excellular and intracellular events in MVA infected BMDCs

CLSM is a fast developing technique for obtaining high-resolution optical images with depth selectivity. The basic key to the confocal approach is the use of spatial filtering techniques to eliminate the focus light or glare in samples where the thickness exceeds the immediate plane of focus. Therefore, images can be acquired point-by-point and reconstructed with a computer, even allowing three-dimensional reconstructions of images acquired by different depth levels. In recent years, CLSM became widely established as a research instrument in bio and life sciences, especially in cell biology.¹¹⁷ Additionally, the multicolor immunofluorescence technique applied with CLSM enables us to analyze different cellular organelles and pathogens in one image, thus greatly improving the study of antigen presentation on the cellular level. In this thesis, CLSM has been widely used to investigate the autophagic flux and the endocytosis ability of BMDCs, as well as antigen processing and trafficking upon viral infection and chemical stimulation.

5.3.1 Expression and spatiotemporal distribution pattern of viral products

It is known that late viral gene expression is abolished in human DCs infected by VACV or MVA, including in the absence of viral DNA replication.^{16, 118, 119} Interestingly, when compare the expression of recombinant protein EGFP under the control of an early or late promoter, respectively, it was possible to detect EGFP expression in murine BMDCs (Fig. 23). Additionally, the late viral antigen-H3 was also observed in MVA-infected murine BMDCs (Fig. 26). The reasons for the abortive late gene expression in human DCs, but not in murine DCs upon infection with VACV or MVA have not been assessed in the publications. While it is also difficult to directly compare the two kinds of DCs, as the entire DC system in response to viral infections is considered to be quite dynamic. The BMDCs used in this thesis are of myeloid origin generated from inbred laboratory mice, while most readily available source of human DCs is blood. It is concluded that culture-generated DCs might be more like the immunogenic type of DC that is incline to response to infections and pathogens, whereas DCs freshly isolated from blood might be involved in the steady-state maintenance of self-tolerance.¹²⁰ The discrepancies of mouse and human DC population are not going to be extensively discussed here, but it should be

taken into account when comparing the outcome of viral gene expression in these DCs.

From the observation of the spatiotemporal distribution pattern of the two viral antigens H3 and A27, it was concluded that viral factories could play an important role in antigen generation and function. Both viral proteins were initially detected around the viral factories, whereas only H3 translocated to the cell surface at later time points after infection (Fig. 26). Up to date, there is only limited information indicating that envelope protein H3 present on mature virions (MV) binds to heparin sulfate on the cell surface and might provide virion attachment to target cells. McCausland *et al.* have published that by using human mAb against H3 in the combination therapy of VACV infection in a small animal model provides protection similar to vaccinia immune globulin, suggesting H3 is an immunodominant antigen.¹²¹ According to the literature so far, it is the first hand image to elucidate the subcellular pattern of H3 after infection. Further research may be required to interpret the intracellular behavior of H3.

It was reported that the A27 is required for the transport of intracellular mature virions (IMV) between the virus factory to the site of intracellular enveloped virions (IEV) formation.¹²² They argued that A27 participates in microtubule-dependent dispersal of accumulated IMV particles. Moreover, A27 binds to cell surface heparin sulfate, providing an anchor for A26 protein packaging into MV, which results in MV progeny with increased plasma membrane fusion activity upon cell entry.⁸⁰ From these findings, it is thought that A27 is an important structural protein involved in virion development. In this thesis, A27 was found to be located surrounding the viral factories and partially close to nuclei. Even in the later infection period, A27 was not translocated to the marginal areas of the infected cells. Although, in BMDCs or Hela cells, MVA is not able to finish its viral replication cycle, viral factories are formed between 3h to 5h post infection. Both, the immunodominant protein (H3) and envelope structure protein (A27) were synthesized around the viral factories, demonstrating that viral factories are not only the viral DNA replication site, but also the viral proteins packing center for viral proteins which is crucial for viral particle generation.

5.3.2 Co-localization of viral factory, MIIC and Golgi complex

Earlier reports suggested that the Golgi complex might participate in virus assembly as it was found that the first VACV envelope originated from a cellular tubulovesicular

compartment, which was related to the endoplasmic reticulum-Golgi intermediate compartment (ERGIC).³⁹ Cluett *et al.* found that the acquisition of the membrane envelope by VACV has occurred at the *cis*- and *trans*-Golgi-network site.⁸⁴ Though it is not clear whether viral factories have direct interaction with the Golgi, these findings prove that viral factories are crucial compartments that might usurp the Golgi to serve for viral protein processing and assembly of new virions. Fig. 29 showed that the co-localization between Golgi and viral factories was prominent in MVA infected HeLa cells as well as BMDCs. However, some differences concerning the interaction of Golgi and viral factories during MVA infection were noticed between the two cell types: 1) the Golgi complex almost completely overlapped with viral factories in BMDCs, whereas the co-localization in HeLa cells was only partial; 2) the Golgi in HeLa cells seemed to maintain a network-like structure, while it exhibited a spherical shape in BMDCs. The morphological diversity might be due to a more abundant and stretchable cytoplasm in HeLa cells, which allows for more space for cellular organelles. BMDCs are generally smaller than HeLa cells, and they are specialized in antigens uptake so that the endosomal systems (e.g. endosomes and lysosomes) are much bigger than that in HeLa cells with regard to the LAMP-2 staining pattern in HeLa cells (Fig. 12) or BMDCs (Fig. 29 and 31). Therefore, the Golgi complex in BMDCs looks more compact than in HeLa cells.

Another important finding in this thesis is that the MIIC was observed to transform into a large tubular structure only upon MVA infection and consequently co-localized with viral factories (Fig. 30). The fusion structure of MIIC displayed at the later time points after infection suggests that MVA infection may change the cytoskeleton which may provide a scaffold for the MHC II complex transport. Although it needs more evidence to prove that the three compartments directly interact with each other, the co-localization could provide an opportunity e.g. a tunnel which delivers viral products to MIIC where MHC II molecules, lysozymes and HLA-DM are accumulated. Therefore, the morphological changes of MIIC in BMDCs could represent an immune defense mechanism to protect these cells from viral invasion. This observation is partially in accordance with the previous report that a similar spatial transformation of MIIC was found in the murine dendritic cell line-D1, which had been stimulated with LPS for 6h.¹²³ However, the detection of this MIIC transformation upon treatment with the same dose of LPS for the same time failed in BMDCs (Fig. 30B). Hence, it was assumed that this unique

conformational change of MIIC triggered by MVA infection is in favor for the antigen presentation in BMDCs.

6. Conclusions and Outlook

The results obtained in this thesis contribute to the better understanding of the processing and presentation of endogenous MVA antigens by MHC class II molecules assisted by the autophagy system and the spatiotemporal co-localization of cellular organelles with sites of viral antigens production following infection. First of all, the study provides evidences that MVA-induced autophagy delivers the cytosolic components to the lysosomal compartment, which provides an opportunity for endogenous antigens to gain access to the MHC II antigen presentation pathway. The data demonstrates that the TLR adaptor protein MyD88 and Atg7, are crucial for the induction of the autophagy upon MVA infection, which correlates with enhanced expression of the autophagy-related protein Beclin-1. Moreover, viral DNA replicates or subsequent intermediate/late viral gene products are necessary for the activation of autophagy, suggesting that MVA may be recognized by PRRs like TLR7/8 or TLR9 that recruit both MyD88 and Beclin-1 to trigger the stimulation of autophagy. Secondly, by utilizing a recombinant MVA construct expressing the model antigen HEL, this study provides for the first time the direct evidence that the endogenous HEL peptide 46-61 is endogenously processed, bound to MHC II molecules and presented on the cell surface. Finally, a functional immunofluorescence protocol for confocal laser scan microscope observation was established to monitor the transport and spatiotemporal distribution pattern of MVA-produced recombinant and viral antigens, as well as to demonstrate their connection with cellular organelles. For the first time, a triple co-localization between the Golgi complex, MHC II loading compartment and the viral DNA replication site namely MVA-induced viral factories could be discovered. The distinct partial co-localization among the three compartments might provide a place where viral products are simultaneously processed in Golgi for viral particle packaging and can be delivered to endosomal vesicles for degradation and subsequent presentation via MHC class II molecules.

The above findings extend our knowledge about MVA antigen presentation in dendritic cells and the induction of adaptive immunity towards viral infection. The MVA-induced autophagy, which contributes to intracellular antigen processing and transport might be important to expand memory CD4⁺ T cells in secondary response after direct infection of

DCs. Although immature DCs are very specialized in the endocytosis of exogenous antigens, infection-triggered autophagy could be beneficial for mature DCs which are no longer able to ingest extracellular antigens, or which are infected by noncytolytic pathogens that leave infected host cells intact. Our findings can be exploited for future vaccine design, i.e. to improve stimulation of T helper cells by using a recombinant MVA vaccine, which delivers antigens that are targeted by autophagy to promote antigen presentation by MHC II.

In general, the above findings represent the first attempt to characterize the cellular components that control and shape the endogenous antigen presentation pathway in the course of viral infection. To acquire a deeper understanding of the underlying molecular mechanisms, the following experiments are planned for future research:

- 1) Investigate the interaction between MyD88 and Beclin-1 in virus-infected cells by co-transfecting Flag-MyD88 and HA-Beclin-1 plasmids and perform immunoprecipitation (IP) on the cell lysate. By detection of Flag- and HA-tagged proteins, the question whether MyD88 indeed targets Beclin-1 to initiate autophagy can be addressed.
- 2) Decipher the possible TLR pathway(s) which is/are responsible for the recognition of MVA upon infection and which regulate autophagy through the TLR adaptor protein MyD88 by analyzing LC3 levels mice lacking individual TLR. Since MyD88 participates in the downstream signaling of all TLRs except TLR3, it is important to pinpoint the TLR pathway for subsequent characterization of the underlying mechanisms.
- 3) Monitor the intracellular distribution of pHEL46-61/I-A^k and autophagic compartments, as well as the presentation of pHEL46-61/I-A^k on the cell surface in the presence or absence of autophagy inhibitors. By utilizing methods such as CLSM and FACS, the impact of autophagy on processing and presentation pathways of endogenous HEL peptides can be visualized and quantified.

7. References

1. Trombetta ES, Mellman I. Cell biology of antigen processing in vitro and

-
- in vivo. Annual review of immunology 2005; 23:975-1028.
2. Banchereau J, Briere F, Caux C, Davoust J, Lebecque S, Liu YJ, et al. Immunobiology of dendritic cells. Annual review of immunology 2000; 18:767-811.
 3. Parham P. The Immune System, 3rd Edition. 2009.
 4. Neefjes J, Jongstra ML, Paul P, Bakke O. Towards a systems understanding of MHC class I and MHC class II antigen presentation. Nature reviews Immunology 2011; 11:823-36.
 5. Lutz MB, Schuler G. Immature, semi-mature and fully mature dendritic cells: which signals induce tolerance or immunity? Trends in immunology 2002; 23:445-9.
 6. Segura E, Villadangos JA. Antigen presentation by dendritic cells in vivo. Current opinion in immunology 2009; 21:105-10.
 7. Mellman I, Steinman RM. Dendritic cells: specialized and regulated antigen processing machines. Cell 2001; 106:255-8.
 8. Thery C, Amigorena S. The cell biology of antigen presentation in dendritic cells. Current opinion in immunology 2001; 13:45-51.
 9. Kenneth P. Murphy PT, Mark Walport, Charles Janeway. Janeway's Immuno Biology, Seventh Edition. 2008.
 10. Xu RH, Remakus S, Ma X, Roscoe F, Sigal LJ. Direct presentation is sufficient for an efficient anti-viral CD8⁺ T cell response. PLoS pathogens 2010; 6:e1000768.
 11. Kloetzel PM, Ossendorp F. Proteasome and peptidase function in MHC-class-I-mediated antigen presentation. Current opinion in immunology 2004; 16:76-81.
 12. Heath WR, Carbone FR. Cross-presentation in viral immunity and self-tolerance. Nature reviews Immunology 2001; 1:126-34.
 13. Kurts C, Robinson BW, Knolle PA. Cross-priming in health and disease. Nature reviews Immunology 2010; 10:403-14.
 14. Bevan MJ. Cross-priming for a secondary cytotoxic response to minor H antigens with H-2 congenic cells which do not cross-react in the cytotoxic assay. The

Journal of experimental medicine 1976; 143:1283-8.

15. Ramachandra L, Simmons D, Harding CV. MHC molecules and microbial antigen processing in phagosomes. *Current opinion in immunology* 2009; 21:98-104.
16. Kastenmuller W, Drexler I, Ludwig H, Erfle V, Peschel C, Bernhard H, et al. Infection of human dendritic cells with recombinant vaccinia virus MVA reveals general persistence of viral early transcription but distinct maturation-dependent cytopathogenicity. *Virology* 2006; 350:276-88.
17. Gasteiger G, Kastenmuller W, Ljapoci R, Sutter G, Drexler I. Cross-priming of cytotoxic T cells dictates antigen requisites for modified vaccinia virus Ankara vector vaccines. *Journal of virology* 2007; 81:11925-36.
18. Kastenmuller W, Gasteiger G, Gronau JH, Baier R, Ljapoci R, Busch DH, et al. Cross-competition of CD8+ T cells shapes the immunodominance hierarchy during boost vaccination. *The Journal of experimental medicine* 2007; 204:2187-98.
19. Dengjel J, Schoor O, Fischer R, Reich M, Kraus M, Muller M, et al. Autophagy promotes MHC class II presentation of peptides from intracellular source proteins. *Proceedings of the National Academy of Sciences of the United States of America* 2005; 102:7922-7.
20. Dongre AR, Kovats S, deRoos P, McCormack AL, Nakagawa T, Paharkova-Vatchkova V, et al. In vivo MHC class II presentation of cytosolic proteins revealed by rapid automated tandem mass spectrometry and functional analyses. *European journal of immunology* 2001; 31:1485-94.
21. Rudensky A, Preston-Hurlburt P, Hong SC, Barlow A, Janeway CA, Jr. Sequence analysis of peptides bound to MHC class II molecules. *Nature* 1991; 353:622-7.
22. Schmid D, Munz C. Immune surveillance of intracellular pathogens via autophagy. *Cell death and differentiation* 2005; 12 Suppl 2:1519-27.
23. Aichinger G, Karlsson L, Jackson MR, Vestberg M, Vaughan JH, Teyton L, et al. Major histocompatibility complex class II-dependent unfolding, transport, and degradation of endogenous proteins. *The Journal of biological chemistry* 1997; 272:29127-36.

-
24. Malnati MS, Marti M, LaVaute T, Jaraquemada D, Biddison W, DeMars R, et al. Processing pathways for presentation of cytosolic antigen to MHC class II-restricted T cells. *Nature* 1992; 357:702-4.
 25. Paludan C, Schmid D, Landthaler M, Vockerodt M, Kube D, Tuschl T, et al. Endogenous MHC class II processing of a viral nuclear antigen after autophagy. *Science* 2005; 307:593-6.
 26. Schmid D, Pypaert M, Munz C. Antigen-loading compartments for major histocompatibility complex class II molecules continuously receive input from autophagosomes. *Immunity* 2007; 26:79-92.
 27. Moss B. *Field's Virology, Fifth Edition, Chapter 84 Poxviridae, the viruses and their replication.* 2007.
 28. Frank F. *Smallpox and Its Eradication (History of International Public Health, No.6).* 1988.
 29. Knight J. Prairie-dog model offers hope of tackling monkeypox virus. *Nature* 2003; 423:674.
 30. Kennedy RB, Ovsyannikova IG, Jacobson RM, Poland GA. The immunology of smallpox vaccines. *Current opinion in immunology* 2009; 21:314-20.
 31. Drexler I, Staib C, Sutter G. Modified vaccinia virus Ankara as antigen delivery system: how can we best use its potential? *Current opinion in biotechnology* 2004; 15:506-12.
 32. Moss B, Carroll MW, Wyatt LS, Bennink JR, Hirsch VM, Goldstein S, et al. Host range restricted, non-replicating vaccinia virus vectors as vaccine candidates. *Advances in experimental medicine and biology* 1996; 397:7-13.
 33. Meyer H, Sutter G, Mayr A. Mapping of deletions in the genome of the highly attenuated vaccinia virus MVA and their influence on virulence. *The Journal of general virology* 1991; 72 (Pt 5):1031-8.
 34. Chahroudi A, Garber DA, Reeves P, Liu L, Kalman D, Feinberg MB. Differences and similarities in viral life cycle progression and host cell physiology after infection of

human dendritic cells with modified vaccinia virus Ankara and vaccinia virus. *Journal of virology* 2006; 80:8469-81.

35. Earl PL, Americo JL, Wyatt LS, Eller LA, Whitbeck JC, Cohen GH, et al. Immunogenicity of a highly attenuated MVA smallpox vaccine and protection against monkeypox. *Nature* 2004; 428:182-5.

36. Moss B. Poxvirus cell entry: how many proteins does it take? *Viruses* 2012; 4:688-707.

37. Tolonen N, Doglio L, Schleich S, Krijnse Locker J. Vaccinia virus DNA replication occurs in endoplasmic reticulum-enclosed cytoplasmic mini-nuclei. *Molecular biology of the cell* 2001; 12:2031-46.

38. Novoa RR, Calderita G, Arranz R, Fontana J, Granzow H, Risco C. Virus factories: associations of cell organelles for viral replication and morphogenesis. *Biology of the cell / under the auspices of the European Cell Biology Organization* 2005; 97:147-72.

39. Risco C, Rodriguez JR, Lopez-Iglesias C, Carrascosa JL, Esteban M, Rodriguez D. Endoplasmic reticulum-Golgi intermediate compartment membranes and vimentin filaments participate in vaccinia virus assembly. *Journal of virology* 2002; 76:1839-55.

40. Herrero-Martinez E, Roberts KL, Hollinshead M, Smith GL. Vaccinia virus intracellular enveloped virions move to the cell periphery on microtubules in the absence of the A36R protein. *The Journal of general virology* 2005; 86:2961-8.

41. Backes S, Sperling KM, Zwilling J, Gasteiger G, Ludwig H, Kremmer E, et al. Viral host-range factor C7 or K1 is essential for modified vaccinia virus Ankara late gene expression in human and murine cells, irrespective of their capacity to inhibit protein kinase R-mediated phosphorylation of eukaryotic translation initiation factor 2alpha. *The Journal of general virology* 2010; 91:470-82.

42. Ludwig H, Mages J, Staib C, Lehmann MH, Lang R, Sutter G. Role of viral factor E3L in modified vaccinia virus ankara infection of human HeLa Cells: regulation of the virus life cycle and identification of differentially expressed host genes. *Journal of virology* 2005; 79:2584-96.

-
43. McFadden G. Poxvirus tropism. *Nature reviews Microbiology* 2005; 3:201-13.
 44. Senkevich TG, Ward BM, Moss B. Vaccinia virus entry into cells is dependent on a virion surface protein encoded by the A28L gene. *Journal of virology* 2004; 78:2357-66.
 45. Seet BT, Johnston JB, Brunetti CR, Barrett JW, Everett H, Cameron C, et al. Poxviruses and immune evasion. *Annual review of immunology* 2003; 21:377-423.
 46. Guerra S, Lopez-Fernandez LA, Conde R, Pascual-Montano A, Harshman K, Esteban M. Microarray analysis reveals characteristic changes of host cell gene expression in response to attenuated modified vaccinia virus Ankara infection of human HeLa cells. *Journal of virology* 2004; 78:5820-34.
 47. Hung JJ, Chung CS, Chang W. Molecular chaperone Hsp90 is important for vaccinia virus growth in cells. *Journal of virology* 2002; 76:1379-90.
 48. Garcia-Arriaza J, Arnaez P, Gomez CE, Sorzano CO, Esteban M. Improving Adaptive and Memory Immune Responses of an HIV/AIDS Vaccine Candidate MVA-B by Deletion of Vaccinia Virus Genes (C6L and K7R) Blocking Interferon Signaling Pathways. *PloS one* 2013; 8:e66894.
 49. Liu L, Chavan R, Feinberg MB. Dendritic cells are preferentially targeted among hematolymphocytes by Modified Vaccinia Virus Ankara and play a key role in the induction of virus-specific T cell responses in vivo. *BMC immunology* 2008; 9:15.
 50. Jing L, Davies DH, Chong TM, Chun S, McClurkan CL, Huang J, et al. An extremely diverse CD4 response to vaccinia virus in humans is revealed by proteome-wide T-cell profiling. *Journal of virology* 2008; 82:7120-34.
 51. Yin L, Calvo-Calle JM, Cruz J, Newman FK, Frey SE, Ennis FA, et al. CD4+ T cells provide intermolecular help to generate robust antibody responses in vaccinia virus-vaccinated humans. *Journal of immunology* 2013; 190:6023-33.
 52. Sette A, Moutaftsi M, Moyron-Quiroz J, McCausland MM, Davies DH, Johnston RJ, et al. Selective CD4+ T cell help for antibody responses to a large viral pathogen: deterministic linkage of specificities. *Immunity* 2008; 28:847-58.
 53. Kaushik S, Massey AC, Mizushima N, Cuervo AM. Constitutive activation of

chaperone-mediated autophagy in cells with impaired macroautophagy. *Molecular biology of the cell* 2008; 19:2179-92.

54. Mizushima N, Yoshimori T, Levine B. Methods in mammalian autophagy research. *Cell* 2010; 140:313-26.

55. Maiuri MC, Zalckvar E, Kimchi A, Kroemer G. Self-eating and self-killing: crosstalk between autophagy and apoptosis. *Nature reviews Molecular cell biology* 2007; 8:741-52.

56. Shi CS, Kehrl JH. MyD88 and Trif target Beclin 1 to trigger autophagy in macrophages. *The Journal of biological chemistry* 2008; 283:33175-82.

57. Munz C. Beclin-1 targeting for viral immune escape. *Viruses* 2011; 3:1166-78.

58. Deretic V, Saitoh T, Akira S. Autophagy in infection, inflammation and immunity. *Nature reviews Immunology* 2013; 13:722-37.

59. Sanjuan MA, Dillon CP, Tait SW, Moshiah S, Dorsey F, Connell S, et al. Toll-like receptor signalling in macrophages links the autophagy pathway to phagocytosis. *Nature* 2007; 450:1253-7.

60. Thurston TL, Ryzhakov G, Bloor S, von Muhlinen N, Randow F. The TBK1 adaptor and autophagy receptor NDP52 restricts the proliferation of ubiquitin-coated bacteria. *Nature immunology* 2009; 10:1215-21.

61. Watts C, West MA, Zaru R. TLR signalling regulated antigen presentation in dendritic cells. *Current opinion in immunology* 2010; 22:124-30.

62. Delgado MA, Elmaoued RA, Davis AS, Kyei G, Deretic V. Toll-like receptors control autophagy. *The EMBO journal* 2008; 27:1110-21.

63. Lee HK, Lund JM, Ramanathan B, Mizushima N, Iwasaki A. Autophagy-dependent viral recognition by plasmacytoid dendritic cells. *Science* 2007; 315:1398-401.

64. Shi CS, Kehrl JH. Traf6 and A20 differentially regulate TLR4-induced autophagy by affecting the ubiquitination of Beclin 1. *Autophagy* 2010; 6:986-7.

65. Schmid D, Munz C. Innate and adaptive immunity through autophagy. *Immunity*

2007; 27:11-21.

66. Lee HK, Mattei LM, Steinberg BE, Alberts P, Lee YH, Chervonsky A, et al. In vivo requirement for Atg5 in antigen presentation by dendritic cells. *Immunity* 2010; 32:227-39.
67. Delaloye J, Roger T, Steiner-Tardivel QG, Le Roy D, Knaup Reymond M, Akira S, et al. Innate immune sensing of modified vaccinia virus Ankara (MVA) is mediated by TLR2-TLR6, MDA-5 and the NALP3 inflammasome. *PLoS pathogens* 2009; 5:e1000480.
68. Klionsky DJ, Abeliovich H, Agostinis P, Agrawal DK, Aliev G, Askew DS, et al. Guidelines for the use and interpretation of assays for monitoring autophagy in higher eukaryotes. *Autophagy* 2008; 4:151-75.
69. Mizushima N, Yoshimori T. How to interpret LC3 immunoblotting. *Autophagy* 2007; 3:542-5.
70. Kuma A, Matsui M, Mizushima N. LC3, an autophagosome marker, can be incorporated into protein aggregates independent of autophagy: caution in the interpretation of LC3 localization. *Autophagy* 2007; 3:323-8.
71. Scott RC, Schuldiner O, Neufeld TP. Role and regulation of starvation-induced autophagy in the *Drosophila* fat body. *Developmental cell* 2004; 7:167-78.
72. Komatsu M, Waguri S, Ueno T, Iwata J, Murata S, Tanida I, et al. Impairment of starvation-induced and constitutive autophagy in Atg7-deficient mice. *The Journal of cell biology* 2005; 169:425-34.
73. Katayama H, Yamamoto A, Mizushima N, Yoshimori T, Miyawaki A. GFP-like proteins stably accumulate in lysosomes. *Cell structure and function* 2008; 33:1-12.
74. Kimura S, Noda T, Yoshimori T. Dissection of the autophagosome maturation process by a novel reporter protein, tandem fluorescent-tagged LC3. *Autophagy* 2007; 3:452-60.
75. Cuervo AM, Dice JF. Unique properties of lamp2a compared to other lamp2 isoforms. *Journal of cell science* 2000; 113 Pt 24:4441-50.

-
76. Gannage M, Ramer PC, Munz C. Targeting Beclin 1 for viral subversion of macroautophagy. *Autophagy* 2010; 6:166-7.
77. Loschko J, Heink S, Hackl D, Dudziak D, Reindl W, Korn T, et al. Antigen targeting to plasmacytoid dendritic cells via Siglec-H inhibits Th cell-dependent autoimmunity. *Journal of immunology* 2011; 187:6346-56.
78. Zhong G, Reis e Sousa C, Germain RN. Production, specificity, and functionality of monoclonal antibodies to specific peptide-major histocompatibility complex class II complexes formed by processing of exogenous protein. *Proceedings of the National Academy of Sciences of the United States of America* 1997; 94:13856-61.
79. Inaba K, Turley S, Iyoda T, Yamaide F, Shimoyama S, Reis e Sousa C, et al. The formation of immunogenic major histocompatibility complex class II-peptide ligands in lysosomal compartments of dendritic cells is regulated by inflammatory stimuli. *The Journal of experimental medicine* 2000; 191:927-36.
80. Chang TH, Chang SJ, Hsieh FL, Ko TP, Lin CT, Ho MR, et al. Crystal structure of vaccinia viral A27 protein reveals a novel structure critical for its function and complex formation with A26 protein. *PLoS pathogens* 2013; 9:e1003563.
81. Sancho MC, Schleich S, Griffiths G, Krijnse-Locker J. The block in assembly of modified vaccinia virus Ankara in HeLa cells reveals new insights into vaccinia virus morphogenesis. *Journal of virology* 2002; 76:8318-34.
82. Mu FT, Callaghan JM, Steele-Mortimer O, Stenmark H, Parton RG, Campbell PL, et al. EEA1, an early endosome-associated protein. EEA1 is a conserved alpha-helical peripheral membrane protein flanked by cysteine "fingers" and contains a calmodulin-binding IQ motif. *The Journal of biological chemistry* 1995; 270:13503-11.
83. Husain M, Moss B. Similarities in the induction of post-Golgi vesicles by the vaccinia virus F13L protein and phospholipase D. *Journal of virology* 2002; 76:7777-89.
84. Cluett EB, Machamer CE. The envelope of vaccinia virus reveals an unusual phospholipid in Golgi complex membranes. *Journal of cell science* 1996; 109 (Pt 8):2121-31.

-
85. Orvedahl A, Levine B. Viral evasion of autophagy. *Autophagy* 2008; 4:280-5.
86. Knodler LA, Celli J. Eating the strangers within: host control of intracellular bacteria via xenophagy. *Cellular microbiology* 2011; 13:1319-27.
87. Klionsky DJ, Abdalla FC, Abeliovich H, Abraham RT, Acevedo-Arozena A, Adeli K, et al. Guidelines for the use and interpretation of assays for monitoring autophagy. *Autophagy* 2012; 8:445-544.
88. Huang WP, Scott SV, Kim J, Klionsky DJ. The itinerary of a vesicle component, Aut7p/Cvt5p, terminates in the yeast vacuole via the autophagy/Cvt pathways. *The Journal of biological chemistry* 2000; 275:5845-51.
89. Dugina V, Zwaenepoel I, Gabbiani G, Clement S, Chaponnier C. Beta and gamma-cytoplasmic actins display distinct distribution and functional diversity. *Journal of cell science* 2009; 122:2980-8.
90. Humphries AC, Dodding MP, Barry DJ, Collinson LM, Durkin CH, Way M. Clathrin potentiates vaccinia-induced actin polymerization to facilitate viral spread. *Cell host & microbe* 2012; 12:346-59.
91. Moloughney JG, Monken CE, Tao H, Zhang H, Thomas JD, Lattime EC, et al. Vaccinia virus leads to ATG12-ATG3 conjugation and deficiency in autophagosome formation. *Autophagy* 2011; 7:1434-47.
92. Ni HM, Bockus A, Wozniak AL, Jones K, Weinman S, Yin XM, et al. Dissecting the dynamic turnover of GFP-LC3 in the autolysosome. *Autophagy* 2011; 7:188-204.
93. Alcantara LM, Kim J, Moraes CB, Franco CH, Franzoi KD, Lee S, et al. Chemosensitization potential of P-glycoprotein inhibitors in malaria parasites. *Experimental parasitology* 2013; 134:235-43.
94. Zhao H, Cai Y, Santi S, Lafrenie R, Lee H. Chloroquine-mediated radiosensitization is due to the destabilization of the lysosomal membrane and subsequent induction of cell death by necrosis. *Radiation research* 2005; 164:250-7.
95. Fan C, Wang W, Zhao B, Zhang S, Miao J. Chloroquine inhibits cell growth and induces cell death in A549 lung cancer cells. *Bioorganic & medicinal chemistry* 2006;

14:3218-22.

96. Komatsu M, Wang QJ, Holstein GR, Friedrich VL, Jr., Iwata J, Kominami E, et al. Essential role for autophagy protein Atg7 in the maintenance of axonal homeostasis and the prevention of axonal degeneration. *Proceedings of the National Academy of Sciences of the United States of America* 2007; 104:14489-94.
97. Chang TK, Shrivage BV, Hayes SD, Powers CM, Simin RT, Wade Harper J, et al. Uba1 functions in Atg7- and Atg3-independent autophagy. *Nature cell biology* 2013; 15:1067-78.
98. Nishida Y, Arakawa S, Fujitani K, Yamaguchi H, Mizuta T, Kanaseki T, et al. Discovery of Atg5/Atg7-independent alternative macroautophagy. *Nature* 2009; 461:654-8.
99. Whilding LM, Archibald KM, Kulbe H, Balkwill FR, Oberg D, McNeish IA. Vaccinia virus induces programmed necrosis in ovarian cancer cells. *Molecular therapy : the journal of the American Society of Gene Therapy* 2013.
100. Elmore S. Apoptosis: a review of programmed cell death. *Toxicologic pathology* 2007; 35:495-516.
101. Into T, Inomata M, Takayama E, Takigawa T. Autophagy in regulation of Toll-like receptor signaling. *Cellular signalling* 2012; 24:1150-62.
102. Salminen A, Kaarniranta K, Kauppinen A, Ojala J, Haapasalo A, Soininen H, et al. Impaired autophagy and APP processing in Alzheimer's disease: The potential role of Beclin 1 interactome. *Progress in neurobiology* 2013; 106-107:33-54.
103. Nakagawa I, Amano A, Mizushima N, Yamamoto A, Yamaguchi H, Kamimoto T, et al. Autophagy defends cells against invading group A Streptococcus. *Science* 2004; 306:1037-40.
104. Ogawa M, Yoshimori T, Suzuki T, Sagara H, Mizushima N, Sasakawa C. Escape of intracellular Shigella from autophagy. *Science* 2005; 307:727-31.
105. Xu Y, Jagannath C, Liu XD, Sharafkhaneh A, Kolodziejaska KE, Eissa NT. Toll-like receptor 4 is a sensor for autophagy associated with innate immunity. *Immunity* 2007; 27:135-44.

-
106. Lysakova-Devine T, Keogh B, Harrington B, Nagpal K, Halle A, Golenbock DT, et al. Viral inhibitory peptide of TLR4, a peptide derived from vaccinia protein A46, specifically inhibits TLR4 by directly targeting MyD88 adaptor-like and TRIF-related adaptor molecule. *Journal of immunology* 2010; 185:4261-71.
107. Mercer J, Helenius A. Vaccinia virus uses macropinocytosis and apoptotic mimicry to enter host cells. *Science* 2008; 320:531-5.
108. Vanderplasschen A, Hollinshead M, Smith GL. Intracellular and extracellular vaccinia virions enter cells by different mechanisms. *The Journal of general virology* 1998; 79 (Pt 4):877-87.
109. Sandgren KJ, Wilkinson J, Miranda-Saksena M, McInerney GM, Byth-Wilson K, Robinson PJ, et al. A differential role for macropinocytosis in mediating entry of the two forms of vaccinia virus into dendritic cells. *PLoS pathogens* 2010; 6:e1000866.
110. Lim JP, Gleeson PA. Macropinocytosis: an endocytic pathway for internalising large gulps. *Immunology and cell biology* 2011; 89:836-43.
111. West MA, Wallin RP, Matthews SP, Svensson HG, Zaru R, Ljunggren HG, et al. Enhanced dendritic cell antigen capture via toll-like receptor-induced actin remodeling. *Science* 2004; 305:1153-7.
112. Wilson NS, Behrens GM, Lundie RJ, Smith CM, Waithman J, Young L, et al. Systemic activation of dendritic cells by Toll-like receptor ligands or malaria infection impairs cross-presentation and antiviral immunity. *Nature immunology* 2006; 7:165-72.
113. Platt CD, Ma JK, Chalouni C, Ebersold M, Bou-Reslan H, Carano RA, et al. Mature dendritic cells use endocytic receptors to capture and present antigens. *Proceedings of the National Academy of Sciences of the United States of America* 2010; 107:4287-92.
114. Ranftler C, Auinger P, Meisslitzer-Ruppitsch C, Ellinger A, Neumuller J, Pavelka M. Electron microscopy of endocytic pathways. *Methods in molecular biology* 2013; 931:437-47.
115. Unanue ER. From antigen processing to peptide-MHC binding. *Nature immunology* 2006; 7:1277-9.

-
116. Dadaglio G, Nelson CA, Deck MB, Petzold SJ, Unanue ER. Characterization and quantitation of peptide-MHC complexes produced from hen egg lysozyme using a monoclonal antibody. *Immunity* 1997; 6:727-38.
117. Pawley JE. *Handbook of Biological Confocal Microscopy*. 2006.
118. Bronte V, Carroll MW, Goletz TJ, Wang M, Overwijk WW, Marincola F, et al. Antigen expression by dendritic cells correlates with the therapeutic effectiveness of a model recombinant poxvirus tumor vaccine. *Proceedings of the National Academy of Sciences of the United States of America* 1997; 94:3183-8.
119. Drillien R, Spehner D, Bohbot A, Hanau D. Vaccinia virus-related events and phenotypic changes after infection of dendritic cells derived from human monocytes. *Virology* 2000; 268:471-81.
120. Shortman K, Liu YJ. Mouse and human dendritic cell subtypes. *Nature reviews Immunology* 2002; 2:151-61.
121. McCausland MM, Benhnia MR, Crickard L, Laudenslager J, Granger SW, Tahara T, et al. Combination therapy of vaccinia virus infection with human anti-H3 and anti-B5 monoclonal antibodies in a small animal model. *Antiviral therapy* 2010; 15:661-75.
122. Sanderson CM, Hollinshead M, Smith GL. The vaccinia virus A27L protein is needed for the microtubule-dependent transport of intracellular mature virus particles. *The Journal of general virology* 2000; 81:47-58.
123. van Nispen tot Pannerden HE, Geerts WJ, Kleijmeer MJ, Heijnen HF. Spatial organization of the transforming MHC class II compartment. *Biology of the cell / under the auspices of the European Cell Biology Organization* 2010; 102:581-91.

8. Appendix

8.1 Equipment

Device	Manufacture/Distributor
BD FACS Canto II	BD Biosciences (Heidelberg)
CO₂ incubator	Heraeus (Hanau)
Confocal Laser Scan Microscope (Fluoview FV10i)	Olympus (Hamburg)
Cup sonicator	Bandelin (Berlin)
Electrophoresis power supply	Bio-Rad (Munich)
Electrophoresis system Mini Protean	Bio-Rad (Munich)
Fluo cytometer	Agfa (Köln)
Freezer (-20 °C)	Bauknecht (Stuttgart)
Freezer (-80 °C)	Heraeus (Hanau)
Fridge (4 °C)	Bauknecht (Stuttgart)
Gel documentation system	Bio-Rad chemi-Doc XRS+ (Munich)
Haematocytometer	Karl Hecht KG (Sonderheim)
Ice machine	Scotsman (Milan Italy)
Incubator shaker	New Brunswick Scientific (Nürtingen)
Laminar flow	Heraeus (Hanau)

Micropipette	Gilson (Middleton, USA)
Microwave	Siemens (Munich)
Multi channel pipette	Brand (Wertheim)
Nitrogen freezing tank	Forma Scientific (Marietta, OH, USA)
UV/VIS Bio-photometer	Pharmacia Biotech (Uppsala, Sweden)
pH-meter	InoLab (Weilheim)
Pipettor	Eppendorf (Hamburg)
Rotor	Model 200/2.0 Bio-rad (Munich)
Sealing apparatus Folio	Rische+Herfurth GMBH (Hamburg)
Trans-Blot Electrophoretic Transfer cell	Bio-Rad (Munich)
Ultracentrifuge	Beckmann (Munich)
Universal Hood	Bio-Rad (Munich)
Vortexer	Scientific Industries (Bohemia, NY, USA)
Waterbath	Julabo (seelbach)

8.2 Consumables

Item	Manufacturer/Distributor
Cell culture flask with vented screw (25 cm², 75 cm² and 185 cm²)	BD Falcon (Franklin Lakes, NJ, USA)

Cell culture plates (6-well)	BD Falcon (Franklin Lakes, NJ, USA)
Cell scraper	Sarstedt (Nümbrecht)
CL-X posure film	Thermo (Rockford, IL, USA)
Conical Tubes (15ml and 50 ml)	BD Falcon (Franklin Lakes, NJ, USA)
Filter tips	Greiner Bio-One (Frickenhausen)
Nitrocellulose membrane	GE Healthcare
Parafilm	Roth (Karlsruhe)
Petri dish	Nunc (Wiesbaden)
Petri dish (100 mm x 15mm)	BD Falcon (Franklin Lakes, NJ, USA)
Safe lock microcentrifuge tubes (0.5 ml, 1.5 ml and 2 ml)	Eppendorf (Hamburg)
Syringe filter (0.2 μM)	Corning (Lowell, MA, USA)
Syringe sterile (1 ml)	B.Braun (Melsungen)
Ultracentrifuge tubes (Ultra clear)	Beckmann (Munich)
Whatman 3 mm blotting paper	GE Healthcare

Acknowledgment

First of all, I would like to thank my supervisor Prof. Dr. Ingo Drexler for giving me the opportunity to carry out my PhD thesis in his lab. In particular, I am thankful for his supports and patience for maintenance a successful supervision in such a long distance for more than two years. I am grateful for his trusts, the stimulating discussion as well as the kind criticism that I am able to learn so much lab skills and gain the scientific way of thinking to become independent in research.

I want to thank Prof. Anne Krug and Dr. Klaus-Peter Janssen for external supervision for my PhD thesis. Especial gratefulness to Anne, for the inspiring discussion in the thesis committee meeting and the following collaboration that make this project more interesting.

Many thanks go to Dr. Katharina Eisenächer for all the help in experiments optimization, thesis writing and most importantly her warm hugs that light up the way in the darkest moments. I further want to thank Dr. Jacob Loschko for initiating the collaboration.

I want to thank Prof. Ulrike Protzer for giving me the chance to finish PhD study when my group moved to Düsseldorf. I am grateful for the nice discussion and the precious mice sources from Prof. Percy Knolle and Prof. Dirk H. Busch.

All the thanks to my group members: Andi, Frank, Sha, David, Borja, Ronny and Robert for providing materials, technical supports and helpful discussions. In particular, I want to thank Andi for your friendship and humors from time to time during the painful writing.

Beate, Vera, Clemens, Claudia, Jessi, Judith, Flo and all the members in Schneckenburgerstr.8: thank you for all the fun we had together.

And thanks for our secretaries Barbara and Andrea to solve all the “bothers” I ask for.

I want to give the deepest gratefulness to my parents for supporting and encouraging me in the past thirty years. Thank you my aunt Dr. Wenge Ma and uncle Dr. Jiangkai Chen that I have learned so much from you. Last but not least, thank my husband for the love and accompany.

Curriculum Vitae

PERSONAL INFORMATION

Yi Zhang

Date of birth: May 14th, 1983

Place of birth: Chongqing, China

Citizenship: Chinese

Current address: Prinzregenten Strasse 135, 81677, Munich, Germany

Email address: anniezhang514@me.com

EDUCATION

09/2009 to date PhD Thesis entitled: “Characterization of Endogenous Major Histocompatibility Complex Class II Antigen Processing Pathways for Modified Vaccinia Virus Ankara Infection” in the Research Group of Prof. Dr. med. Ingo Drexler at Institute of Virology of Technische Universität München, Germany

09/2006-06/2009 M.S. Pharmaceutical Science, West China School of Pharmacy, Sichuan University, China. Master Thesis entitled: “Preparation of antisense oligodeoxynucleotide -Protamine sulfate-human serum α -PLGA nanoparticles and evaluation of their nucleus targeting property *in vitro*”

09/2002-06/2006 B.S. Biotechnology, School of Life Science, Sichuan University, China. Bachelor Thesis entitled: “Study on the preparation of antisense oligodeoxynucleotide nanoparticles and evaluation of their related properties”

09/1999-06/2002 High School, Bashu Middle School, Chongqing, China

PUBLICATIONS AND CONFERENCE ATTENDING

Inhibition of the EGFR with nanoparticles encapsulating antisense oligonucleotides of the

EGFR enhances radiosensitivity in SCCVII cells. Ping Y, Jian Z, **Yi Z**, Huoyu Z, Feng L, Yuqiong Y, Shixi L. *Med Oncol*. 2010 Sep;27(3):715-21.

Inhibition of ataxia-telangiectasia mutated by antisense oligonucleotide nanoparticles induces radiosensitization of head and neck squamous-cell carcinoma in mice. Zou J, Qiao X, Ye H, **Zhang Y**, Xian J, Zhao H, Liu S. *Cancer Biother Radiopharm*. 2009 Jun;24(3):339-46.

Preparation of ASODN-Protamine-HSA-PLGA nanoparticles and initial evaluation of their nucleus targeting property in vitro. Part I: Physicochemical characterization. **Zhang Yi**, Yuan Li, Yan Xiaoling, Gong Tao, Liu Jiu, Zhang Zhirong, Sun Xun. *Journal of Sichuan University (Medical Science Edition)*, 2009 (03): 555-558

Study on the preparation of antisense oligodeoxynucleotide-PLGA nanoparticles and its properties. YAN Xiao-ling, **ZHANG Yi**, GONG Tao, ZHANG Zhi-rong, SUN Xun. *West China Journal of Pharmaceutical Science*, 2009 (2): 136- 138

2012 XIX International Poxvirus, Asfarvirus and Iridovirus Conference, Spain, poster section: Endogenous MHC class II Antigen Processing Pathway in Modified Vaccinia Virus Ankara Infection. **Yi Zhang**, Frank Thiele, and Ingo Drexler

MVA-infected Dendritic Cells Activate CD4+ T cells via Endogenous MHC Class II Presentation Pathways. Frank Thiele, **Yi Zhang**, Sha Tao, Andreas Muschaweckh, Tina Zollmann, Ulrike Protzer, Rubert Abele and Ingo Drexler. *Journal of Virology* (in submission).